TU/e EINDHOVEN UNIVERSITY OF TECHNOLOGY

Eindhoven University of Technology

MASTER

H-infinity robust control design for an electromechanical servo system

Falkus, H.M.

Award date:
1990

Link to publication

EINDHOVEN UNIVERSITY OF TECHNOLOGY
DEPARTMENT OF ELECTRICAL ENGINEERING
Measurement ans Control Section

H∞ Robust Control Design
for an Electromechanical
Servo System

by Heinz M. Falkus

H$_\infty$ Robust Control Design for an Electromechanical Servo System

Heinz M. Falkus

Summary

In this report, the application of H$_\infty$ control to an electromechanical servo system is discussed. One of the reasons of introducing the H$_\infty$ theory is that according to literature the obtained controllers are expected to be robust. A system is called robust if it maintains certain properties, like stability and performance of the closed-loop system, in spite of plant perturbations or external disturbances. A servo mechanism for High performance applications with one dominant mechanical resonance frequency has to be controlled. This resonance frequency can change due to tolerances in the mechanics of the servo system illustrating the problem of robustness.

To solve the H$_\infty$ optimization problem, two different techniques can be used. The state-space approach is recommended above the polynomial approach because of the explicitness of the formulas involving only the solution to two algebraic Riccati equations together with a substantial reduction in computation. For the calculation of the controllers with the H$_\infty$ theory, a software program which is described in a separate manual has been developed. This program is based on the formulas derived by K. Glover and J.C. Doyle [12] and has been implemented in PC-Matlab (Robust Control Toolbox). A Two-Degree-of-Freedom configuration is introduced to optimize the trade off between robustness and performance. To design a controller which is robust with respect to stability as well as performance, stable factor perturbations are used for the uncertainty modelling. Practical design specifications are translated into weighting functions in the frequency domain and simulations are carried out with the controllers obtained with the H$_\infty$ theory. Important criteria, like Model Robustness, Disturbance Reduction, Input Saturation and Signal Tracking are examined.

To obtain an optimal performance and to satisfy the robustness constraints, high order weighting functions are necessary, which implies also high order controllers. Uncertainty modelling using stable factor perturbations lead only to sufficient and not necessary conditions. Therefore an alternative design is presented as well. In this design all the effort is put in performance optimization and no robustness information at all is included. Finally recommendations are made for further investigations to optimize the results.

Preface & Acknowledgement

This report describes the results obtained when the H_∞ control theory is applied on an electromechanical servo system. This project was a part of my study at the Eindhoven University of Technology (TUE) to obtain my master degree. The research has been performed at the Centre for manufacturing Technology (CFT), department Signal Processing, group Machine and Process Control. The CFT is a part of the N.V. Philips Gloeilampenfabrieken.

For the help, guidance and many useful suggestions I would like to thank both my coaches Ir. J.E.D. Geerts - van Dalen and Ir. B.G.M.G. Tosseram of the CFT. The stimulating discussions with Dr. Ir. A.A.H. Damen and Dr. Ir. A.J.W. v.d. Boom of the TUE during our monthly meetings have inspired and formed many of the ideas presented here. Dr. Ir. P. Boekhoudt is thanked for the detailed explanation and information about using the polynomial approach solving the H_∞ control problem. I would like to thank Ir. A.J.J. v.d. Boom (TUE) , Dr. Ir. M. Steinbuch and Ir. S. Smit (both Natlab) for their ideas and information about applying the state-space approach which helped me in a better understanding of the basic problems. Finally I would like to thank Prof. Dr. Ir. P. Eykhoff for his support and Dr. Ir. K.C.P. Machielsen for giving me the opportunity to do my research in his group. The members of the Machine and Process Control group are thanked for the pleasant time I spent at Philips.

<div align="right">Heinz Falkus, June 1990</div>

Contents

1 Introduction

A number of methods exist in control theory to design and analyze controllers for a given system. During the 1940s and 1950s the frequency domain approaches have been developed to control a system, often referred to as the 'classical' methods. The more 'modern' state-space approach of control theory, has been developed during the late 1950s and 1960s. Although the state-space approach appeared to have a lot of advantages, it is difficult to include uncertainties in the process dynamics into the state-space design and system properties such as bandwidth, stability margin etc. are difficult to study by state-space methods. These are the reasons for a new interest in the frequency domain approach. In H_∞ optimal control a symbiosis of 'classical' and 'modern' control theory seems to be achieved : 'classical' control system design objectives such as robustness, are defined in terms of an H_∞ optimization problem and a solution is obtained via fairly standard modern linear multivariable control techniques. The H_∞ theory applied in this report uses the state-space approach advocated by J.C. Doyle and K. Glover . This approach is entirely based on standard state-space techniques.

Up to the present more attention has been payed to the development of the H_∞ theory in contradistinction to the practical applications of this theory. An explanation for this is probably the strong mathematical character of the H_∞ theory. It is not the case in our opinion that the H_∞ control problems are unpractical formulated control problems. Earlier the opposite is true. It seems inevitable to design the more complicated control strategies on the basis of the robustness demands with respect to stability and performance.

In the Machine and Process Control (MPC) group of the CFT the attention is focused on the control of electromechanical servo systems with one dominant mechanical resonance frequency. It is expected that the control of these kind of systems can be improved significantly by the practical application of the H_∞ theory. The application is focused on the more complicated servo problems, e.g. problems which demand high bandwidth and high performance for the controlled system. The dynamical behaviour can be modelled as a Single-Input Single-Output system.

It is the goal of this master thesis to show how an advanced control theory such as the H_∞ theory can be applied to practical control problems, in our case an electromechanical servo system with one dominant mechanical resonance frequency. The main problem is to translate design specifications such as desired behaviour, robustness, performance etc. into weighting functions in the frequency domain in order to obtain proper closed-loop behaviour. The choices of the weighting functions and the analysis of the obtained results at simulation level will be the most important subjects.

The practical control problem in our case is an electromechanical servo system. The modelling of this electromechanical servo system is described in Chapter 2. In Chapter 3 the solution method of the H_∞ optimization problem is emphasized including a short historical description on the H_∞ theory. Before using the H_∞ theory, the most important properties of the H_∞ theory together with the basic design considerations such as robustness, process uncertainties etc. , are described in Chapter 4. To describe the process uncertainties we use stable factor perturbations. In the Chapters 5 and 6 controllers are designed from different points of view. In Chapter 5 the robustness approach is emphasized to design a controller which is robust with respect to stability as well as performance. An alternative design method using the performance approach to derive an optimal performance is emphasized in Chapter 6. Time response analysis and robustness behaviour with respect to stability as well as performance of the control system are simulated. Conclusions and recommendations for further examinations are pointed out in Chapter 7.

2 Description of the Servo System

2.1 Introduction

This chapter describes an electromechanical servo system. Before we can design controllers for position servos, a model of the servo mechanism is needed. If we assume that the mechanical part of the system is infinitely stiff, a simple second order model is sufficient. In reality, however, the stiffness of the mechanics of a servo system is finite. Therefore a fourth order model will be used. It enables us to improve the design which results in more accurate control systems.

2.2 Modelling of the Servo System

In this section a model of an electromechanical servo system is derived. Fig. 2.1 depicts a block diagram of a position servo system. The mechanics, position sensor, motor, servo-amplifier, in combination with the motion controller determine the overall system behaviour [14].

Commands
Motion Controller U_p Servo Amplifier I DC Motor T_m Mechanics X_p

X_{enc}
Position Sensor
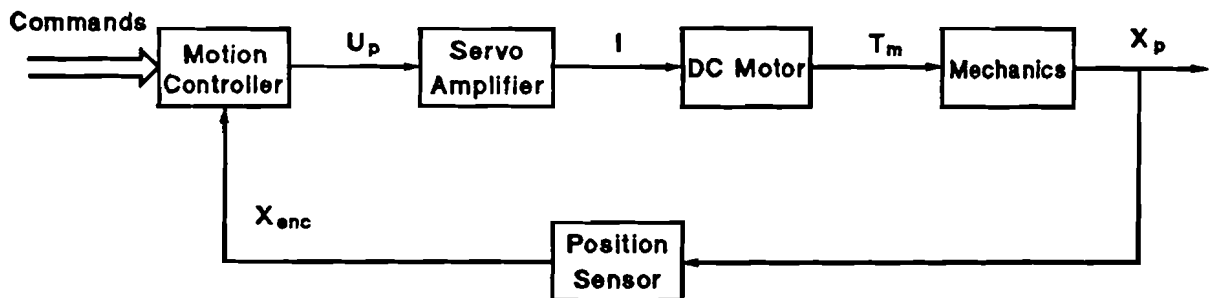
Fig. 2.1 : An Electromechanical Servo System

The controller receives setpoint commands. These commands contain information about the desired position as a function of the time. After receiving a command, a control signal 'u$_p$' is send to the amplifier by the controller. The servo amplifier converts the control voltage into a motor current 'I'. Controlling the current in the motor directly protects the motor and mechanism from overloading. Due to the fast current loop, the electrical time constant caused by the armature resistence and selfinductance can be neglected. The current loop also makes the servo insensitive to variations of the armature resistence due to temperature changes. The DC motor generates a torque 'T$_m$'

6

that is proportional to the armature current 'I' provided by the amplifier. In the motor model the motor constant 'K_r' is the proportional gain. The motor and the mechanics are connected by a fixed transmission ratio 'i'. Due to the torque 'T_m' , generated by the motor, the mechanics will move the load. A position sensor measures the position of the load 'x_p'. For the position sensor several devices can be used such as optical incremental encoders, resolvers and optical sinewave encoders. As the position signal of the sensor is used for digital signal processing, the output signal 'x_{enc}' is expressed in increments. The data processing time in the position sensor is neglected. If an encoder is used which has a considerable processing time in relation to the sample time of the digital controller, this value can be modelled as an additional calculation delay in the controller. The position information is fed back to the controller. The controller now compares the actual position with the desired one and generates the new control signal 'u_p'.

To design a controller, a model of the motor with mechanics is needed. If we assume that the motor and the load are infinitely stiff connected, the motor and the load can be seen as one total mass. The mechanical friction in the bearings has been ignored as well. The resulting model of the motor with load is shown in Fig. 2.2 .
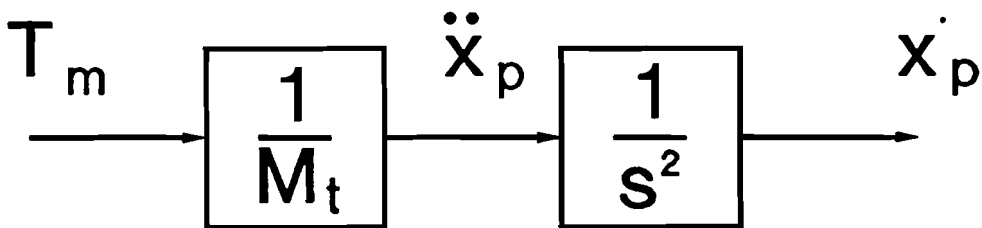
Fig. 2.2 : Second Order Model of Motor with Load

A differential equation for this simple configuration with only inertia forces is derived using the law of Newton.

$$T_m = M_t \ddot{x}_p \tag{2.1}$$

'M_t' can be considered as a converted inertia. This equation results in the following transfer function :

$$P(s) = \frac{x_p}{T_m} = \frac{1}{M_t s^2} = \frac{K_o}{s^2} \qquad with \quad K_o = \frac{1}{M_t} \tag{2.2}$$

7

A better model of the servo system is obtained when the motor and the load are not considered as one total mass. Fig. 2.3 depicts how this connection between the motor and the load can be modelled. The spring represents the mechanical stiffness, 'c', between the rotor and the load. The damper 'd_1' represents the mechanical damping between rotor and load. Finally, the dampers 'd_2' and 'd_3' represent the friction in the bearings between the load respectively the rotor and the stator.
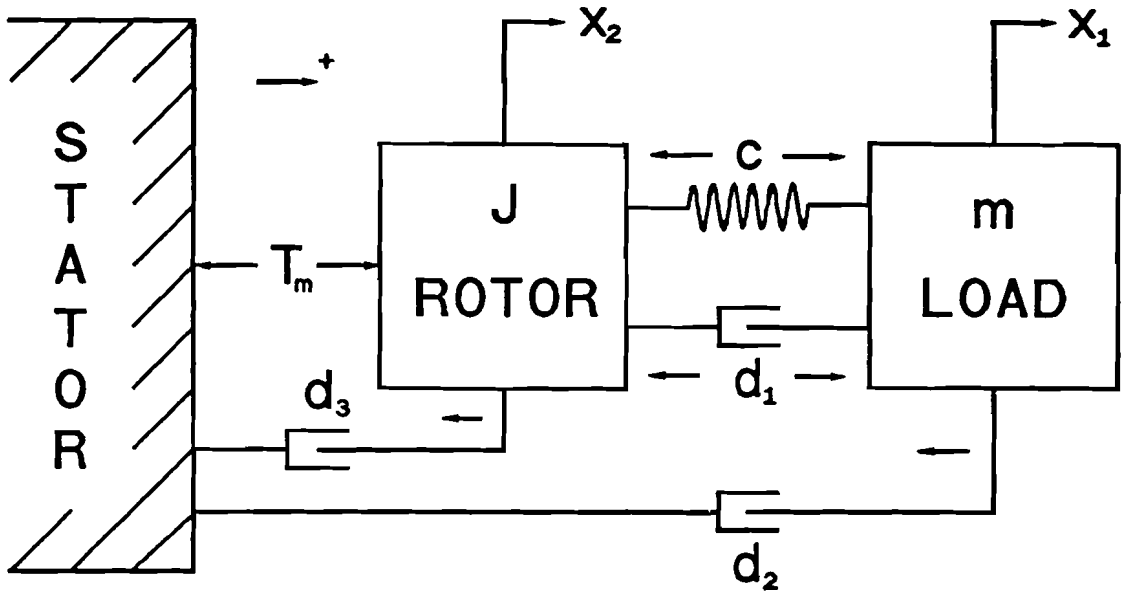
Fig. 2.3 : Model with Friction, Mechanical Damping and Stiffness

The equations of the forces in Fig. 2.3 are given by :

$$F_{spring} - c(ix_2 - x_1)$$

$$F_{damper_1} - d_1(i\dot{x}_2 - \dot{x}_1)$$

$$F_{damper_2} - -d_2\dot{x}_1$$

$$F_{damper_3} - -d_3 i\dot{x}_2$$

(2.3)

In Fig. 2.3 the angle of the rotor is called 'x_2'. The position of the mass 'm' is called 'x_1' which is equal to 'x_p' in the second order model. The motor torque 'T_m' is given by :

$$T_m - K_r * u_p$$

(2.4)

8

The constant 'K$_r$' is the motor constant. The control signal 'u$_p$', send by the controller, is the input signal of the motor. Fig. 2.4 depicts a blockscheme of Fig. 2.3 .

Fig. 2.4 : Blockscheme of Fourth Order Servo Model

For the mechanical model of Fig. 2.3 , two linear differential equations can be derived. One for the torques which act upon the rotor and one for the forces which act upon the load. The differential equations are given by :

$$Force \quad : \Sigma F_m - m\ddot{x}_1$$

$$with \quad \Sigma F_m - F_{spring} + F_{damper_1} + F_{damper_2}$$

(2.5a)

and

$$Torque \quad : \Sigma T_m - J\ddot{x}_2$$

$$with \quad \Sigma T_m - K_r u_p - iF_{spring} - iF_{damper_1} + iF_{damper_3}$$

(2.5b)

The first differential equation is derived by substitution of 2.3 in 2.5a :

$$m\ddot{x}_1 - c(ix_2 - x_1) + d_1(i\dot{x}_2 - \dot{x}_1) - d_2\dot{x}_1$$

(2.6)

Substitution of 2.3 in 2.5b yields the second differential equation :

$$J\ddot{x}_2 - K_r u_p - ic(ix_2 - x_1) - id_1(i\dot{x}_2 - \dot{x}_1) - id_3 i\dot{x}_2$$

(2.7)

9

Using the Laplace transformation, Eq. 2.6 and 2.7 become :

$$mx_1s^2 = c(ix_2-x_1)+d_1s(ix_2-x_1)-d_2x_1s$$

$$Jx_2s^2 = K_ru_p-ic(ix_2-x_1)-id_1s(ix_2-x_1)-i^2d_3x_2s$$

(2.8)

Elimination of 'x$_2$' results now in the final transfer function from the control signal 'u$_p$' to the position of the load 'x$_1$' :

$$P(s) = \frac{x_1}{u_p} = \frac{\frac{K_ri}{Jm}(c+d_1s)}{s^4+\left(\frac{d_1+d_2}{m}+\frac{i^2(d_1+d_3)}{J}\right)s^3+\left(\frac{c}{m}+\frac{i^2(d_1d_2+d_1d_3+d_2d_3)}{Jm}+\frac{ci^2}{J}\right)s^2+\left(\frac{ci^2(d_2+d_3)}{Jm}\right)s}$$

(2.9)

The derived transfer function contains a large number of parameters and is rather complex. We can reduce the transfer function P(s) by assuming that the friction in the bearings between the load respectively the rotor and the stator can be neglected compared to the mechanical damping between the rotor and the load. This results in the following transfer function :

$$P(s) = \frac{x_1}{u_p} = \frac{\frac{K_ri}{Jm}(c+d_1s)}{s^2\left[s^2+\left(\frac{d_1i^2}{J}+\frac{d_1}{m}\right)s+\left(\frac{ci^2}{J}+\frac{c}{m}\right)\right]}$$

(2.10)

We can rewrite the transfer function given by 2.10 in a more compact form by defining the following variables :

$$K_o = \frac{K_ri}{J+mi^2} \quad , \quad \omega_o = \sqrt{\frac{J+mi^2}{Jm}c} \quad , \quad \beta_o = \frac{d_1}{2}\sqrt{\frac{J+mi^2}{Jmc}}$$

(2.11)

The constant 'K_o' is a gain factor. The parameter 'ω_o' is the natural angular frequency due to the finite stiffness of the mechanics and 'β_o' is the servo damping ratio. The compact transfer function with the variables defined in 2.16 is now given by :

$$P_o(s) = \frac{K_o \left(2\beta_o \omega_o s + \omega_o^2 \right)}{s^2 \left(s^2 + 2\beta_o \omega_o s + \omega_o^2 \right)} \qquad (2.12)$$

To illustrate the form of the transfer function $P_o(s)$, Fig. 2.5 depicts the Bode plots of $P_o(s)$ for $K_o = 1$, $\omega_o = 1$ rad/s, and $\beta_o = 0.01$. The resonance peak of the servo system is clearly visible. This peak is characterized by the variables 'ω_o' and 'β_o', which are highly depending on the mass of the load 'm' and the mechanical stiffness 'c'.
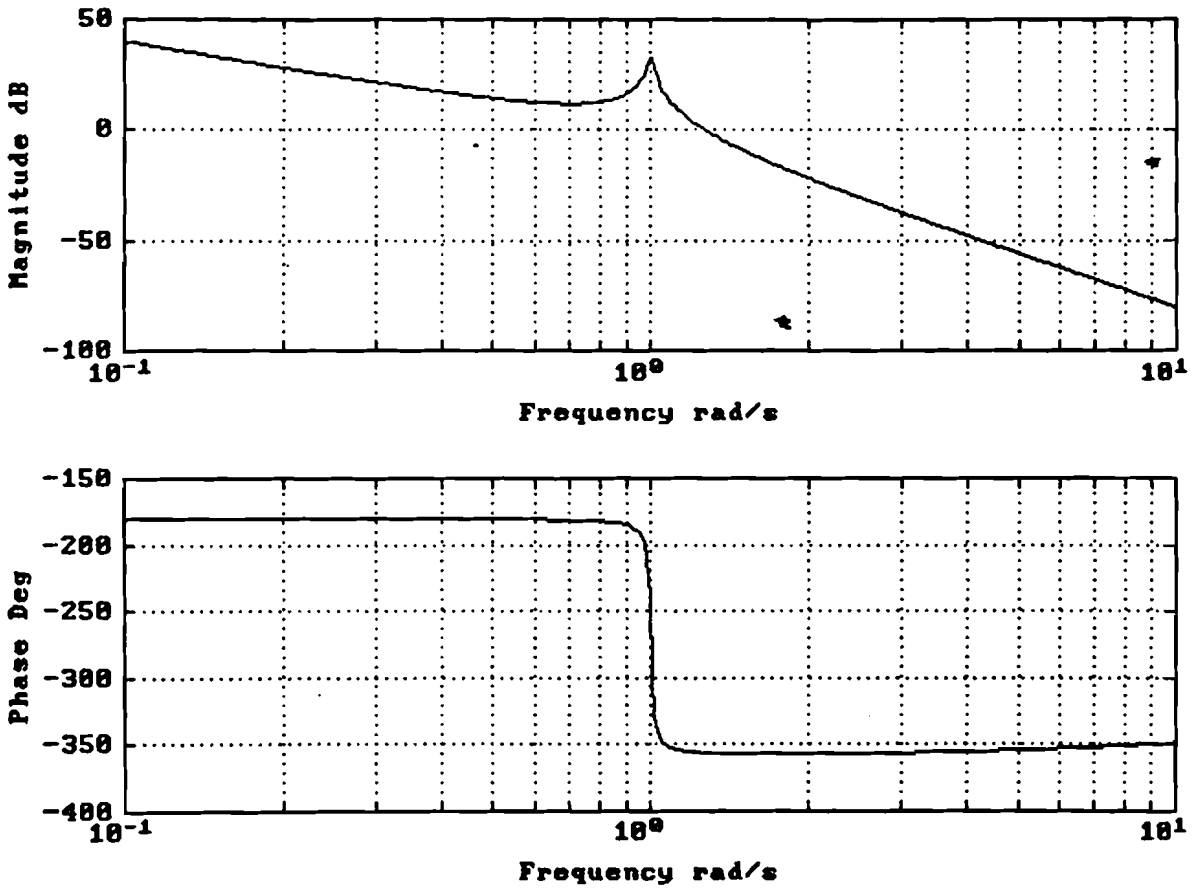

Fig. 2.5 : Bode Plots of $P_o(s)$

11

3 The H∞ Theory

3.1 Introduction

With the knowledge of the process described in Chapter 2, we can design a controller. Our goal is to design a robust controller for an electromechanical servo system with one dominant mechanical resonance frequency. A system is called robust if it maintains certain properties in spite of plant perturbations. First of all it is necessary to know which control system properties need to be maintained in spite of plant changes. The robustness can be divided into stability robustness and performance robustness. Stability robustness is a fundamental robustness property. It expresses that the closed-loop system remains stable in spite of plant changes. Performance robustness ensures that the response of the closed-loop system to important inputs, in particular command and disturbance inputs, remains acceptable in spite of plant changes. Secondly, it is necessary to specify against what range of plant variations the control system is required to be robust. For this purpose the H∞ theory is selected, because it is possible to specify robustness criteria as well as performance criteria. In H∞ optimal control a symbiosis of 'classical' and 'modern' control theory seems to be achieved : 'classical' control system design objectives such as robustness, are defined in terms of an H∞ optimization problem and a solution is obtained via fairly standard modern linear multivariable control techniques.

This chapter describes now the method for designing robust multivariable feedback control with H∞ synthesis. First of all we will give a short historical description on the the H∞ control theory. The choice of the solution method will be explained as well. In Section 3.3 the H∞ standard problem is introduced because many control problems can be reduced to a similar problem where the H∞ criterion will have the same form. Finally the solution method is described in more details.

3.2 A Short Historical Description on the H∞ Theory

Frequency domain feedback design goes back to the work of Nyquist in the 1930s. His and Bode's work led to what is nowadays referred to as 'classical' control. In the 1940s Wiener's work was directed towards optimal filtering, where for the first time stochastic processes and an optimization criterion where used for design purposes. During the 1950s the study of optimization in control theory led in the early 1960s to the work of Kalman: LQG optimal control and related subjects. The new theory based on time domain models and tools (the state-space approach to systems and control) was paramount in control theory during the 1960s and 1970s. Those who where opposed to LQG optimal control generalized classical frequency domain techniques to multivariable systems.

At the end of the 1970s it became clear that LQG control cannot cope with model

uncertainties, so that robustness could not be guaranteed. The white noise assumption in LQG also was not always the right way to represent disturbances. The study of robust control problems took control theory in the early 1980s back to the frequency domain. The work of Zames was the beginning of the H_∞ optimal control era. The mathematical and practical challenge of H_∞ optimization is generally recognized.

The first contributions to the H_∞ optimal control literature considered sensitivity minimization problems. In Kwakernaak [17] it was recognized that H_∞ optimal sensitivity controllers suffer from two important drawbacks. Firstly, the optimal controllers were generally improper, and therefore needed to be truncated at high frequencies to yield suboptimal physically realizable proper controllers. Secondly, robustness and other important control system properties, such as bandwidth and input power constraints, were not taken into account. Thus a frequency weighted combination of the sensitivity and the complementary sensitivity (or the control sensitivity) was considered, for which an H_∞ optimal solution was derived in terms of solutions to polynomial equations. Doyle introduced the "standard" H_∞ control design problems. This formulation is adopted in most publications on H_∞ optimal control. In Francis [9] a factorization approach to the solution of H_∞ optimal control problems is given. This method, however, suffered from severe cancellation problems. Kwakernaak solved the "standard" problem polynomially ; this method, however, also introduced spurious factors which cause the same delicate cancellation problems. In Boekhoudt [2] this cancellation phenomenon is avoided. In Appendix C the method to solve the "standard" H_∞ optimization problem via a polynomial approach is discussed shortly.

More recent publications give substantial simplifications and improvements of earlier methods. The latest solution method of the H_∞ optimization problem using the state-space approach is described by K. Glover and J.C. Doyle [12]. This characterization involves only the solution to two algebraic Riccati equations, each with the same order as the system, and further gives feasible controllers also with this order. The polynomial approach has no such explicit solution, and involves complicated matrix fraction conversions to derive a set of polynomial matrix equations. After converting these equations to algebraic equations, by equating coefficients of like powers, a solution is found through iteration by decreasing λ (scaling factor) gradually starting at ∞. The optimal solution using the state-space approach can be found through iteration by finding the minimal γ (scaling factor) for which a solution exists. Because it is much easier to implement the state-space approach (PC-Matlab, Robust Control Toolbox, 'hinfkgjd' procedure), together with a substantial reduction in computation and the explicitness of the formulas of Glover and Doyle, are the main reasons for using these formulas to solve the H_∞ control problem.

3.3 The H_∞ Standard Problem

Many control problems can be reduced to a similar problem, where the H_∞ criterion will have the same form. Therefore the standard problem is introduced. Suppose we have a MIMO - System, with transfer matrix G. The input and output signals 'w', 'u', 'z' and 'y' are defined as follows :

w(t)　　: exogeneous input　　e.g. command, disturbance inputs
u(t)　　: control input　　　　e.g. controller output
z(t)　　: output to be controlled　e.g. error, process input signal
y(t)　　: measured output　　　e.g. process output, reference signal
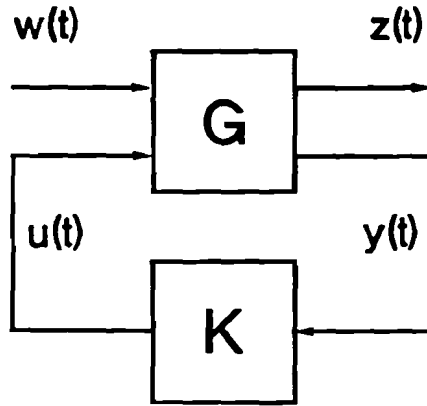
Fig. 3.1 : The Standard Problem

G can be partitioned as follows :

$$G - \begin{pmatrix} G_{11} & G_{12} \\ G_{21} & G_{22} \end{pmatrix} \qquad (3.1)$$

so the algebraic equations become :

$$z - G_{11}w + G_{12}u$$

$$y - G_{21}w + G_{22}u$$

$$u - Ky \qquad (3.2)$$

$$z - M_k w$$

The partitioning of G corresponds to the partitioning of the inputs and outputs.
　The transfer matrix M_k from 'w' to 'z' is now a linear fractional transformation matrix of K.

$$z - M_k w - \left[G_{11} + G_{12} K (I - G_{22} K)^{-1} G_{21} \right] w \qquad (3.3)$$

14

M_k is the closed-loop transfer function matrix from the external input 'w' to the controlled output 'z'. The problem is to minimize the H_∞ - norm of the transfer matrix M_k over all stabilizing controllers K_{st} which results in the following criterion :

$$\alpha := \inf_{K_{st}} \left[\sup_{w \in L_2} \frac{\| z \|_2}{\| w \|_2} \right] = \inf_{K_{st}} \| M_k \|_\infty \qquad (3.4)$$

The H_∞ - norm of M_k is defined as :

$$\| M_k \|_\infty := \sup_{w \in \mathbf{R}} \| M_k \|_2 = \sup_{w \in \mathbf{R}} (\sigma_{max} (M_k)) \qquad (3.5)$$

where $\| M_k \|_\infty = \sigma_{max} (M_k)$ denotes the largest singular value of the matrix M_k (square root of the largest eigenvalue of $M_k^* M_k$).

The standard problem is now defined as follows :

Standard Problem : Find a real rational proper controller K to minimize the H_∞ - norm of the transfer matrix M_k from 'w' to 'z' under the constraint that K stabilizes G :

$$\alpha := \inf_{K_{st}} \| G_{11} + G_{12} K (I - G_{22} K)^{-1} G_{21} \|_\infty$$

3.4 A State - Space Approach

In this section we discuss the state-space approach to H_∞ optimization described by K. Glover and J.C. Doyle [12]. Let a linear system be described by the following state equation :

$$\dot{x}(t) = Ax(t) + B_1 w(t) + B_2 u(t)$$

$$z(t) = C_1 x(t) + D_{11} w(t) + D_{12} u(t) \qquad (3.6)$$

$$y(t) = C_2 x(t) + D_{21} w(t) + D_{22} u(t)$$

The signals are defined as follows :

$w(t) \in \mathbb{R}^{m_1}$: The exogeneous input vector.

$u(t) \in \mathbb{R}^{m_2}$: The control input vector.

$z(t) \in \mathbb{R}^{p_1}$: The output control vector.

$y(t) \in \mathbb{R}^{p_2}$: The measured output vector.

$x(t) \in \mathbb{R}^{n}$: The state vector.

Any frequency - dependent weights are included in this model. The transfer function can be denoted as :

$$G(s) = \begin{pmatrix} G_{11} & G_{12} \\ G_{21} & G_{22} \end{pmatrix} = \begin{bmatrix} D_{11} & D_{12} \\ D_{21} & D_{22} \end{bmatrix} + \begin{bmatrix} C_1 \\ C_2 \end{bmatrix} (sI - A)^{-1} [\, B_1 \quad B_2 \,] \qquad (3.7)$$

The corresponding Rosenbrock state-space matrix is :

$$\left[\begin{array}{c|cc} A & B_1 & B_2 \\ \hline C_1 & D_{11} & D_{12} \\ C_2 & D_{21} & D_{22} \end{array} \right] =: \left[\begin{array}{c|c} A & B \\ \hline C & D \end{array} \right] \qquad (3.8)$$

For a linear controller with transfer function K(s), connected from 'y' to 'u', the closed-loop transfer function M_k is already described in section 3.3 .

The state-space approach described by K. Glover and J.C. Doyle [12] involves only the solution to two algebraic Riccati equations, each with the same order as the system, and further gives feasible controllers also with this order. Given a state-space characterization of all stabilizing controllers $K_{st}(s)$ such that

$$| M_k(G, K_{st}) |_\infty < \gamma \qquad (3.9)$$

where γ is the H_∞ - norm of the transfer matrix $M(G, K_{st})$ and the optimal solution is defined by $\alpha = \min(\gamma)$ (Eq. 3.4) , the following conditions must be satisfied :

1) (A, B_2) is stabilizable and (A, C_2) is detectable. This is required for the existence of a stabilizing K_{st} . If the state matrix A contains unstable poles, these poles have to be stabilizable and detectable otherwise no stabilizing solution exists.

16

2) rank(D_{12}) = m_2 , rank(D_{21}) = p_2 . This is sufficient to ensure that the controllers are proper. Otherwise the controllers might become improper which makes truncation at high frequencies necessary to obtain suboptimal physically realizable proper controllers.

3) A scaling of 'u' and 'y', together with a unitary transformation of 'w' and 'z', enables us to assume without loss of generality :

$$
D_{12} - \begin{bmatrix} 0 \\ I \end{bmatrix} \quad , \quad D_{21} - \begin{bmatrix} 0 & I \end{bmatrix} \quad , \quad D_{11} - \begin{bmatrix} D_{11,11} & D_{11,12} \\ D_{11,21} & D_{11,22} \end{bmatrix} \begin{matrix} \updownarrow p_1 - m_2 \\ \updownarrow m_2 \end{matrix}
$$
$$
\underset{m_1 - p_2 \quad \quad p_2}{}
$$

This is necessary for the derivation of the formulas.

4) $D_{22} = 0$ (This condition will be removed later).

The final assumptions ensure that the solution to the corresponding LQG problem is closed-loop asymptotically stable.

5)
$$
rank \begin{pmatrix} A - j\omega I & B_2 \\ C_1 & D_{12} \end{pmatrix} \begin{matrix} \updownarrow n \\ \updownarrow p_1 \end{matrix} - n + m_2 \quad \quad \forall \omega \in \mathbf{R}
$$
$$
\underset{n \quad \quad m_2}{}
$$

which implies : 1) No zeros on the $j\omega$-axis.
2) $p_1 \geq m_2$.

6)
$$
rank \begin{pmatrix} A - j\omega I & B_1 \\ C_2 & D_{21} \end{pmatrix} \begin{matrix} \updownarrow n \\ \updownarrow p_2 \end{matrix} - n + p_2 \quad \quad \forall \omega \in \mathbf{R}
$$
$$
\underset{n \quad \quad m_1}{}
$$

which implies : 1) No zeros on the $j\omega$-axis.
2) $m_1 \geq p_2$.

The solution to the algebraic Riccati equation (ARE) :

$$
A^* X + X A - X P_r X + Q_r - 0 \tag{3.10}
$$

17

will be denoted via its Hamiltonian matrix, as :

$$X - Ric \begin{pmatrix} A & -P_r \\ -Q_r & -A^* \end{pmatrix} \quad , \quad P_r - P_r^* \quad , \quad Q_r - Q_r^* \tag{3.11}$$

where this implies that $X = X^*$ and

$$\begin{pmatrix} A & -P_r \\ -Q_r & -A^* \end{pmatrix} \begin{pmatrix} I \\ X \end{pmatrix} - \begin{pmatrix} I \\ X \end{pmatrix} (A - P_r X) \tag{3.12}$$

$$Re \ \lambda_i (A - P_r X) < 0 \tag{3.13}$$

Now define

$$R - D_{1.}^* D_{1.} - \begin{pmatrix} \gamma^2 I_{m_1} & 0 \\ 0 & 0 \end{pmatrix} \tag{3.14}$$

where $D_{1.} - [\ D_{11} \ D_{12} \ ]$, and

$$\tilde{R} - D_{.1} D_{.1}^* - \begin{pmatrix} \gamma^2 I_{p_1} & 0 \\ 0 & 0 \end{pmatrix} \tag{3.15}$$

where $D_{.1} - \begin{bmatrix} D_{11} \\ D_{21} \end{bmatrix}$.

X_∞ and Y_∞ are now defined as solutions to the following algebraic Riccati equations :

$$X_\infty - Ric \left\{ \begin{pmatrix} A & 0 \\ -C_1^* C_1 & -A^* \end{pmatrix} - \begin{pmatrix} B \\ -C_1^* D_{1.} \end{pmatrix} R^{-1} [\ D_{1.}^* C_1 \ B^* \ ] \right\}$$

$$- Ric \begin{pmatrix} A_{X_\infty} & -P_{X_\infty} \\ -Q_{X_\infty} & -A_{X_\infty}^* \end{pmatrix} - Ric (\ H_{X_\infty}) \tag{3.16}$$

18

$$Y_\infty = Ric \left\{ \begin{pmatrix} A^* & 0 \\ -B_1 B_1^* & -A \end{pmatrix} - \begin{pmatrix} C^* \\ -B_1 D_{.1}^* \end{pmatrix} \tilde{R}^{-1} \begin{bmatrix} D_{.1} B_1^* & C \end{bmatrix} \right\}$$

$$= Ric \begin{pmatrix} A_{Y_\infty} & -P_{Y_\infty} \\ -Q_{Y_\infty} & -A_{Y_\infty} \end{pmatrix} = Ric \left(H_{Y_\infty} \right)$$

(3.17)

and the 'state feedback' and 'output injection' (~ Kalman gain) matrices as :

$$F = \begin{pmatrix} F_{11} \\ F_{12} \\ F_2 \end{pmatrix} \begin{matrix} \updownarrow m_1 - p_2 \\ \updownarrow p_2 \\ \updownarrow m_2 \end{matrix} = -R^{-1} \begin{bmatrix} D_{.1}^* C_1 + B^* X_\infty \end{bmatrix}$$

(3.18)

$$H = \begin{bmatrix} H_{11} & H_{12} & H_2 \end{bmatrix} = - \begin{bmatrix} D_{.1}^* C_1 + Y_\infty C^* \end{bmatrix} \tilde{R}^{-1}$$

$$\qquad\quad \underset{p_1 - m_2}{\cdots} \quad \underset{m_2}{\cdots} \quad \underset{p_2}{\cdots}$$

(3.19)

For the system described by 3.6 and satisfying the assumptions 1-6 :

a) There exists an internally stabilizing controller $K_{st}(s)$ such that $\| M(G,K_{st}) \|_\infty < \gamma$ if and only if
i) $\gamma > \max \left(\bar{\sigma} \begin{bmatrix} D_{11.11} & D_{11.12} \end{bmatrix} , \bar{\sigma} \begin{bmatrix} D_{11.11}^* & D_{11.21}^* \end{bmatrix} \right)$ and
ii) there exists $X_\infty \geq 0$ and $Y_\infty \geq 0$ satisfying 3.16 and 3.17
$\Rrightarrow$ respectively and such that $\rho(X_\infty Y_\infty) < \gamma^2$
($\rho(.)$ denotes the largest eigenvalue)
b) Given that the conditions of part (a) are satisfied then all rational internally stabilizing controllers satisfying $\| M(G,K_{st}) \|_\infty < \gamma$ are given by $K_{st} = M(K_a,\varphi)$ for arbitrary $\varphi \in RH_\infty$ such that $\| \varphi \|_\infty < \gamma$.

where

$$K_a = \left[\begin{array}{c|cc} \hat{A} & \hat{B}_1 & \hat{B}_2 \\ \hline \hat{C}_1 & \hat{D}_{11} & \hat{D}_{12} \\ \hat{C}_2 & \hat{D}_{21} & 0 \end{array} \right]$$

(3.20)

19

$$\hat{D}_{11} - -D_{11,21}D_{11,11}^{\cdot}\left(\gamma^{2}I - D_{11,11}D_{11,11}^{\cdot}\right)^{-1}D_{11,12} - D_{11,22} \qquad (3.21)$$

and $\hat{D}_{12} \in \mathbf{R}^{m_2 \times m_2}$ and $\hat{D}_{21} \in \mathbf{R}^{p_2 \times p_2}$ are any matrices satisfying :

$$\hat{D}_{12}\hat{D}_{12}^{\cdot} - I - D_{11,21}\left(\gamma^{2}I - D_{11,11}^{\cdot}D_{11,11}\right)^{-1}D_{11,21}^{\cdot} \qquad (3.22)$$

$$\hat{D}_{21}^{\cdot}\hat{D}_{21} - I - D_{11,12}^{\cdot}\left(\gamma^{2}I - D_{11,11}D_{11,11}^{\cdot}\right)^{-1}D_{11,12} \qquad (3.23)$$

Further we have

$$\hat{B}_2 - \left(B_2 + H_{12}\right)\hat{D}_{12}$$

$$\hat{C}_2 - -\hat{D}_{21}\left(C_2 + F_{12}\right)Z$$

$$\hat{B}_1 - -H_2 + \hat{B}_2\hat{D}_{12}^{-1}\hat{D}_{11} \qquad (3.24)$$

$$\hat{C}_1 - F_2Z + \hat{D}_{11}\hat{D}_{21}^{-1}\hat{C}_2$$

$$\hat{A} - A + HC + \hat{B}_2\hat{D}_{12}^{-1}\hat{C}_1$$

where

$$Z - \left(I - \gamma^{-2}Y_{\infty}X_{\infty}\right)^{-1} \qquad (3.25)$$

Until now it was assumed that $D_{22} = 0$. Suppose K_{st} is a stabilizing controller for the case with D_{22} is set to zero and satisfying :

$$\left\| M_k\left(G - \begin{pmatrix} 0 & 0 \\ 0 & D_{22} \end{pmatrix}, K_{st}\right) \right\|_{\infty} < \gamma \qquad (3.26)$$

Then

$$M_k\left(G, K_{st}\left(I + D_{22}K_{st}\right)^{-1}\right) - G_{11} + G_{12}K_{st}\left(I + D_{22}K_{st} - G_{22}K_{st}\right)^{-1}G_{21}$$

$$- M_k\left(G - \begin{pmatrix} 0 & 0 \\ 0 & D_{22} \end{pmatrix}, K_{st}\right) \qquad (3.27)$$

Hence all controllers in this case are given by :

$$\tilde{K}_{s\!t} - K_{s\!t} \left(I + D_{22} K_{s\!t} \right)^{-1} \tag{3.28}$$

which leads to :

$$\tilde{K}_{s\!t} - M_k \left(\tilde{K}_a , \varphi \right) \quad \textit{for } \varphi \in \mathbf{RH}_\infty , \ \| \varphi \|_\infty < \gamma \tag{3.29}$$

where assuming that $\det \left(I + \hat{D}_{11} D_{22} \right) \neq 0$ and :

$$\tilde{K}_a - \left[\begin{array}{c|c} \hat{A} - \hat{B} \left(I - M_k \right) \hat{D}^{-1} \hat{C} & \hat{B} M_k \\ \hline \tilde{M}_k \hat{C} & \hat{D} M_k \end{array} \right] \tag{3.30}$$

with :

$$M_k - \left[I + \begin{pmatrix} D_{22} & 0 \\ 0 & 0 \end{pmatrix} \hat{D} \right]^{-1}$$

$$\tilde{M}_k - \left[I + \hat{D} \begin{pmatrix} D_{22} & 0 \\ 0 & 0 \end{pmatrix} \right]^{-1} \tag{3.31}$$

When $D_{22} \neq 0$ there is a possibility of the feedback system becoming ill-posed due to $\det \left(I + D_{22} K(\infty) \right) - 0$. Such possibilities need to be excluded from the above parametrization.

4 Application of H_∞ Control

4.1 Introduction

This chapter describes the basic design considerations together with the control system. To design a controller with the aid of the H_∞ theory, which is robust with respect to stability and performance , a computer program has been developed (implemented in PC-Matlab using the 'hinfkgjd' procedure in the Robust Control Toolbox as basic). This program is menu-structured through which it's easy to enter variables, calculate the controller and check the results afterwards [8]. Finally the unmodelled dynamics are specified, including the robustness description and the range of plant variations for which the control system is required to be robust, together with the design goals.

The design is focused on two different goals. The first goal (constraint) is to design a controller which is robust for a certain range of plant variations. The second goal (objective) is to optimize the signal tracking performance.

4.2 Two-Degree-of-Freedom Problem

To satisfy the goals with respect to robustness and performance in an optimal way, we have chosen to use a two-degree-of-freedom configuration, with a feed-forward and a feed-back controller, as depicted in Fig. 4.1 .
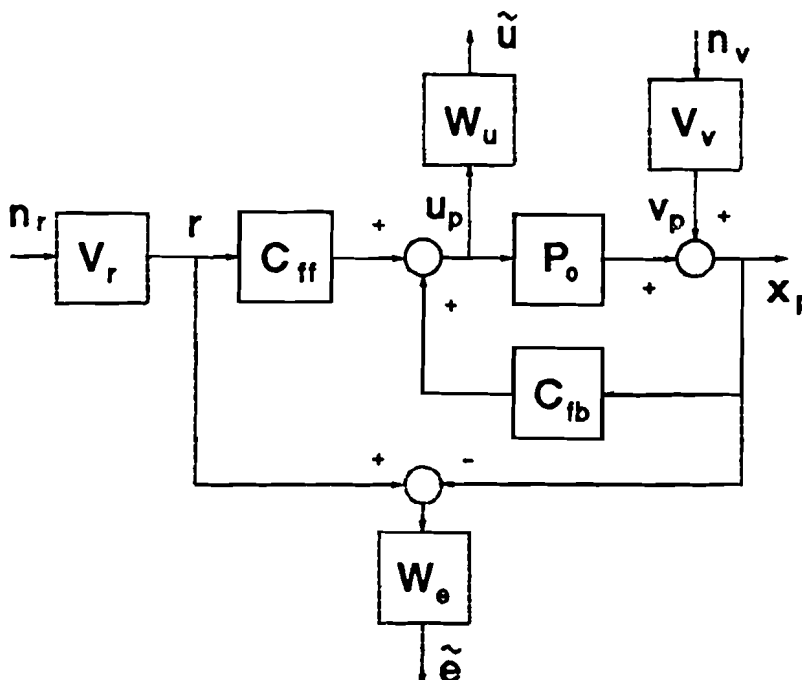

Fig. 4.1 : Two-Degree-of-Freedom Configuration

The robustness and performance optimization are opposite criteria. Using the two-degree-of-freedom configuration we have an extra degree of freedom in the design (C_{ff} , instead of only C_{fb}) to optimize the trade off between robustness and performance. The solid lines are the basic controller system including the electromechanical process. To be able to apply the H_∞ theory, we added the dashed lines, consisting of the shaping and weighting filters.

The two-degree-of-freedom problem is a multiple-input multiple-output (MIMO) configuration. The filters (boxes) in Fig. 4.1 , however, are single-input single-output (SISO) transfer functions which are defined in more detail in Table 4.1 .

Table 4.1 : Two-Degree-of-Freedom Filters
(All filters are SISO transfer functions. For the ease of notation the Laplace operator 's' is omitted.)

Filter	Description
P_o	Nominal process
V_v	Shaping model disturbances
V_r	Shaping reference signal
W_e	Weighting error signal
W_u	Weighting process input signal
C_{fb}	Feed-back controller
C_{ff}	Feed-forward controller

The shaping filters (V_r and V_v) can be used to model the exogeneous inputs (command input 'n_r' and disturbance input 'n_v'). With the weighting filters (W_e and W_u) we can weigh the controlled outputs (error signal 'e' and process input 'u_p') in the frequency domain. This is necessary to obtain a predefined behaviour of the several transfer functions which will be explained in more details in the following chapters.

We wish to optimize the closed-loop system response to the reference input 'r' and the disturbance input 'v_p' . The signal tracking error is defined as : $e = r - x_p$. The output signal 'x_p' has to follow the reference signal 'r', where 'r' is a unknown fixed signal, but is modelled as belonging to a class of signals θ satisfying :

$$\theta = \left\{ r : r = V_r n_r \text{ for some } n_r \in L_2 \text{ , } \| n_r \|_{L_2} < 1 \right\} \qquad (4.1)$$

Likewise 'r' , we define now the disturbance 'v_p' :

$$\phi = \left\{ v_p : v_p = V_v n_v \ \ for \ some \ \ n_v \in L_2 , \left| n_v \right|_{L_2} < 1 \right\} \tag{4.2}$$

'n_r' and 'n_v' are the two components of the exogeneous input 'w' and V_r and V_v are the corresponding shaping filters.

$$w = \begin{pmatrix} n_v \\ n_r \end{pmatrix} \tag{4.3}$$

Furthermore we choose the components of the control output 'z' as :

$$z = \begin{pmatrix} \tilde{e} \\ \tilde{u} \end{pmatrix} = \begin{pmatrix} W_e \left(r - x_p \right) \\ W_u \, u_p \end{pmatrix} \tag{4.4}$$

where W_e and W_u are the frequency dependent weighting filters, 'x_p' is the plant output and 'u_p' is the plant input. Thus, '$\tilde{e}$' is the weighted signal tracking error and '$\tilde{u}$' the weighted plant input. From Eq. 4.2 and

$$x_p = v_p + P_o \, u_p = V_v \, n_v + P_o \, u_p \tag{4.5}$$

it follows from Eq. 4.4 that :

$$z = \begin{pmatrix} \tilde{e} \\ \tilde{u} \end{pmatrix} = \begin{pmatrix} W_e \left(V_r \, n_r - V_v \, n_v - P_o \, u_p \right) \\ W_u \, u_p \end{pmatrix} \tag{4.6}$$

The components 'r' and 'x_p' of the observed output 'y' are defined as :

$$y = \begin{pmatrix} x_p \\ r \end{pmatrix} = \begin{pmatrix} V_v \, n_v + P_o \, u_p \\ V_r \, n_r \end{pmatrix} \tag{4.7}$$

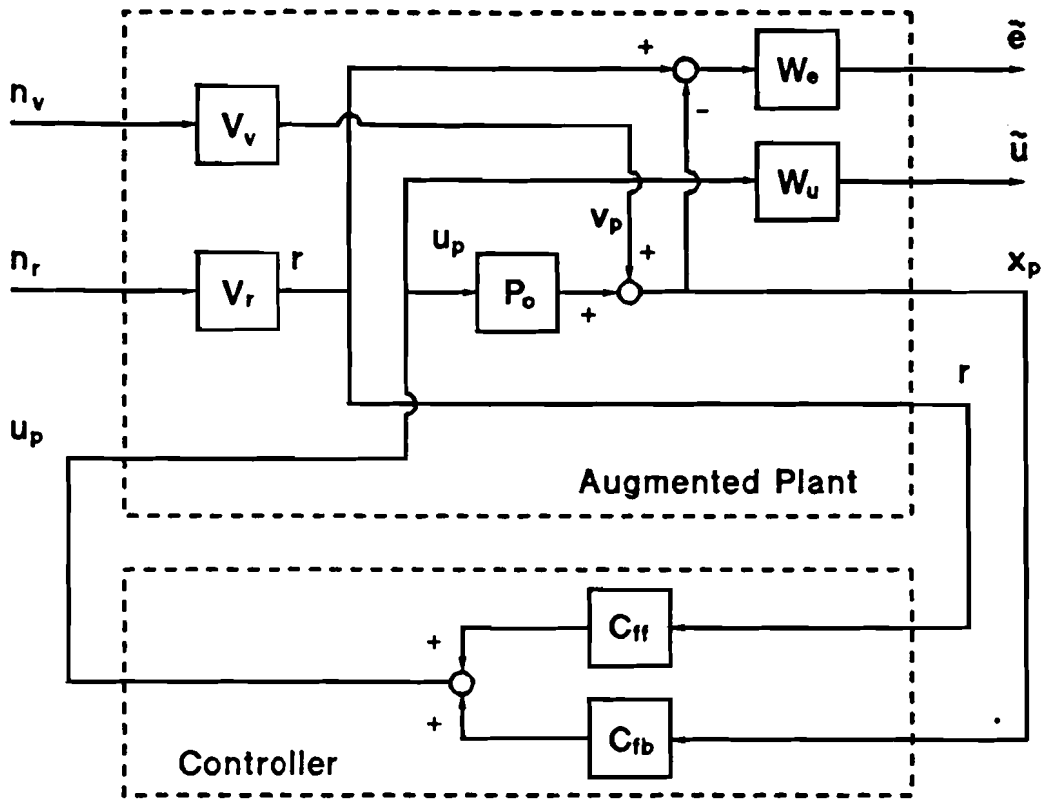Finally, the control input is of course the plant input 'u_p' .

Fig. 4.2 : Two-Degree-of-Freedom Configuration in "Standard" Form

Fig. 4.2 depicts the two-degree-of-freedom configuration in "standard" form (Section 3.3). It follows, after combining the various relations, that in terms of the "standard" H_∞ optimization problem we have :

$$
\begin{pmatrix} z \\ y \end{pmatrix} = \begin{pmatrix} \tilde{e} \\ \tilde{u} \\ \hline x_p \\ r \end{pmatrix} = \left(\begin{array}{cc|c} -W_e V_v & W_e V_r & -W_e P_o \\ 0 & 0 & W_u \\ \hline V_v & 0 & P_o \\ 0 & V_r & 0 \end{array} \right) \begin{pmatrix} n_v \\ n_r \\ \hline u_p \end{pmatrix}
$$

(4.8)

$$
= \left(\begin{array}{c|c} G_{11} & G_{12} \\ \hline G_{21} & G_{22} \end{array} \right) \begin{pmatrix} w \\ u \end{pmatrix} = G \begin{pmatrix} w \\ u \end{pmatrix}
$$

25

$$u - u_p - \left(C_{fb} \mid C_{ff} \right) \begin{pmatrix} x_p \\ r \end{pmatrix} - K_x \left(y \right) \qquad (4.9)$$

Table 4.2 :   State-space Representation Filters
(Observer Canonical Form)

Filter	State-space Representation
P_o , V_v	$\dot{x}_{P_o} - A_p x_{P_o} + B_p u_p + B_v n_v$ $x_p - C_p x_{P_o} + D_p u_p + D_v n_v$
V_r	$\dot{x}_{V_r} - A_r x_{V_r} + B_r n_r$ $r - C_r x_{V_r} + D_r n_r$
W_e	$\dot{x}_{W_e} - A_e x_{W_e} + B_e e$ $\tilde{e} - C_e x_{W_e} + D_e e$
W_u	$\dot{x}_{W_u} - A_u x_{W_u} + B_u u_p$ $\tilde{u} - C_u x_{W_u} + D_u u_p$

In this state-space realization it is assumed that the process P_0 and the model disturbance filter V_v have the same poles. Using an observer canonical form as state-space representation implies that the states of two transfer functions with the same poles will be the same. In our situation this makes a reduction of the number of states of the augmented plant G possible because of $A_v = A_p$ and $C_v = C_p$. The purpose of this assumption will be explained in Section 4.4 .

Combining the state-space representations of the filters in Table 4.2 in terms of the H_∞ standard problem with the state, input and output vectors defined as :

$$states : \begin{pmatrix} x_{P_o} \\ x_{V_r} \\ x_{W_e} \\ x_{W_u} \end{pmatrix} , \; inputs : \begin{pmatrix} w \\ u \end{pmatrix} - \begin{pmatrix} n_v \\ n_r \\ \hline u_p \end{pmatrix} , \; outputs : \begin{pmatrix} z \\ y \end{pmatrix} - \begin{pmatrix} \tilde{e} \\ \tilde{u} \\ \hline x_p \\ r \end{pmatrix} \qquad (4.10)$$

26

results in the following state-space representation of the augmented plant :

$$G(s) = \begin{bmatrix} D_{11} & D_{12} \\ D_{21} & D_{22} \end{bmatrix} + \begin{bmatrix} C_1 \\ C_2 \end{bmatrix} (sI - A)^{-1} [B_1 \ B_2]$$

$$\overset{s}{=} \left[\begin{array}{c|cc} A & B_1 & B_2 \\ \hline C_1 & D_{11} & D_{12} \\ C_2 & D_{21} & D_{22} \end{array} \right] \tag{4.11}$$

$$= \left[\begin{array}{cccc|cc|c} A_p & 0 & 0 & 0 & B_v & 0 & B_p \\ 0 & A_r & 0 & 0 & 0 & B_r & 0 \\ -B_e C_p & B_e C_r & A_e & 0 & -B_e D_v & B_e D_r & -B_e D_p \\ 0 & 0 & 0 & A_u & 0 & 0 & B_u \\ \hline -D_e C_p & D_e C_r & C_e & 0 & -D_e D_v & D_e D_r & -D_e D_p \\ 0 & 0 & 0 & C_u & 0 & 0 & D_u \\ \hline C_p & 0 & 0 & 0 & D_v & 0 & D_p \\ 0 & C_r & 0 & 0 & 0 & D_r & 0 \end{array} \right]$$

where 's' denotes the Laplace operator.

A last remark about the design of the shaping and weighting filters affecting the state-space realization in Eq. 4.11 . In Section 3.4 we mentioned a few conditions which must be satisfied to ensure that a solution exists. We will first derive now the design specifications to satisfy these conditions.

1) The requirement that (A,B_2) is stabilizable and (A,C_2) is detectable is obvious. The augmented plant is stabilizable and detectable if every eigenvalue greater than or equal to zero is controllable respectively observable. Assuming that the shaping and weighting filters are stable (eigenvalues less than zero), the only unstable eigenvalues are the two poles of the process in the origin. Both poles are controllable and observable in our system satisfying condition 1.

2) The rank conditions on the matrices D_{12} and D_{21} can be satisfied by designing the filters V_v , V_r and W_u biproper. Because our process is proper ($D_p = 0$) it is necessary that the process input weighting filter W_u is biproper, otherwise matrix D_{12} has less than full rank. The same

is true for D_{21}. In this situation the D matrices of the filters exist and the condition of full rank is satisfied.

3) The scaling of 'u' and 'y' and the unitary transformation of 'w' and 'z' can be carried out without loss of generality. The scaling of 'u' and 'y' only implies that the inputs and outputs of the controllers have different units and the input output behaviour of the controller remains the same under these scalings and so does the transfer from 'w' to 'z'. The unitary scaling of 'w' and 'z' may be carried out without loss of generality since the ∞ - norm is invariant under unitary transformations. The scaling and unitary transformation is directly implemented in the existing Matlab procedure.

4) The assumption that $D_{22} = 0$ can be removed without loss of generality (Only some possibilities need to be excluded). However, because we are dealing with a proper process, this condition is automatically satisfied.

5,6) The final two conditions can be satisfied if there are no zeros on the $j\omega$-axis , $p_l \geq m_2$ (condition 5) and $m_1 \geq p_2$ (condition 6). Designing the shaping and weighting filters well, we can avoid zeros on the $j\omega$-axis. The other conditions are automatically satisfied because of the chosen augmented plant.

4.3 The Formulation of the Optimization Problem

The optimization problem is formulated in the H_∞ standard problem of Section 3.2 . Substitution of the transfer function matrix (Eq. 4.8) in the optimization problem, defined by :

$$\| M_k \|_\infty - \| G_{11} + G_{12} K_s (I - G_{22} K_s)^{-1} G_{21} \|_\infty \qquad (4.12)$$

results in :

$$\| M_k \|_\infty - \left\| \begin{matrix} M_{11} & M_{12} \\ M_{21} & M_{22} \end{matrix} \right\|_\infty$$

$$- \left\| \begin{matrix} -W_e(I-P_oC_{fb})^{-1}V_v & W_e[I-(I-P_oC_{fb})^{-1}P_oC_{ff}]V_r \\ W_uC_{fb}(I-P_oC_{fb})^{-1}V_v & W_u(I-P_oC_{fb})^{-1}C_{ff}V_r \end{matrix} \right\|_\infty \qquad (4.13)$$

The four sub-criteria are named in Table 4.3 .

Table 4.3 : H_∞ Optimization Criteria in a Two-Degree-of-Freedom Configuration

Criterion	Description	Weighting Function (scaled)	Transfer Function
$M_{11} - \dfrac{\tilde{e}}{n_v}$	*Disturbance Reduction*	$\dfrac{1}{\gamma}\,W_e\,V_v$	$-\left(I - P_o C_{fb}\right)^{-1}$
$M_{12} - \dfrac{\tilde{e}}{n_r}$	*Signal Tracking*	$\dfrac{1}{\gamma}\,W_e\,V_r$	$I - \left(I - P_o C_{fb}\right)^{-1} P_o C_{ff}$
$M_{21} - \dfrac{\tilde{u}}{n_v}$	*Model Robustness*	$\dfrac{1}{\gamma}\,W_u\,V_v$	$C_{fb}\left(I - P_o C_{fb}\right)^{-1}$
$M_{22} - \dfrac{\tilde{u}}{n_r}$	*Input Saturation*	$\dfrac{1}{\gamma}\,W_u\,V_r$	$\left(I - P_o C_{fb}\right)^{-1} C_{ff}$

In Eq. 3.9 γ has been defined as the upper bound of the ∞ - norm. If we scale the ∞ - norm to 1, γ becomes a scaling factor in the weighting functions (Table 4.3). It will be our goal to find a solution with $\gamma \le 1$, because in this situation the final transfer function of a criterion will be bounded by the inverse weighting function.

Without the scaling factor γ we might not find a solution for a certain choice of weighting functions. In this situation we don't know which criterion is the limiting function and also the frequency range where the limitation occurs is unknown. To avoid the problem of not knowing which filter has to be redesigned, γ is used as a scaling factor. By adjusting γ a solution is found for almost every choice of weighting functions. The H_∞ optimization problem can be reformulated as follows :

$$\left| \frac{1}{\gamma} M(G, K_{st}) \right| < 1 \qquad (4.14)$$

where every sub-criterion of $M(G, K_{st})$ consists of a scaled weighting function and a transfer function (Table 4.3). The weighting function can be designed as the inverse of the desired transfer function if a solution is found with $\gamma \le 1$.

4.4 Uncertainty Modelling
Stable Factor Perturbation

Designing a robust controller for a certain range of parameter variations implies the derivation of an uncertainty model. For this purpose we will consider stable factor perturbations [4,18,23]. In robust stability analysis, factor perturbation uncertainty allows a very general class of errors to be considered; more general than the corresponding classes allowed by additive or multiplicative models. Additive and multiplicative uncertainties are in fact a sub-set of stable factor perturbations. An immediate benefit of the factor perturbation uncertainty approach is that the uncertainty class is not restricted to perturbations which preserve the number of RHP poles of the plant. This enables a much greater confidence in the robust stability conditions obtained, as a wider class of perturbations is being considered [18].

Let P_o be the nominal model where we factorize

$$P_o - P_i P_s \qquad (4.15)$$

with P_i unstable (P_i^{-1} is stable) and P_s stable.
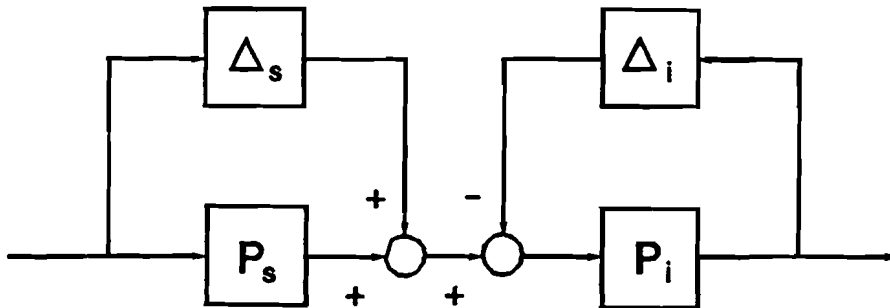

Fig. 4.2 : Factor Perturbation

We introduce now Δ_s to be the model error on the stable part P_s, defined as :

$$\tilde{P}_s - P_s + \Delta_s \qquad (4.16)$$

and Δ_i to be the model error on the inverse of the unstable part P_i, defined as :

$$\tilde{P}_i - P_i^{-1} + \Delta_i \qquad (4.17)$$

We can write the perturbed plant combining 4.16 and 4.17 as :

$$\tilde{P} = \left(P_i^{-1} + \Delta_i \right)^{-1} \left(P_s + \Delta_s \right) \qquad (4.18)$$

and we get a configuration as depicted in Fig. 4.2 . This factorization can be formulated in a more formal way as a left coprime factorization and we can give a robustness constraint by considering the H_∞-bounds of the perturbations on the coprime factors.

Considering the perturbed plant in Eq. 4.18 we have Δ_i and Δ_s as stable unknown functions (model uncertainties) with :

$$\left| \Delta_i \, W_i^{-1} \quad \Delta_s \, W_s^{-1} \right|_\infty < \epsilon \qquad , \qquad W_s \,, W_s^{-1} \,, W_i \,, W_i^{-1} \in \mathbf{RH}_\infty \qquad (4.19)$$

(W_s and W_i are known weighting functions) while K_{st} stabilizes the nominal plant P_o . The controller K_{st} will stabilize all perturbed plants $\tilde{P}$ if and only if [23] :

$$\left| \begin{array}{c} W_i \left(I - P_o K_{st} \right)^{-1} P_i \\ W_s K_{st} \left(I - P_o K_{st} \right)^{-1} P_i \end{array} \right|_\infty \leq \epsilon^{-1} \qquad (4.20)$$

So the optimization of the plant robustness with respect to stable factor perturbations is equal to :

$$\min_{K_{st}} \left| \begin{array}{c} W_i \left(I - P_o K_{st} \right)^{-1} P_i \\ W_s K_{st} \left(I - P_o K_{st} \right)^{-1} P_i \end{array} \right|_\infty \qquad (4.21)$$

Comparing the mentioned requirements with the optimization criteria formulated as a standard problem in Table 4.3 , it is easy to see that if we choose $V_v = P_i$, $W_u = W_s$ and $W_e = W_i$, then the optimization of the plant robustness with respect to stable factor perturbations is equal to the **Disturbance Reduction** and **Model Robustness** criterion formulated in Section 4.3 . Of course we lose some degrees of freedom by this choice of W_u and W_e , but solving the problem will become much easier.

We can rewrite the nominal and perturbed plant as follows by polynomials :

$$P_o = \frac{n_o}{d_o} = \frac{n_o}{d_s d_i} = P_s P_i = \frac{n_o}{d_s d_f} \frac{d_f}{d_i} \qquad (4.22)$$

31

$$\tilde{P} - \frac{n_o + \Delta_n}{d_o + \Delta_d} - \tilde{P}_s \tilde{P}_i - \left(P_s + \Delta_s \right) \left(P_i^{-1} + \Delta_i \right)^{-1}$$

$$- \left(\frac{n_o}{d_s d_f} + \Delta_s \right) \left(\frac{d_i}{d_f} + \Delta_i \right)^{-1} \tag{4.23}$$

where

$$\lambda \left(d_i \right) \in \mathbf{C}^+ \quad \rightarrow \quad d_i - s^2$$

$$\lambda \left(d_s \right) \in \mathbf{C}^- \quad \rightarrow \quad d_s - s^2 + 2\beta_o \omega_o s + \omega_o^2 \tag{4.24}$$

$$\lambda \left(d_f \right) \in \mathbf{C}^- \quad \rightarrow \quad d_f : \textit{Stable polynomial of } 2^{nd} \textit{ order}$$

We find now :

$$\Delta_s - \frac{\Delta_n}{d_s d_f} \quad , \quad \Delta_i - \frac{\Delta_d}{d_s d_f} \tag{4.25}$$

The derived descriptions of the uncertainties Δ_s and Δ_i can be used in the design of the weighting filter W_u respectively W_e . It follows from Eq. 4.19 :

$$\left| W_e^{-1} \Delta_i \quad W_u^{-1} \Delta_s \right|_{\mathbf{L}} < \epsilon \tag{4.26}$$

if $V_v = P_i$. The uncertainties are the lower bound descriptions of the corresponding weighting filters. Δ_s and Δ_i are known functions now and depend only on the disturbed part of the process , defined in Δ_n and Δ_d , and the design of disturbance filter V_v (numerator d_f).

4.5 Plant Perturbations

Continuing our design, we first have to derive the plant perturbations. Therefore we have to specify which process parameters can vary and the range of plant variations for which the controller is required to be robust. In Chapter 2 we derived a fourth order model of an electromechanical servo system :

$$P_o(s) - \frac{K_o \left(2\beta_o \omega_o s + \omega_o^2 \right)}{s^2 \left(s^2 + 2\beta_o \omega_o s + \omega_o^2 \right)} \tag{4.27}$$

with the variables K_o, ω_o and β_o defined as :

$$K_o - \frac{K_i}{J + mi^2} \quad , \quad \omega_o - \sqrt{\frac{J + mi^2}{Jm}c} \quad , \quad \beta_o - \frac{d_1}{2}\sqrt{\frac{J + mi^2}{Jmc}} \qquad (4.28)$$

Considering the electromechanical servo system in a practical situation, all physical parameters can vary within a certain range. We are mainly interested in designing a controller which is robust for variations of the mechanical stiffness 'c' and the mass of the load 'm'. We assume that the variations of the other physical parameters can be neglected compared to the two dominant parameter variations. Because of these physical parameter variations, the variables of the process can be rewritten as a nominal part and a disturbed part :

$$\bar{K} - K_o + \Delta_k$$

$$\bar{\omega} - \omega_o + \Delta_\omega \qquad (4.29)$$

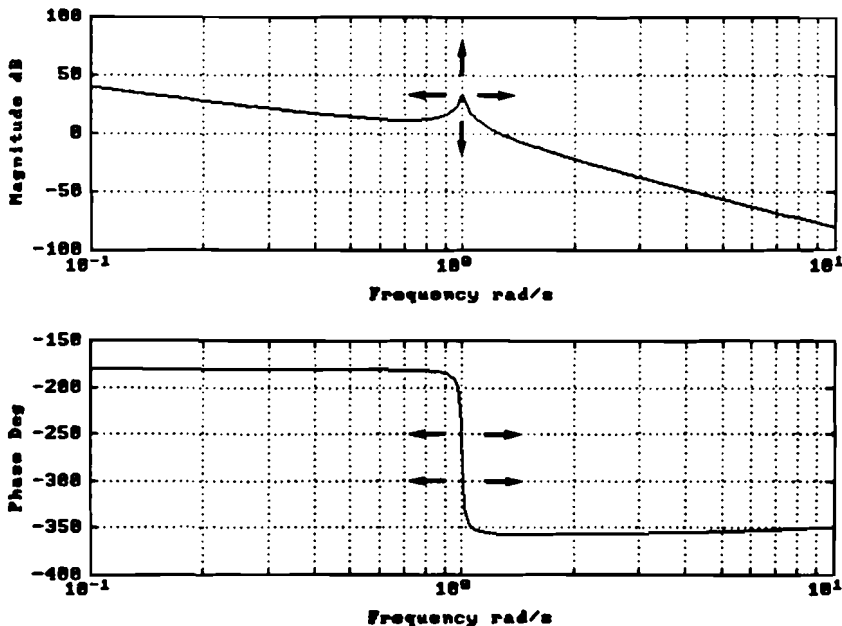$$\tilde{\beta} - \beta_o + \Delta_\beta$$

Fig. 4.3 : Consequences Process Perturbations

The arrows in Fig. 4.3 show the consequences of these parameter variations.

The main problem in our robustness design is the variation of the resonance peak. The controller has to be robust for variations of the resonance peak caused by variations of the resonance frequency $\bar{\omega}$ and the damping $\tilde{\beta}$.

Using Eq. 4.27 , the perturbed plant $\bar{P}$ can be written as follows :

$$\bar{P} = \frac{(K_o + \Delta_k)\left[\,2\,(\,\beta_o + \Delta_\beta\,)\,(\,\omega_o + \Delta_\omega\,)\,s + (\,\omega_o + \Delta_\omega\,)^2\,\right]}{s^2\left[\,s^2 + 2\,(\,\beta_o + \Delta_\beta\,)\,(\,\omega_o + \Delta_\omega\,)\,s + (\,\omega_o + \Delta_\omega\,)^2\,\right]}$$

$$= \frac{n_o + \Delta_n}{d_o + \Delta_d} \tag{4.30}$$

with

$$n_o = K_o\left(\,2\beta_o\omega_o + \omega_o^2\,\right)$$

$$\Delta_n = \left[\,2K_o\,(\,\beta_o\Delta_\omega + \Delta_\beta\omega_o + \Delta_\beta\Delta_\omega\,) + 2\Delta_k\,(\,\beta_o + \Delta_\beta\,)\,(\,\omega_o + \Delta_\omega\,)\,\right]s$$

$$\quad + \left[\,K_o\,(\,2\omega_o\Delta_\omega + \Delta_\omega^2\,) + \Delta_k\,(\,\omega_o + \Delta_\omega\,)^2\,\right] \tag{4.31}$$

$$d_o = s^2\left(\,s^2 + 2\beta_o\omega_o + \omega_o^2\,\right)$$

$$\Delta_d = s^2\left[\,2\,(\,\beta_o\Delta_\omega + \Delta_\beta\omega_o + \Delta_\beta\Delta_\omega\,)\,s + \left(\,2\omega_o\Delta_\omega + \Delta_\omega^2\,\right)\,\right]$$

Table 4.4 : Plant Perturbations

Parameter	Nominal Value	Variation
$\tilde{K}$	$K_o = 1$	$\Delta_k \approx 100\%$
$\tilde{\omega}$	$\omega_o = 1$	$\Delta_\omega \approx 50\%$
$\tilde{\beta}$	$\beta_o = 0.01$	$\Delta_\beta \approx 50\%$

Until now, we assumed that all process parameters can vary. The controller should be robust with respect to stability as well as performance for the variations described in Table 4.4 . The variations in Table 4.4 are global values and we presented them to give an indication of the robustness range we try to achieve.

The uncertainty modelling derived using stable factor perturbations is an upper bound of all possible uncertainties (only amplitude information and no phase information). This implies that H_∞ is minimizing much more uncertainties than in a practical situation will occur by which conservatism is introduced. As **Model Robustness** is reciprocal to

Signal Tracking Performance, a too conservative uncertainty modelling will result automatically in loss of performance. Therefore we have to design our uncertainty modelling very carefully to reduce the conservatism and achieve an optimal signal tracking performance.

Because the gain $\bar{K}$ is directly related to the uncertainty Δ_g, increasing the gain $\bar{K}$ will also increase the gain of the process input weighting filter W_u. By weighting the process input too strong, the controller becomes very passive. To avoid this problem, it is much easier to check the robustness for variations of the gain $\bar{K}$ afterwards. If we design the controller for the worst-case value of $\bar{K}$ and we make sure that at the end a gain margin of 6 dB is achieved, we don't have to take variations of $\bar{K}$ into account in our uncertainty modelling.

The same holds for variations of the damping $\bar{\beta}$. If the envelop description of the uncertainties Δ_g and Δ_l using the weighting filters W_u respectively W_e is critical (filters match uncertainties) around the resonance frequency, we will not satisfy the robustness constraints anymore if $\bar{\beta}$ becomes smaller. In this situation the peak value will increase and the weighting filters are no longer an envelop description. Larger values of $\bar{\beta}$, however, will decrease the peak value and the envelop descriptions still hold. So, if we design the controller also for the worst case value of $\bar{\beta}$, we always satisfy the robustness constraints if $\bar{\beta}$ varies, i.e. becomes larger.

There is now only one parameter left we have to take into account in our uncertainty modelling, the resonance frequency $\bar{\omega}$. The resonance peak is caused by two complex conjugated poles (with small damping) in the process. A nominal controller will try to eliminate this resonance peak through pole-zero cancellation. This means the controller has two zeros with the same values. The actual resonance frequency of the process can vary around the nominal value. If the actual resonance frequency is greater than the nominal value, we first have the positive phase shift of the controller, caused by the zeros, and then the negative phase shift due to the process. If the actual resonance frequency is smaller than the nominal value, the situation is just the other way around and because we have to deal first with the negative phase shift (-180°) of the process, the system might become unstable much easier. Less problems are expected for the first situation ($\bar{\omega} > \omega_e$). For this reason we will design the controller for the worst-case value of the resonance frequency and consider only positive variations.

We reduced the robustness design to only one parameter. Of course we have to check afterwards whether the controller is robust for variations of the gain $\bar{K}$ and the damping $\bar{\beta}$ or not and determine the robustness ranges. The uncertainty expressions we derived in Eq. 4.30 can be reduced as well. To meet the robustness constraints considering variations of the resonance frequency, the weighting filters W_u and W_e must satisfy the conditions in Eq. 4.32 .

$$- \quad V_v - P_i - \frac{d_f}{s^2}$$

$$- \quad |W_u| \geq \overset{sup}{\underset{\Delta_\omega}{}} |\Delta_s|$$

$$\forall \, \omega$$

$$- \overset{sup}{\underset{\Delta_\omega}{}} \left| \frac{2K_o\beta_o\Delta_\omega s + K_o\left(2\omega_o\Delta_\omega + \Delta_\omega^2\right)}{d_f\left(s^2 + 2\beta_o\omega_o s + \omega_o^2\right)} \right| \qquad (4.32)$$

$$- \quad |W_e| \geq \overset{sup}{\underset{\Delta_\omega}{}} |\Delta_i|$$

$$\forall \, \omega$$

$$- \overset{sup}{\underset{\Delta_\omega}{}} \left| \frac{s^2\left(2\beta_o\Delta_\omega s + 2\omega_o\Delta_\omega + \Delta_\omega^2\right)}{d_f\left(s^2 + 2\beta_o\omega_o s + \omega_o^2\right)} \right|$$

with $s - j\omega$. The lower bound descriptions of the weighting filters W_u and W_e , Δ_s and Δ_i , are completely known functions now. The filters depend on the uncertainty Δ_ω (= 0 - 50 % of the nominal value) and the design of the disturbance filter V_v (numerator d_f).

According to the theory of stable factor perturbation the disturbance filter V_v contains only the unstable poles of the process P_o ($V_v = P_i$). In Section 4.2 however we assumed that the disturbance filter V_v contains all the poles of the process P_o to reduce the order of the augmented plant G. This might seem a contradistinction. But by adding the stable poles of the process P_o in the denominator as well as in the numerator of V_v , we can satisfy both conditions.

$$V_v - \frac{d_f}{s^2} - \frac{d_f\left(s^2 + 2\beta_o\omega_o s + \omega_o^2\right)}{s^2\left(s^2 + 2\beta_o\omega_o s + \omega_o^2\right)} \qquad (4.33)$$

We achieved now that the process P_o and the disturbance filter V_v have the same poles, but because of the pole-zero cancellation the disturbance filter V_v contains in fact only the unstable part of the process P_i .

4.6 Performance Design Criteria

Until now we considered only robustness criteria. For this purpose we use stable factor perturbation to derive uncertainty models which results in a lower bound

description of the weighting filters W_e and W_u. The first goal is indeed to design a controller which is robust for a certain range of parameter variations. The second goal, performance optimization with respect to maximum position error, steady state position error and settling time, is probably just as important. Because servo systems are often used for high performance applications it is necessary to take some additional design criteria with respect to performance into account. First of all however we have to specify the type of reference signal which will be used. In theory step inputs are quite often used for design purposes. In practice however, step inputs are seldom used for motion trajectories. They cause saturation of the controller due to the limited acceleration and velocity of the motor and servo amplifier and therefore result in a poor position accuracy. High order set point functions are used to overcome these saturation problems. A well known function is the parabolic position profile (second order) which is pointed out further in Appendix D. We will use this parabolic position profile as reference signal in the simulations to check the performance of the designed closed-loop system. The performance objectives are now specified in Table 4.5 .

Table 4.5 : Performance Objectives

Description	Value
Displacement	1 cm
Maximum Acceleration	$2.5 \ 10^{-4} \ \text{cm/s}^2$
Maximum Velocity	$1.3 \ 10^{-2} \ \text{cm/s}$
Motion Time	129 s
Settling Time	63 s
Maximum Position Error during Motion	10^{-3} cm
Maximum Steady State Position Error	10^{-6} cm

The resonance frequency we use in our simulation model is $\omega_o = 1$ rad/s. This is in fact a scaled value. Because of this low resonance frequency we find the large motion and settling time.

An practical example will give a better impression of these values. Suppose a practical servo system has a dominant resonance frequency at $\omega_p = 100$ Hz $= 628$ rad/s . A multiplication of ω_p on the frequency axis is the same as a division of ω_p in the time domain. The corresponding motion and settling time for the servo system would be about 0.2 s respectively 0.1 s .

4.7 Design Procedure

In this section a global design procedure is presented which will be used in the following chapters. Fig. 4.4 depicts a block diagram of this procedure.
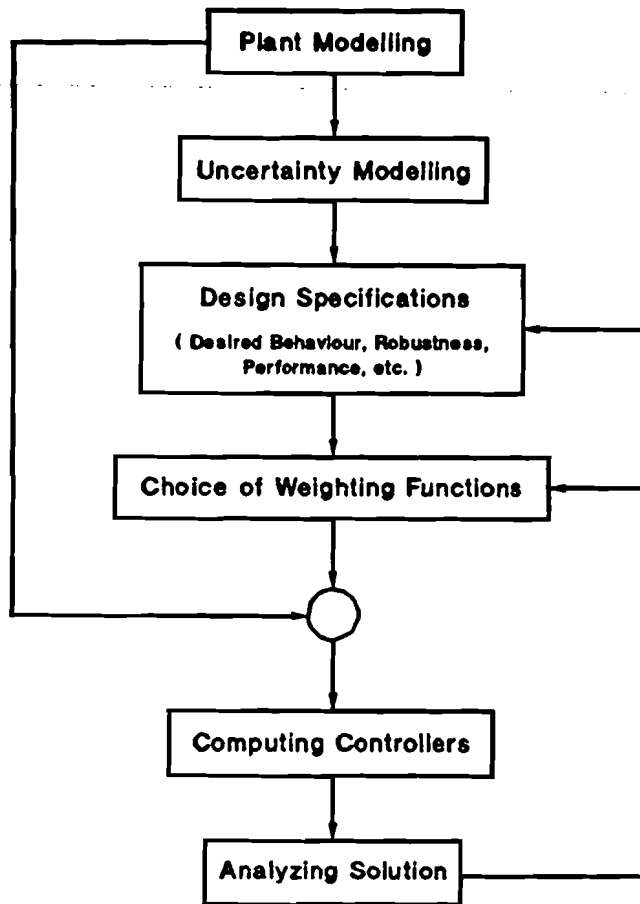
Fig. 4.4 : Design Procedure

A model of the electromechanical servo system has been derived in Chapter 2. In Section 4.4 we described the uncertainty modelling using stable factor perturbations. Finally the design specifications with respect to robustness and performance have been presented in the Sections 4.5 and 4.6 . The actual design, the choice of the weighting functions, computing the controllers and analyzing the solution will be the subject of the following chapters.

In Section 4.3, "Formulation of the Optimization Problem", we introduced a scaling factor γ . By adjusting γ a solution is found for almost every choice of weighting functions. Our goal however is to find a solution satisfying :

$$\alpha - \min(\gamma) \leq 1 \tag{4.34}$$

If a solution is found with $\gamma \leq 1$, we know that the final transfer functions in the two-degree-of-freedom configuration will be bounded by the corresponding inverse weighting function (Table 4.3). This is necessary to satisfy the robustness constraints.

Until a solution is found satisfying Eq. 4.34 , we will continue the design which consists of analyzing the results, redesigning the weighting functions and computing the controllers again.

38

5 Controller Design Robustness Approach

5.1 Introduction

In this chapter we start the controller design from the point of view of robustness maximization. To achieve this goal, we will use the robustness constraints derived with stable factor perturbations (Eq. 4.32) and the parameter variations described in Chapter 4. A scaling factor γ has been introduced to ensure that a solution is found for almost every choice of shaping and weighting filters (numerical problems excluded). However, to make sure that the final transfer functions are bounded by the inverse of the predefined weighting functions, a solution with $\gamma \leq 1$ is needed. This is an additional limiting condition because with $\gamma > 1$, it is not guaranteed anymore that the robustness constraints will be satisfied.

5.2 Design Strategy for Robustness Approach

We will introduce now a global design strategy to show how robustness maximization can be achieved. Experiments showed that this design approach is the appropriate way to achieve maximum robustness. As mentioned before, the H_∞ theory will minimize the ∞ - norm of the design criteria (Table 4.3) which consist of a weighting and a transfer function. If a transfer function of a design criterion matches the corresponding inverse weighting function in a certain frequency range (For example from 0.1 rad/s to 1 rad/s), we will call this criterion a limiting function.

The design can be divided in two major parts. The first part is the robustness maximization which has the following phases :

1)   Design the reference filter V_r in such a way that the **Signal Tracking** criterion, defined by :

$$M_{12} - W_e \left[I - \left(I - PC_{fb} \right)^{-1} PC_{ff} \right] V_r$$

and the **Input Saturation** criterion, defined by :

$$M_{22} - W_u \left(I - PC_{fb} \right)^{-1} C_{ff} V_r$$

are not the limiting functions.

2)   Design the disturbance filter V_v (the denominator is the same as the unstable part of the process, Eq. 4.32).

39

3)   With the selected parameter variations, the uncertainty Δ_u is a lower bound description for the process input weighting filter W_u, and the uncertainty Δ_e is a lower bound description for the error weighting filter W_e.
Design the weighting filters W_u and W_e in such a way that the constraints of the uncertainty modelling will be satisfied and a solution is found for $\gamma \leq 1$.

With this approach so far, the **Model Robustness** constraint, defined by :

$$M_{21} - W_u C_{fb} (I - PC_{fb})^{-1} V_r$$

and the **Disturbance Reduction** constraint, defined by :

$$M_{11} - - W_e (I - PC_{fb})^{-1} V_v$$

will be satisfied. If the robustness is maximized, the **Model Robustness** constraint M_{21} or/and the **Disturbance Reduction** constraint M_{11} have reached their limitation. Both criteria are used to satisfy the uncertainty modelling, but have different names for distinction. One or both of the transfer functions will match the corresponding inverse weighting function (Table 4.3) for a certain frequency range. We will show in the following sections that in our design the **Model Robustness** constraint becomes the limiting function.
    The second part of the design is the performance optimization which can be divided in the following phases :

4)   Improve the **Signal Tracking** by optimizing the error weighting filter W_e. This can be achieved by weighting low frequencies stronger and increasing the bandwidth of the filter W_e (The bandwidth of a filter is defined as the 0 dB intersection). The bandwidth should be maximized as much as possible (to decrease the maximum position error) until no solution is found satisfying $\gamma \leq 1$. A further optimization is not possible, because the **Disturbance Reduction** constraint has reached its limitation and γ will become larger than 1.

5)   Using the last degree of freedom, we can further improve the **Signal Tracking** by optimizing the reference filter V_r. As we did with W_e, V_r will be designed in such a way that low frequencies will be weighted stronger and the bandwidth is increased as much as possible. This can be done until either the **Signal Tracking** criterion or/and the **Input Saturation** criterion will reach their limitations.

We optimized the solution as much as possible (satisfying the robustness constraints and optimizing the performance) for a certain choice of the disturbance filter V_v. If the results are not satisfying, we can use this last degree of freedom, redesigning the disturbance filter V_v and restart the design procedure, to improve the results.

Until so far, we didn't mention the order of the shaping and weighting filters. Our goal is however, to design controllers of the lowest possible order which satisfy the robustness constraints. The order of the controllers obtained with the aid of the H_∞ theory, depends on the order of the augmented plant. **The final order of the system is the sum of orders of the process P_0 and the filters V_r, W_e and W_u**. The shaping filter V_v will not increase the order of the system, because it has the same poles as the nominal process (Table 4.2). In order to keep the controller design as simple as possible and to reduce the order of the controllers as far as possible, we will start the controller design with low order filters. The order of the shaping and weighting filters is only increased if robustness constraints cannot be satisfied or to optimize the performance objectives.

The controller design strategy presented here, is meant to give a general impression of the design approach. A more detailed explanation together with the choices for the shaping and weighting filters will be given in the following sections.

5.3 Robustness Maximization

In the previous section a general design strategy has been introduced. Our goal is to design a controller which is robust, with respect to stability as well as performance, for variations of the resonance frequency $\tilde{\omega}$ of 50%.

5.3.1 Design Shaping Filters

The first step in the control design is the design of the shaping filters V_r and V_v. To avoid that the **Signal Tracking** criterion or the **Input Saturation** criterion is the limiting function in any frequency point, we will choose V_r small compared to the ∞ - norm which is scaled to 1 (Section 4.3). Suppose we take (Design step 1) :

$$V_r - 0.001 \qquad (5.1)$$

The next step is to design the disturbance shaping filter V_v. According to the theory of stable factor perturbations the disturbance filter V_v contains the unstable poles of the process P_0 (Section 4.5). Because we have to design V_v biproper (Program condition in Section 4.2), a general form of the transfer function V_v is given by :

$$V_v - \frac{k_v \left(s^2 + b\sqrt{2}s + b^2 \right)}{s^2} \qquad (5.2)$$

41

We are dealing now with two variables, the gain k_v and the choice of the cut-off frequency at b rad/s. The robustness constraints have been formulated in Eq. 4.32 . We can see that the numerator of V_v returns as a part of the denominator in $\Delta_,$ and $\Delta_,$.

Experiments showed that an appropriate choice for the gain is $k_v = 1$ which can be explained as follows. Suppose we choose $k_v > 1$. This would decrease the gains of $\Delta_,$ and $\Delta_,$ which implies a gain reduction of the weighting filters W_u and W_e to satisfy the robustness constraints and therefore more space to optimize the performance. It turned out however that if the high frequency gain of V_v is larger than 1 , problems occur for frequencies at ∞ and no solution is found satisfying $\gamma \le 1$. The scaling factor γ is adjusted in the solution procedure in such a way that the high frequency gain becomes again smaller or equal to 1. For $k_v < 1$, the opposite is true. Satisfying the robustness constraints for $k_v < 1$ implies a stronger weighting with W_u and W_e in the frequency domain and therefore less space to optimize the performance. Weighting the process input stronger, will result also in a more passive controller. For these reasons we have chosen $k_v = 1$, because another value for k_v will cause problems in one way or the other.

The choice of the cut-off frequency at b rad/s is not only important in the uncertainty modelling. From experiments we found that the cut-off frequency of V_v can also be recognized in the open-loop Bode plot of the final control system. The phase-margin which is derived from the open-loop Bode plot is build up after the cut-off frequency. The cut-off frequency at b rad/s should be chosen in such a way that a phase-margin of 45° (Standard design criterion) is achieved. Increasing the cut-off frequency results in a phase-margin smaller than 45° (not acceptable) and decreasing the cut-off makes the phase-margin unnecessary high. The appropriate choice for the cut-off frequency in our situation is b = 0.1 . It will be explained later, together with the final results at the end of this chapter, why this choice is appropriate. We have finished now design step 2.
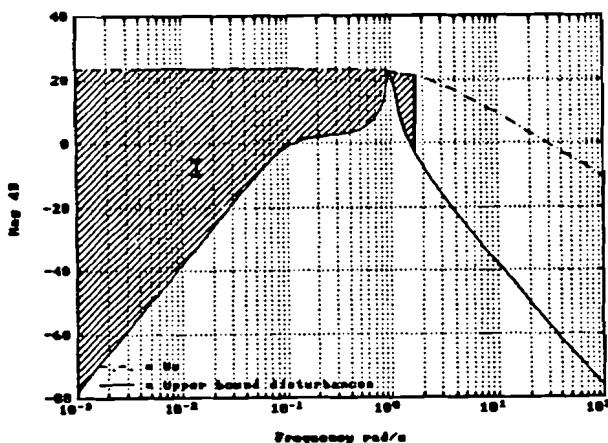
5.3.2 First Order Weighting Filters
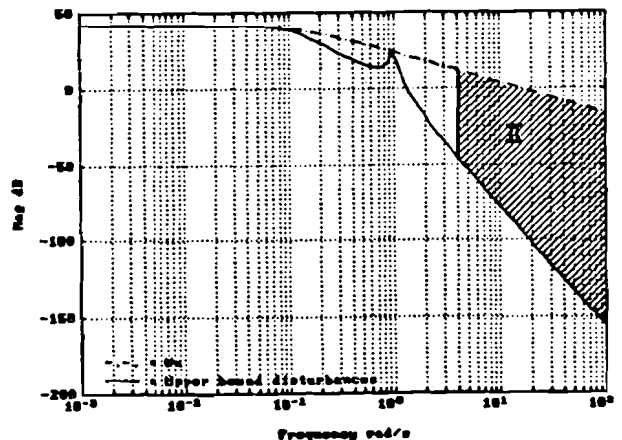

Fig. 5.1 : W_e (1st order, Δ_u - 50%)   Fig. 5.2 : W_u (1st order, Δ_u - 50%)

The design of the disturbance filter V_v, together with the robustness descriptions using stable factor perturbations and the parameter variations of Chapter 4, make it possible to derive the lower bound descriptions of W_e and W_u, Δ_i and Δ_s (Design step 3).

To reduce the order of the controllers, we will start with first order filters W_e and W_u. Fig. 5.1 and 5.2 show the lower bound descriptions and the first order filters given by :

$$W_e - \frac{0.01s + 30}{s + 2} \qquad , \qquad W_u - \frac{0.01s + 16.25}{s + 0.13} \qquad (5.3)$$

The first order weighting filters have been designed in such a way that the low frequency gain fits as good as possible and the high frequency gain is set to 0.01 . This corresponds in fact with a straight line for low frequencies as well as for high frequencies. We can find the poles and the zeros of the weighting filters by drawing a line with slope -1 (First order filter) which fits the lower bound descriptions of W_e and W_u, Δ_i and Δ_s, in an optimal way. The intersection of two lines corresponds of course with a pole or a zero.

It's obvious that the envelop description of the uncertainties Δ_i and Δ_s, using first order weighting filters is very poor. Only the process input weighting filter W_u fits well for frequencies up to 0.1 rad/s (Fig. 5.2). But for high frequencies we are weighting stronger than necessary and therefore we introduce conservatism. For this particular case, all the transfer functions together with the inverse weighting functions (scaled with γ) will be presented. These functions are depicted in Fig. 5.3 , 5.4 , 5.5 and 5.6 .
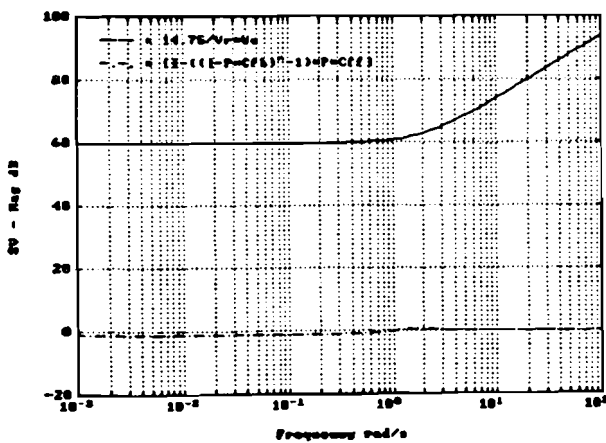
Fig. 5.3 : Signal Tracking
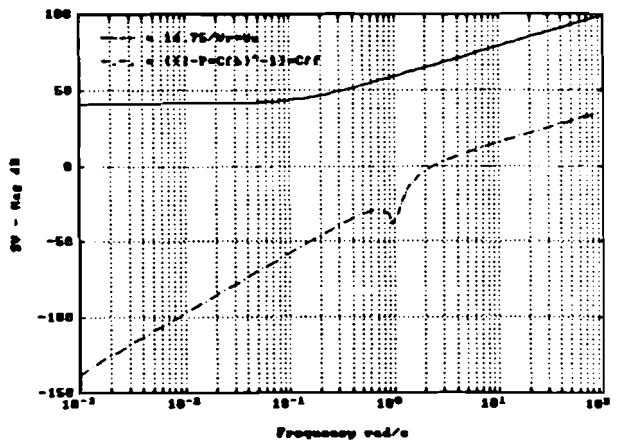
Fig. 5.4 : Input Saturation

Calculating the controller, a solution is found for $\gamma - 14.75$. Fig. 5.3 and 5.4 show that we have chosen the reference filter V_r small enough. The **Signal Tracking** and the **Input Saturation** are not the limiting functions, and therefore we will not show these two transfer functions anymore until we start optimizing the performance in the next section.
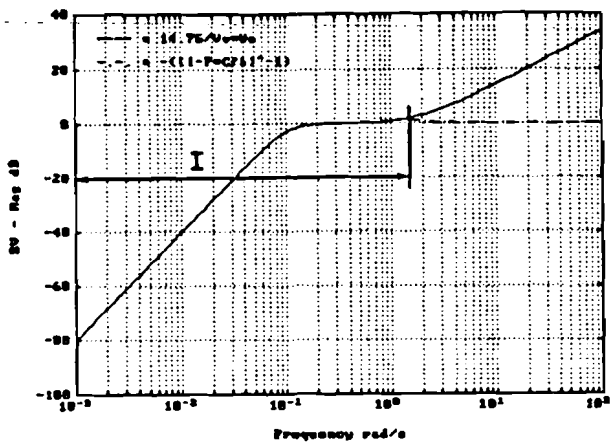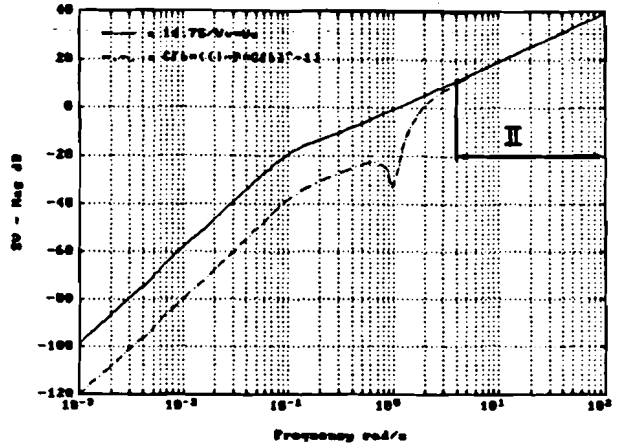
Fig. 5.5 : Disturbance Reduction

Fig. 5.6 Model Robustness

In Fig. 5.5 we see that the **Disturbance Reduction** is limited for frequencies smaller than 1.5 rad/s (Area I). Examining Fig. 5.6, we find the limitations in the frequency range above 4 rad/s (Area II). These areas have been depicted as hatched parts in Fig. 5.1 and 5.2 . These are exactly the frequency ranges where the uncertainty descriptions using first order weighting filters were very poor.

5.3.3 Second Order Weighting Filters

Using first order weighting functions we cannot satisfy the robustness constraints. Because we are interested in a solution with $\gamma \leq 1$, the only way to decrease γ and still satisfy the robustness constraints, is to increase the order of the filters W_c and W_u . We increase the order of both weighting filters because the **Disturbance Reduction** criterion as well as the **Model Robustness** criterion are the limiting function as we can see in Fig. 5.5 and 5.6 .
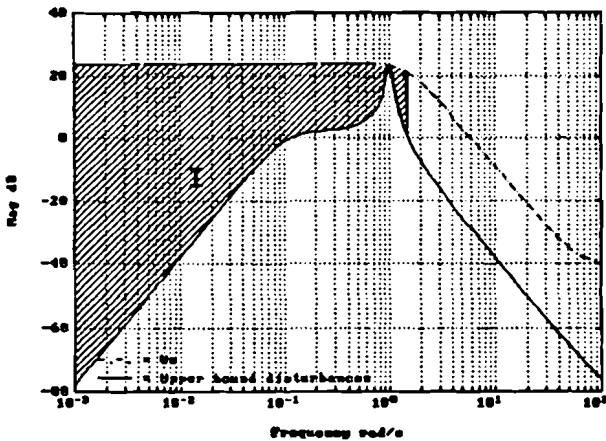
Fig. 5.7 : W_c (2nd order, Δ_ω - 50%)

Fig. 5.8 : W_u (2nd order, Δ_ω - 50%)

44
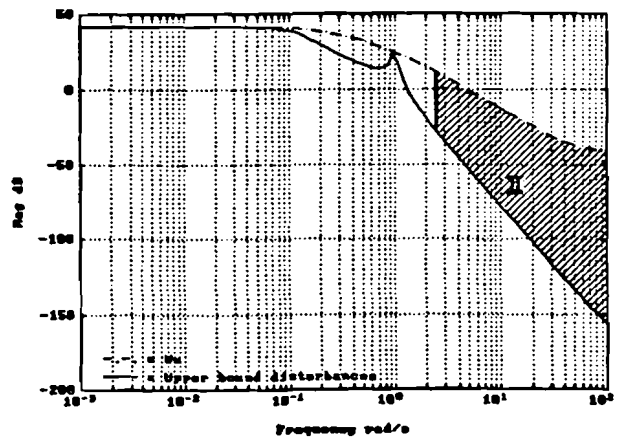
Define now :

$$W_e = \frac{0.01 \left(s^2 + 60\sqrt{2}s + 3600 \right)}{s^2 + 1.5\sqrt{2}s + 2.25} \quad , \quad W_u = \frac{0.01 \left(s^2 + 50\sqrt{2}s + 2500 \right)}{(s + 0.2)(s + 1)} \quad (5.4)$$

The second order weighting filters have been designed the same way as the first order filters. The low frequency behaviour of both, second and first order, weighting filters stayed the same. Only for frequencies above 1.5 rad/s (W_e) respectively 1 rad/s (W_u) we are dealing now with a slope of -2 instead of -1. In these frequency ranges we improved the envelop descriptions of the uncertainties. Fig. 5.7 and 5.8 show the second order filters. The envelop description using second order weighting filters is better as before, but for high frequencies we are still weighting too strong. With these new filters, a solution is found for $\gamma = 14.09$. The hatched parts in Fig. 5.7 and 5.8 correspond again with the frequency ranges where the limitations occur in the **Disturbance Reduction** (Fig. 5.9) and the **Model Robustness** (Fig. 5.10).
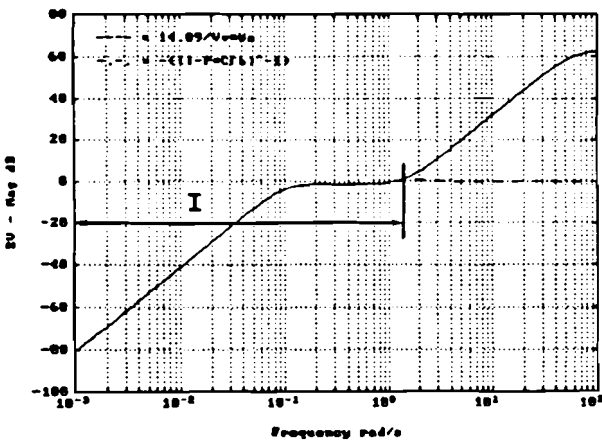
Fig. 5.9 : Disturbance Reduction   Fig. 5.10 Model Robustness
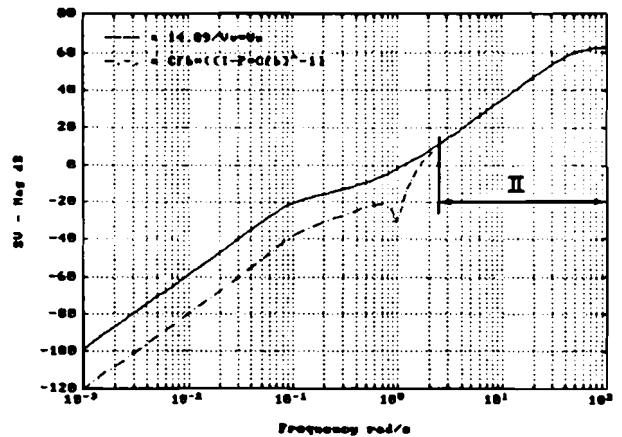
Fig. 5.9 and 5.10 depict the **Disturbance Reduction** and the **Model Robustness** together with the corresponding inverse weighting filters. It is obvious that the second order filters are still not good enough. The decrease of γ is marginal and the limitations occur in the same frequency ranges as before.

Because the limitations occur in the same frequency range it might seem an obvious choice to design the error weighting filter W_e in a different way. The **Disturbance Reduction** is the limiting function for frequencies below 1.5 rad/s. Using a second order filter it is possible to design W_e in such a way that the envelop description fits better also for lower frequencies. This implies that we would weigh lower frequencies less as before. But this is not our intention because satisfying the robustness constraint is only one of the goals we try to achieve using W_e . The weighting filter W_e can also be used to improve the **Signal Tracking**. To optimize the **Signal Tracking** we have to weigh low frequencies stronger and increase the bandwidth as much as possible. Because we know

45

already that we have to use the weighting filter W_e later on in the design to achieve an acceptable **Signal Tracking**, we designed W_e in such a way that both goals, robustness constraint and performance objective, can be satisfied.

To satisfy the condition $\gamma \leq 1$, we have to increase the order of the filters W_u and W_e even more.

5.3.4 Fourth Order Weighting Filters

Until now, the results derived with first as well as second order weighting filters were not acceptable ($\gamma > 1$). Examining the robustness constraints (Eq. 4.32) in more details , we can see that the lower bound descriptions of the weighting filters W_u and W_e are in fact fourth order filters. Because we still don't know which criterion, the **Disturbance Reduction** or the **Model Robustness** is the limiting function, we will increase the order of both filters. Suppose we take the following fourth order filters :

$$W_e = \frac{0.01 \left(s^2 + 3\sqrt{2}s + 9 \right) \left(s^2 + 12\sqrt{2}s + 144 \right)}{\left(s^2 + 0.5\sqrt{2}s + 0.25 \right)^2}$$

$$(5.5)$$

$$W_u = \frac{0.01 \left(s^2 + 3.4\sqrt{2}s + 11.56 \right)^2}{\left(s^2 + 0.02s + 1 \right) \left(s^2 + 0.5\sqrt{2}s + 0.25 \right)^2}$$

The poles of these fourth order weighting functions follow directly from the robustness constraints in Eq. 4.32 . The only degree of freedom left is the choice of the zeros.
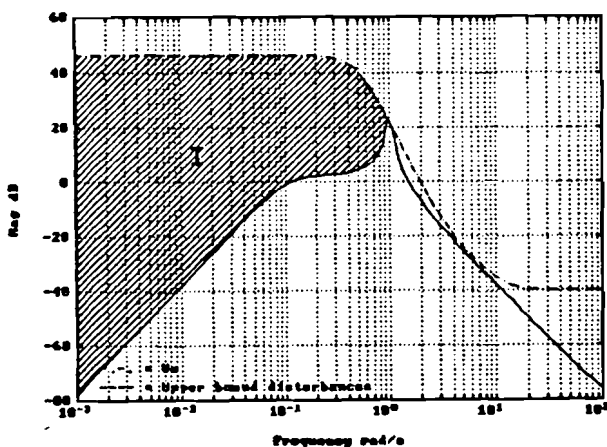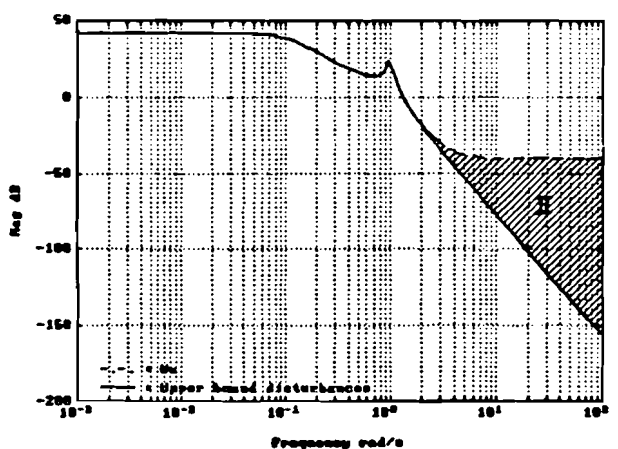

Fig. 5.11 : W_e (4th order, Δ_ω – 50%)   Fig. 5.12 : W_u (4th order, Δ_ω – 50%)

Fig. 5.11 and 5.12 show these fourth order filters together with the lower bound descriptions. We can see that for frequencies up to 2 rad/s , the fourth order filter W_u

is an optimal choice. The frequency range for which the envelop description is exact depends on the choice of the zeros. We have placed now 4 complex conjugated zeros at 3.4 rad/s. Increasing the zeros will also increase the frequency range for which the envelop description of Δ_r with W_u is exact. The fourth order weighting filter W_e has been designed in such a way that the envelop description for the higher frequencies, above the resonance frequency, is as good as possible. The low frequency behaviour of W_e is designed, just as we did for the second order weighting filter W_e, to improve the **Signal Tracking** later in the design. Comparing Fig. 5.1 and 5.7 with Fig. 5.11, we can see that the lower bound description of Δ_l, using W_e, is improved too. With these fourth order filters, a solution is found for $\gamma = 4.69$. Fig. 5.13 and 5.14 depict again the important transfer and inverse weighting functions. γ is reduced with a major factor, so the increase of the order of the weighting filters can be justified. The hatched parts in Fig. 5.11 and 5.12 show the frequency ranges where the limitations occur in the corresponding transfer functions, the **Disturbance Reduction** (Fig. 5.13) respectively the **Model Robustness** (Fig. 5.14).
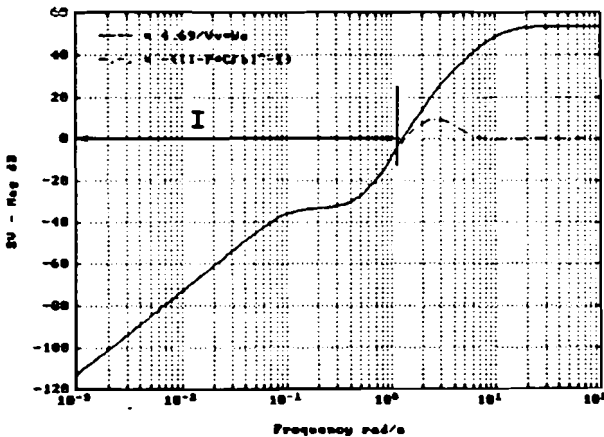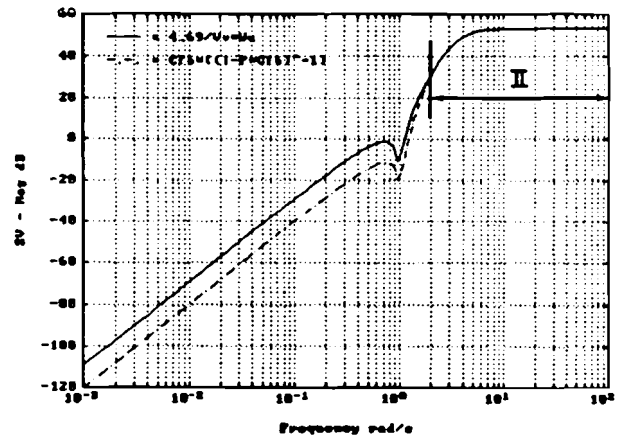

Fig. 5.13 : Disturbance Reduction

Fig. 5.14 : Model Robustness

If we compare Fig. 5.9 and 5.13 we can see that the **Disturbance Reduction** function is different for the lower frequencies, but still matches the inverse weighting function. This might be an indication that this is not really a limiting function and adjustments are possible. For the **Model Robustness** the situation is different, because for frequencies above 2 rad/s the transfer function still matches the inverse weighting function. The envelop description using W_u for high frequencies is not good enough and adjustment of the high frequency gain is necessary. The solution is of course to decrease the gain of W_u and adjust the zeros. Experiments showed that a gain of 10^{-5} is necessary to avoid limitations for high frequencies. Fig. 5.15 depicts the new situation and we can see that the new weighting function W_u, defined by :

$$W_u = \frac{10^{-5} \left(s^2 + 18.8\sqrt{2}s + 353.44 \right)^2}{\left(s^2 + 0.02s + 1 \right)\left(s^2 + 0.1\sqrt{2}s + 0.01 \right)} \tag{5.6}$$

47

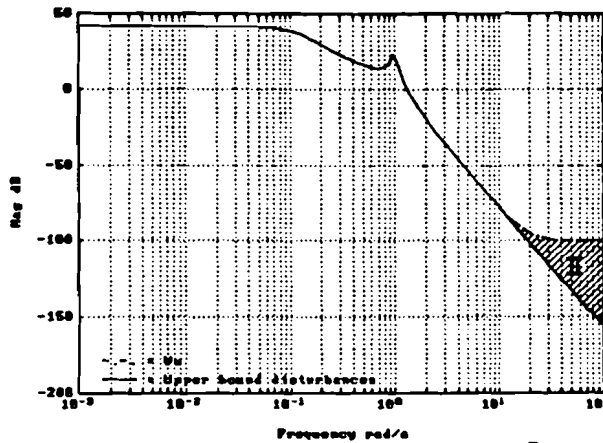describes the disturbances in an optimal way for frequencies almost up to 20 rad/s .

Fig. 5.15 : W_u (4th order, Δ_u - 50%)

A solution is found for γ - 1.55 . Fig. 5.16 and 5.17 depict now the important transfer and weighting functions using the optimized weighting filter W_u . In Fig. 5.16 we can see that the **Disturbance Reduction** is indeed not the limiting function as we expected. The transfer function doesn't match anymore the inverse weighting functions for low frequencies. Until now, we reduced the problem so far that only 1 criterion, the **Model Robustness**, is the limiting function. We can now maximize the robustness, using stable factor perturbations as robustness description, to find a solution with $\gamma \le 1$.
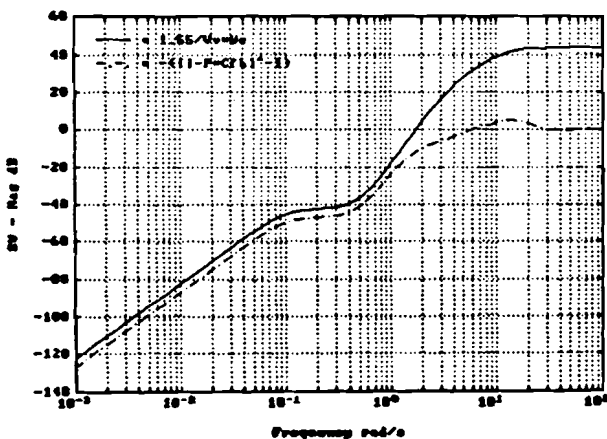
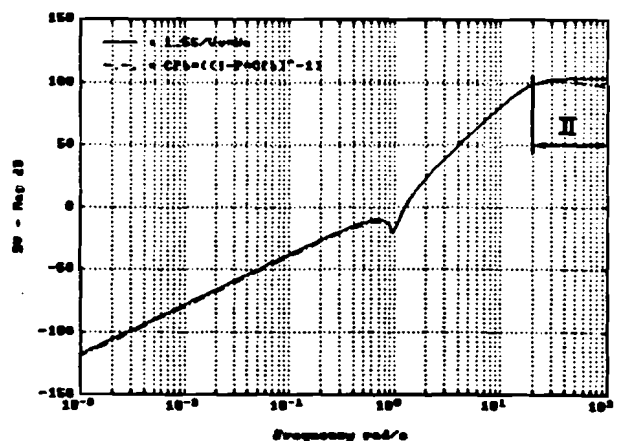

Fig. 5.16 : Disturbance Reduction

Fig. 5.17 : Model Robustness

Fig. 5.17 shows us, that the **Model Robustness** matches the inverse weighting function for almost the whole frequency range. Only for frequencies above 20 rad/s the transfer function doesn't match the inverse weighting function. But this is just the frequency range

where we can improve W_u according to Fig. 5.15 . So, there is no freedom left for a further reduction of γ .

5.3.5 Reduction of Robustness Criteria

The H_∞ optimization problem has been reduced to only one limiting function, the Model Robustness. We optimized the process input weighting filter over the whole frequency range where the limitation occurs (Compare Fig. 5.15 and 5.17). Because we still don't have a solution with $\gamma \leq 1$, we have to reduce our demands concerning the variations of the resonance frequency $\tilde{\omega}$. With a minimal value for γ of 1.55 , it is obvious that we have to decrease the variations of $\tilde{\omega}$ in our robustness design. Using γ as a scaling factor of W_u and if we consider the low frequency gain at $s = 0$ (Eq. 4.32), we can calculate the maximum allowable variation of the resonance frequency $\tilde{\omega}$.

$$\frac{1}{\gamma}\Delta_s \bigg|_{s-0} - \frac{1}{\gamma}\frac{K_o\left(2\omega_o\Delta_\omega + \Delta_\omega^2\right)}{0.01\ \omega_o^2}\bigg|_{\Delta_\omega - 0.5} - 80.65 \quad \rightarrow \quad \Delta_{\omega,max} - 0.34 \qquad (5.7)$$
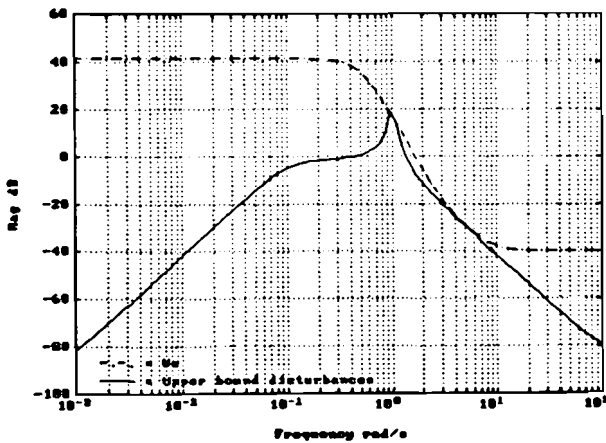
This implies that only variations of 34% are allowed.

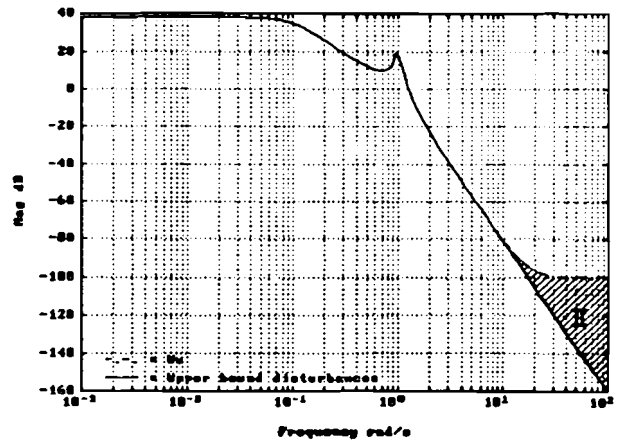Fig. 5.18 : W_e (4th order, Δ_ω - 34%)   Fig. 5.19 : W_u (4th order, Δ_ω - 34%)

With a maximum variation of the resonance frequency of 34%, we have to redesign the weighting filters W_e and W_u . For this new situation, a proper choice for the weighting filters is :

$$W_e = \frac{0.01 \left(s^2 + 3\sqrt{s} + 9 \right) \left(s^2 + 9\sqrt{2}s + 81 \right)}{\left(s^2 + 0.5\sqrt{2}s + 0.25 \right)}$$

$$W_u = \frac{10^{-5} \left(s^2 + 16.8\sqrt{s} + 282.24 \right)^2}{\left(s^2 + 0.02s + 1 \right) \left(s^2 + 0.1\sqrt{2}s + 0.01 \right)}$$

(5.8)

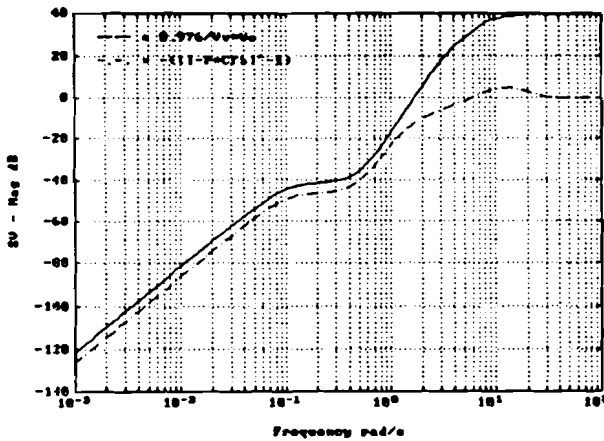as shown in Fig. 5.18 and 5.19 .
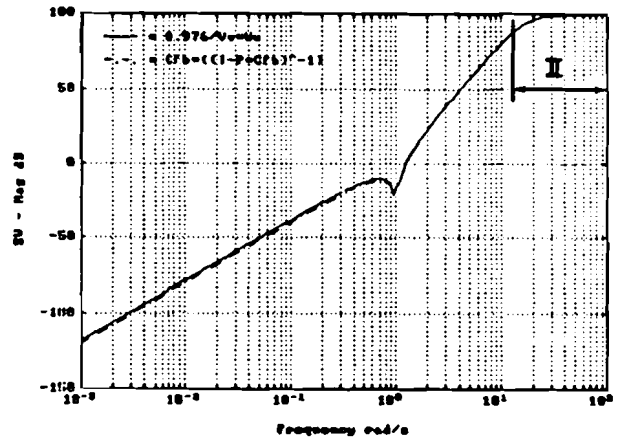

Fig. 5.20 : Disturbance Reduction

Fig. 5.21 : Model Robustness

As expected, a solution is found for $\gamma \leq 1$ ($\gamma = 0.976$). The new transfer and weighting functions are depicted in Fig. 5.20 and 5.21 . The **Model Robustness** matches now the inverse weighting function approximately for the whole frequency range (Fig. 5.21). As before, we can see in Fig. 5.20, that the **Disturbance Reduction** is not the limiting function and optimization is possible. Because we found a solution with $\gamma \leq 1$, we are sure that our robustness constraints are satisfied. Using the factor perturbation theory as robustness description, the resonance frequency may maximally vary 34% . The derived process input weighting filter W_u will be used for the rest of this chapter.

5.4 Performance Optimization

Until now, we satisfied the stability robustness constraints (Eq. 4.32). Our objective in this section is to optimize the **Signal Tracking** (Design step 4).

5.4.1 Optimization of Error Weighting Filter W_e

In the previous section we used a fourth order weighting filter W_e . We saw however,

50

that the **Disturbance Reduction** was not the limiting function and optimization of the **Signal Tracking** with W_e seems possible. Also the shape of the **Disturbance Reduction** function was different in the previous situations (Compare Fig. 5.9 , 5.16 and 5.20), which probably makes an order reduction of the error weighting filter W_e possible. This will also reduce the order of the controllers which is equal to the order of the augmented plant (Chapter 4). Suppose we take a second order weighting filter W_e . We have to design the filter in such a way that on one hand the stability robustness constraint is satisfied, i.e. W_e is still an upper bound description of Δ_i , and on the other hand lower frequencies are weighted stronger to improve the **Signal Tracking**. Suppose we take :

$$W_e = \frac{0.01 \left(s^2 + 30\sqrt{2}s + 900 \right)}{s^2 + 3.10^{-3}\sqrt{2}s + 9.10^{-6}}$$ (5.9)
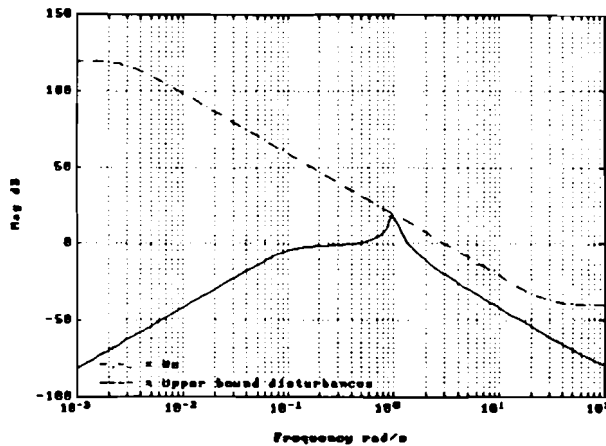

Fig. 5.22 : W_e (2nd order, $\Delta_\omega = 34\%$)

Fig. 5.22 depicts this second order weighting filter W_e . We can see that the critical point in the design of W_e is the peak value of Δ_i at 1 rad/s. Low frequencies are weighted with 120 dB to ensure that the steady state error will reduce to zero.

5.4.2 Zero Order Reference Filter V_r

In the previous section we designed V_r in such a way that no limitations occurred in the **Signal Tracking** and the **Input Saturation** ($V_r = 0.001$). Fig. 5.3 and 5.4 show us, however, that the chosen reference filter V_r is much too small. Increasing V_r (Design step 5) results in :

$$V_r = 0.1$$ (5.10)

Calculating a controller with the new designed second order weighting filter W_e and the optimized reference filter V_r, a solution is found for $\gamma = 1.087$. γ increased slightly. Because of $\gamma > 1$ the robustness constraints are in fact not satisfied anymore. But the increase of γ compared to the limiting condition, $\gamma \leq 1$, is so small that we loose only about 2 % of the stability robustness range. In this design the decrease of the stability robustness range is acceptable because of the obtained order reduction of the controllers.

Reducing the order further or increasing the bandwidth of the error weighting filter W_e, results in an unacceptable γ ($\gamma \gg 1$). For these situations γ will increase significantly which results in a decrease of the stability robustness range of the same order.
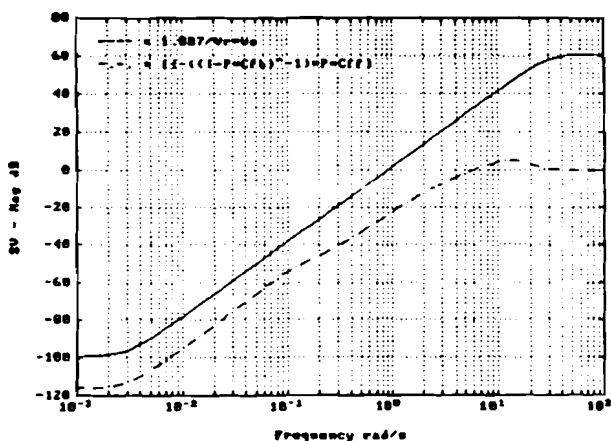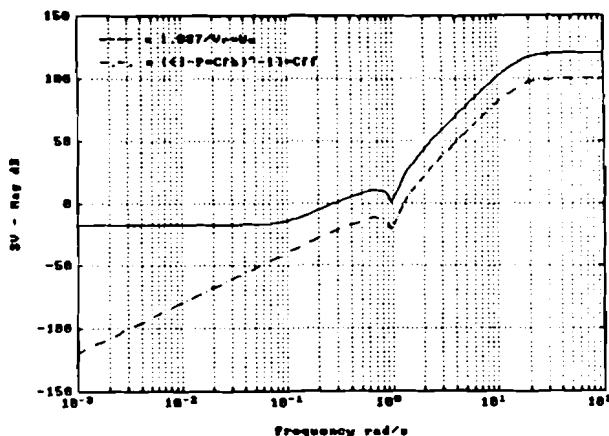

Fig. 5.23 : Signal Tracking
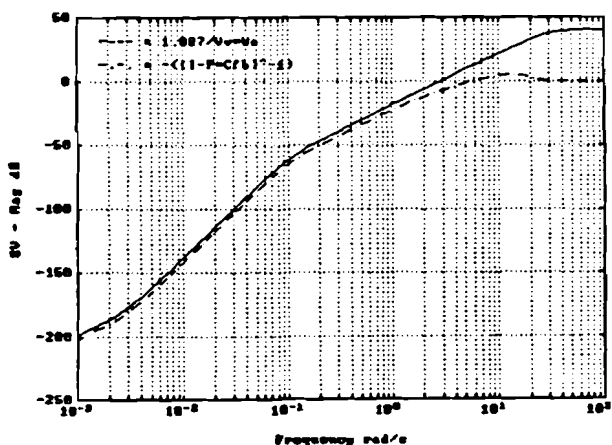

Fig. 5.24 : Input Saturation

Fig. 5.25 : Disturbance Reduction

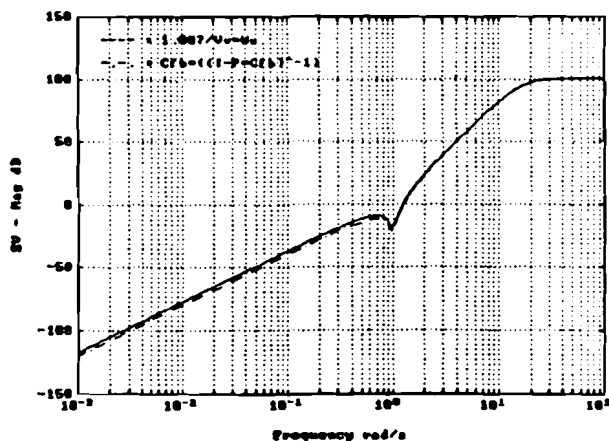Fig. 5.26 : Model Robustness

Fig. 5.23 and 5.24 depict the **Signal Tracking** and the **Input Saturation** function. The transfer functions do not match the inverse weighting functions at any frequency point. This indicates that a further optimization of the reference filter V_r might be possible. In practice, increasing V_r resulted however also in a larger and therefore unacceptable

52

γ . The design became probably so critical considering the whole frequency range, that a further optimization with a constant filter V_r is not possible.

The **Disturbance Reduction** and the **Model Robustness** are depicted in Fig. 5.25 and 5.26 . We can see that for both criteria the transfer functions and the inverse weighting functions almost match completely.

Table 5.1 : Feed-forward Controller (gain C_{ff} : 3.231e+07)
1) Zero at ∞
2) Real zero, imaginary part - 0
3) Pole - zero cancellation

Poles C_{ff}		Zeros C_{ff}	
- 3.1126e+02		1.6424e+46-	- 4.3874e+39 j [1]
- 1.3597e+01	2.1106e+01 j	- 1.6885e+00	8.1390e -17 j [2]
- 1.3597e+01	- 2.1106e+01 j	- 1.0000e -02	9.9995e -01 j [3]
- 2.2587e+01		- 1.0000e -02	9.9995e -01 j
- 9.9997e -03	9.9995e -01 j [3]	- 1.0000e -02	- 9.9995e -01 j [3]
- 9.9997e -03	- 9.9995e -01 j [3]	- 1.0000e -02	- 9.9995e -01 j
- 7.0711e -02	7.0734e -02 j [3]	- 7.0711e -02	7.0711e -02 j [3]
- 7.0711e -02	- 7.0734e -02 j [3]	- 7.0711e -02	7.0711e -02 j
- 2.1213e -03	2.1213e -03 j	- 7.0711e -02	- 7.0711e -02 j [3]
- 2.1213e -03	- 2.1213e -03 j	- 7.0711e -02	- 7.0711e -02 j

Table 5.2 : Feed-back Controller (gain C_{fb} : - 3.366e+07)
1) Zero at ∞
2) Real zero, imaginary part - 0
3) Pole - zero cancellation

Poles C_{fb}		Zeros C_{fb}	
- 3.1126e+02		2.6214e+25	- 4.9920e+18 j [1]
- 1.3597e+01	2.1106e+01 j	- 1.6180e+00	- 6.7085e -17 j [2]
- 1.3597e+01	- 2.1106e+01 j	- 1.0000e -02	9.9995e -01 j [3]
- 2.2587e+01		- 1.0000e -02	9.9995e -01 j
- 9.9997e -03	9.9995e -01 j [3]	- 1.0000e -02	- 9.9995e -01 j [3]
- 9.9997e -03	- 9.9995e -01 j [3]	- 1.0000e -02	- 9.9995e -01 j
- 7.0711e -02	7.0734e -02 j [3]	- 7.0701e -02	7.0836e -02 j
- 7.0711e -02	- 7.0734e -02 j [3]	- 7.0711e -02	7.0711e -02 j [3]
- 2.1213e -03	2.1213e -03 j	- 7.0701e -02	- 7.0836e -02 j
- 2.1213e -03	- 2.1213e -03 j	- 7.0711e -02	- 7.0711e -02 j [3]

Until now, we optimized the **Signal Tracking** with an error weighting filter W_e of lowest possible order, which satisfies the stability robustness constraints (Eq. 4.32) and is optimized with respect to performance, and a constant reference filter V_r. A solution is found with γ close enough to 1. The Tables 5.1 and 5.2 contain the poles and zeros of the feed-forward and the feed-back controller.

Even we designed originally controllers of the 10th order (The augmented plant has order 10, $O(\text{Plant}) = O(P_o) + O(V_r) + O(W_e) + O(W_u) = 4 + 0 + 2 + 4 = 10$), we can reduce the order of the feed-forward as well as the feed-back controller to 6 because of pole-zero cancellation. Due to numerical problems the first two zeros of the feed-forward (Table 5.1) and the feed-back (Table 5.2) controller are not reliable. Considering a pole-zero plot the distance between the first zero and the other roots is so large that we can assume this zero at ∞. Also we can assume that the imaginary part of the second zero is equal to zero. The reduced controllers satisfy the notes in the header of the tables. The Bode-plots of the reduced controllers are depicted in Fig. 5.27 . The Bode-plot of -C_{fb} is depicted because in the two-degree-of-freedom configuration we used a positive feedback. Solving the H_∞ optimization problem results automatically in a feed-back controller with a negative gain. Therefore the minus sign in the feed-back gain is actually the negative feed-back which is normally used.
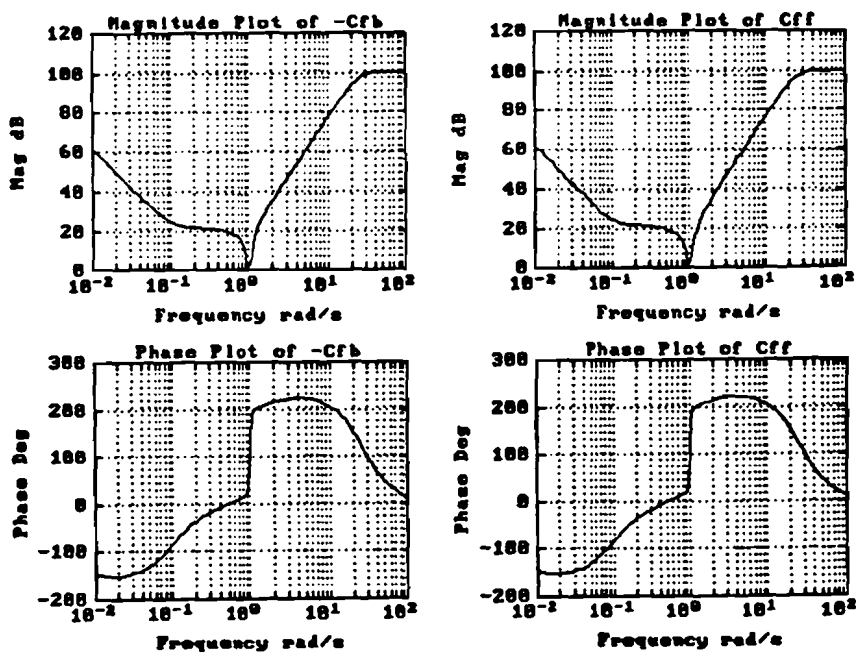

Fig. 5.27 : Bode Plots Controllers

As we can see in Fig. 5.27 together with the numerical results in Table 5.1 and 5.2 , the derived feed-back and feed-forward controller are effectively the same. The minor

54

difference between the zeros and the gain of both controllers can be neglected. In the design so far the **Model Robustness** is the dominant design criterion. The feed-back controller has been designed due to the demands in the frequency domain of this criterion. We optimized the **Signal Tracking** which is obviously not dominant, using a zero order reference filter V_r (V_r = 0.1). The information we added to the control system using V_r is constant over the whole frequency range. Because we didn't add any additional information in the frequency domain, the feed-forward controller is the same as the feed-back controller.

Using the reduced controllers, we excite our control system with a parabolic position signal (reference signal) to test the real time behaviour. This smoother signal consists of a block signal (acceleration signal) which is integrated twice. Fig. 5.28 shows the simulated output signal as a function of the time. It might seem that we have used a very slow position signal (motion time = 129 seconds), but this is in fact not true. The resonance frequency ω_o of our process is scaled to 1 rad/s. Because of the scaling of the resonance frequency, the time axis is scales as well using a real servo system as example which resulted in the used motion time. More information about the parabolic position signal is given in Appendix D.
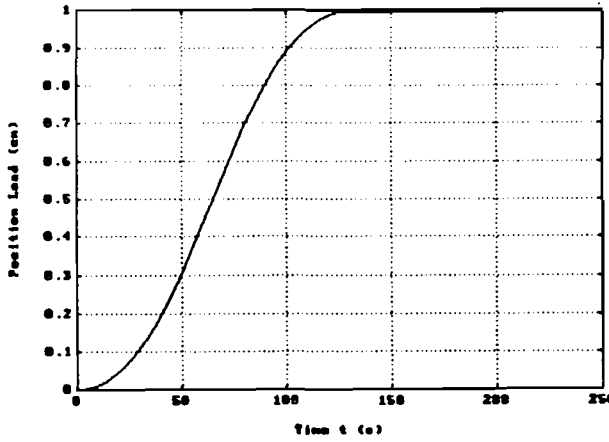

Fig. 5.28 : Simulation Output Signal

The simulation of the error signal is depicted in Fig. 5.29. The design criteria with respect to performance have been specified in Section 4.6 . The absolute maximum position error, 5.5 10^{-5} cm, is within the range we have specified (< 10^{-3} cm). Even we put all the effort in the robustness maximization it was possible to achieve an acceptable position error. Also the settling time (56 seconds) is within the specified 63 seconds. The only problem is that the steady state position error does not reduce to zero. We are dealing with a final position error of about 10^{-6} cm. But this is within the specifications and therefore acceptable . In Fig. 5.23 we can see that low frequencies in the **Signal Tracking** function will be suppressed with about -115 dB = 1.8 10^{-6} . This corresponds with the steady state position error in the simulation of Fig. 5.29 . If we want to reduce the steady state position error further we have to redesign the reference filter V_r to
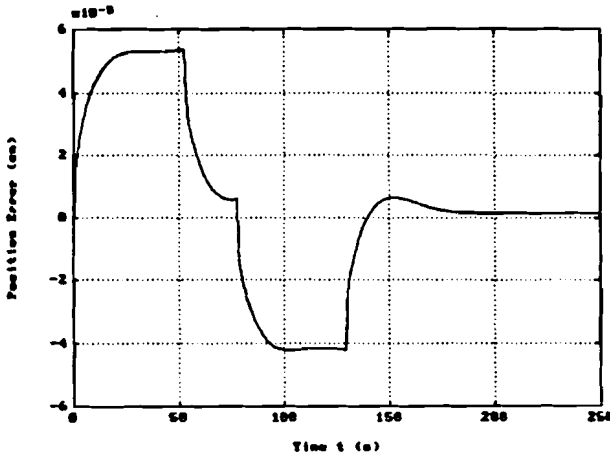
55

improve the Signal Tracking.
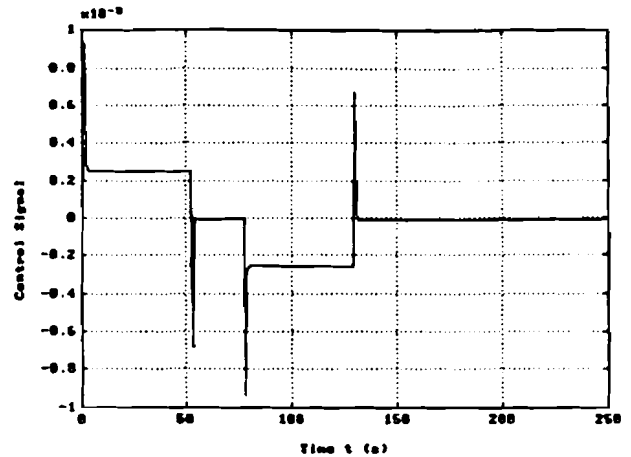

Fig. 5.29 : Simulation Error Signal   Fig. 5.30 : Simulation Control Signal

Another important constraint which we haven't mentioned so far is the **Input Saturation**. Demands about the **Input Saturation** are very difficult to introduce in the frequency domain and result often in very conservative conditions. We didn't specify any input saturation constraints to reduce the conservatism. Of course we have to check wether the control signal 'u_p' would cause saturation or not. Fig. 5.30 depicts the simulation of the control signal. We can see that the shape of the control signal is the same as the acceleration signal we used (Appendix D). Modelling the electromechanical servo system , we used the law of Newton as basic , $T_m - M_r\ddot{x}_p$ (Eq. 2.1). The main purpose of this controller design is to eliminate the resonance peak. For low frequencies we can assume that the law of Newton is still valid. The force of the motor, however, is also equal to $T_m - K_r u_p$ (Eq. 2.4). Therefore, it could be expected that the shape of the control signal 'u_p' is the same as the acceleration signal of the used reference signal at least for low frequencies. The peak values occur due to the steps in the acceleration signal because of the limited bandwidth of the **Signal Tracking** function. These peak vales are limited in Fig. 5.30 . But because of the limited number of points we used in the simulation these peaks might be larger. This can cause problems in a practical implementation because of the limited input signal (Saturation). Using a smoother profile, for example a third order cubic position signal [14], the peak values can be eliminated.

Until now, we have checked only the performance part, which is optimized as far as possible using a constant reference filter V_r . Our basic constraint in this section however, is stability robustness maximization. For this example the controller is robust according to stability for parameter variations of $\tilde{\omega}$ from 0.78 rad/s to 1.6 rad/s . Stability robustness alone however, is not enough. To illustrate the performance robustness, the resonance frequency is varied for the whole stability range. For every value of $\tilde{\omega}$ within the stability range, the maximum position error (positive as well as negative) is derived and the results are depicted in Fig. 5.31 .
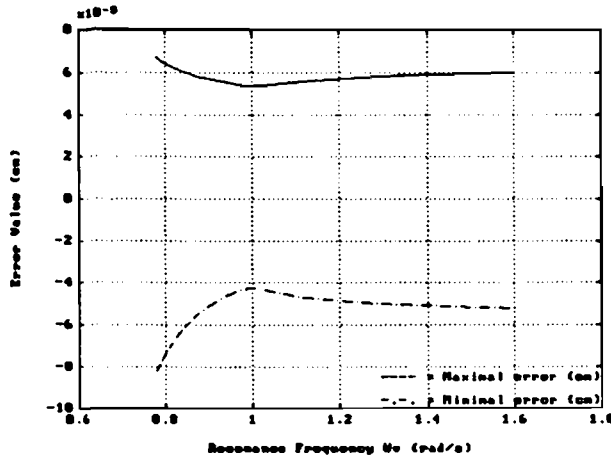
56

Fig. 5.31 :   Performance Robustness ω
              (Maximum Position Error)

An optimal performance robustness, would give a horizontal line for the whole stability range. As we can see in Fig. 5.31, the derived performance robustness so far is not optimal. The maximum position error (positive as well as negative) increases slowly, when the resonance frequency ω is increased.

5.4.3 First Order Reference Filter V_r

In the previous section we optimized the **Signal Tracking** using a constant reference filter V_r. A further optimization is possible, increasing the order of the reference filter V_r. A reference filter of first order, is defined by :

$$V_r = \frac{0.1s + 0.2}{s + 2.10^{-6}}$$ (5.11)

The first order reference filter V_r has been designed in such a way that low frequencies are weighted stronger to reduce the steady state position error further. The zero of V_r at 2 rad/s has been maximized until the increase of the scaling factor γ became significant. With this new reference filter, a solution is found for γ – 1.092 . Comparing this with previous results (V_r = 0.1), we see that γ is hardly increased.

Fig. 5.32 and 5.33 depict again the **Disturbance Reduction** and the **Model Robustness** together with the inverse weighting functions (scaled with γ). The transfer functions match the inverse weighting functions in the same frequency range as we have seen in previous results using a constant reference filter V_r (Fig. 5.25 and 5.26). Changing V_r didn't affect these two functions.
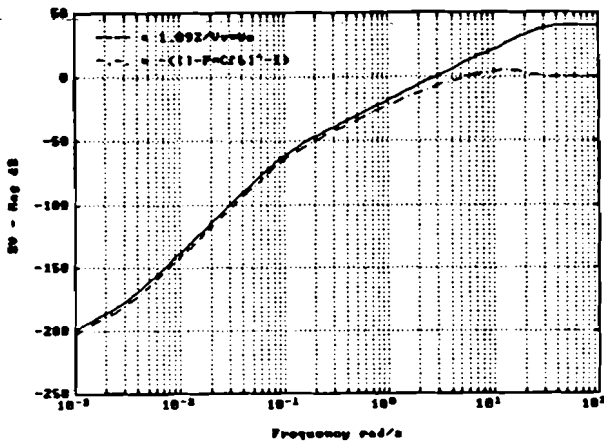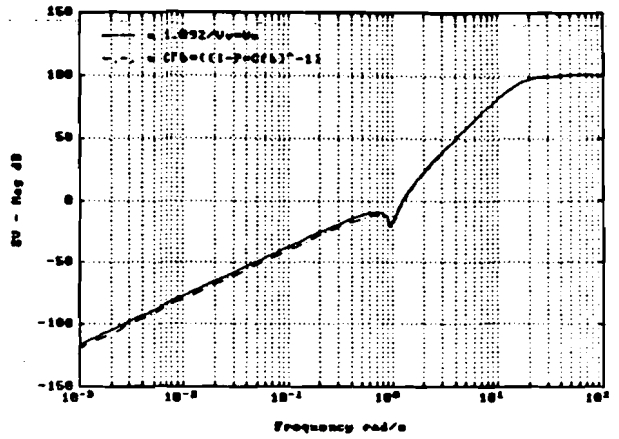
57

Fig. 5.32 : Disturbance Reduction

Fig. 5.33 : Model Robustness

The **Signal Tracking** and the **Input Saturation**, which are affected because of a changing V_r, are depicted in Fig. 5.34 and 5.35. With the chosen reference filter of first order, we see that both transfer functions match the inverse weighting function in the same frequency range around 0.1 rad/s. This means we reached the maximal possible optimization using a first order filter. Comparing Fig. 5.35 with 5.24 , we see that the **Input Saturation** function hardly changed. But the **Signal Tracking** is improved significantly. Low frequencies are weighted much stronger now as before, but the high frequency behaviour of the **Signal Tracking** function is still the same. The hatched area in Fig. 5.34 depicts the gain achieved by optimizing the reference filter V_r compared to Fig. 5.23 .
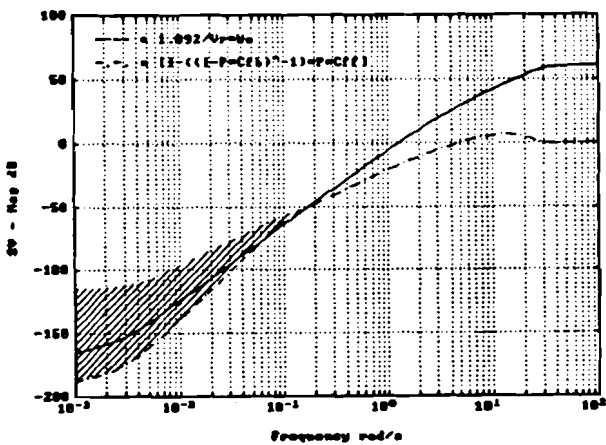

Fig. 5.34 : Signal Tracking
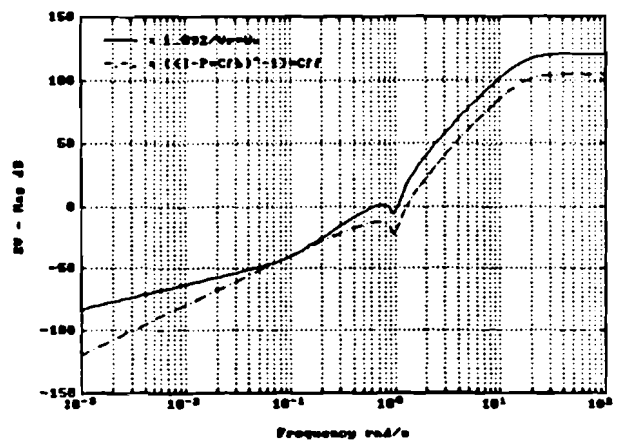

Fig. 5.35 : Input Saturation

We have optimized the **Signal Tracking** as far as possible, because both transfer functions, **Signal Tracking** and **Input Saturation**, match the inverse weighting function in the same frequency range.

58

Table 5.3 :   Feed-forward Controller (gain C_{ff} : 5.494e + 07)
1) Zero at ∞
2) Pole - zero cancellation

Poles C_{ff}		Zeros C_{ff}	
- 3.2167e + 02		- 1.1125e + 41	- 5.8452e + 34 j [1]
- 1.3601e + 01	2.1089e + 01 j	- 1.1125e + 00	8.9071e -01 j
- 1.3601e + 01	- 2.1089e + 01 j	- 1.1125e + 00	- 8.9071e -01 j
- 2.2558e + 01		- 1.0000e -02	9.9995e -01 j [2]
- 1.0000e -02	9.9995e -01 j [2]	- 1.0000e -02	9.9995e -01 j
- 1.0000e -02	- 9.9995e -01 j [2]	- 1.0000e -02	- 9.9995e -01 j [2]
- 7.0711e -02	7.0734e -02 j [2]	- 1.0000e -02	- 9.9995e -01 j
- 7.0711e -02	- 7.0734e -02 j [2]	- 7.0711e -02	7.0711e -02 j [2]
- 2.1212e -03	2.1212e -03 j	- 7.0711e -02	7.0711e -02 j
- 2.1212e -03	- 2.1212e -03 j	- 7.0711e -02	- 7.0711e -02 j [2]
- 2.0000e + 00		- 7.0711e -02	- 7.0711e -02 j

Table 5.4 :   Feed-back Controller (gain C_{fb} : - 3.469e + 07)
1) Zero at ∞
2) Real zero, imaginary part - 0
3) Pole - zero cancellation

Poles C_{fb}		Zeros C_{fb}	
- 3.2167e + 02		- 3.0943e + 25	- 1.2783e -07 j [1]
- 1.3601e + 01	2.1089e + 01 j	- 1.6056e + 00	2.4340e -16 j [2]
- 1.3601e + 01	- 2.1089e + 01 j	- 1.0000e -02	9.9995e -01 j [3]
- 2.2558e + 01		- 1.0000e -02	9.9995e -01 j
- 1.0000e -02	9.9995e -01 j [3]	- 1.0000e -02	- 9.9995e -01 j [3]
- 1.0000e -02	- 9.9995e -01 j [3]	- 1.0000e -02	- 9.9995e -01 j
- 7.0711e -02	7.0707e -02 j [3]	- 7.0689e -02	7.0847e -02 j
- 7.0711e -02	- 7.0707e -02 j [3]	- 7.0711e -02	7.0711e -02 j [3]
- 2.1212e -03	2.1212e -03 j	- 7.0689e -02	- 7.0847e -02 j
- 2.1212e -03	- 2.1212e -03 j	- 7.0711e -02	- 7.0711e -02 j [3]
- 2.0000e + 00 [3]		- 2.0000e + 00 [3]	

The Tables 5.3 and 5.4 contain again the poles and zeros of the controllers for this solution. The order of the controllers found with the aid of the H_∞ theory increased of course with 1, because we increased the order of the reference filter V_r . The extra pole of the controller is exactly the zero of the first order reference filter V_r . But only the

feed-forward controller is affected, the order of the feed-back controller can be reduced again to 6 through pole-zero cancellation. Checking the poles and zeros in the tables, the same numerical problems occur as we noticed before. The Bode-plots of the reduced controllers (satisfying the notes in the header of the tables) are depicted in Fig. 5.36 .
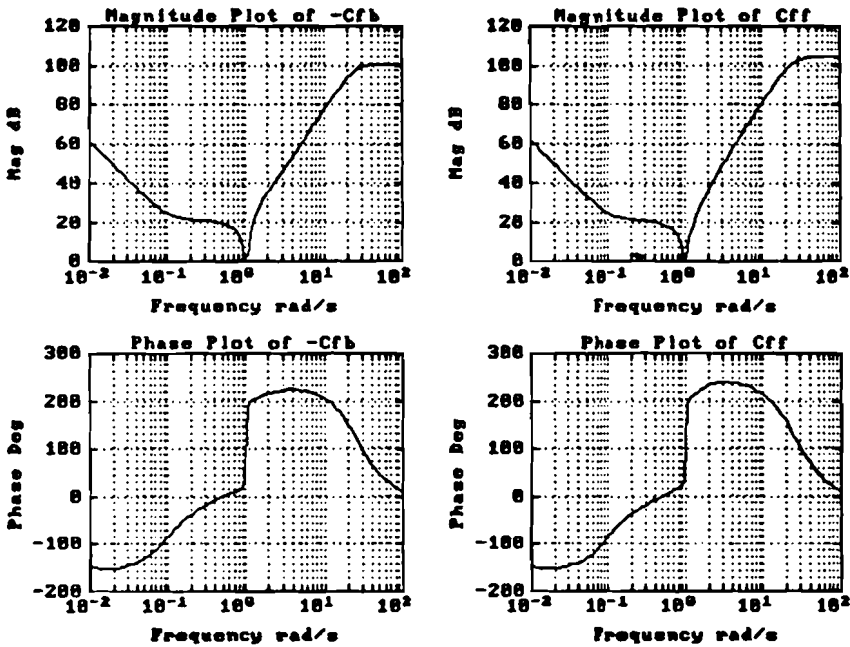

Fig. 5.36 : Bode Plots Controllers

Comparing these results with previous results (Tables 5.1 and 5.2), we can see that the feed-back controller has hardly changed. Only the feed-forward controller is affected by the change of the reference filter V_r . The high frequency behaviour of the feed-forward controller changed slightly compared to the previous results (Fig. 5.27). But we changed the **Signal Tracking** function using a first order reference filter V_r mainly for the lower frequency range, which is not visible in the Bode-plots of Fig. 5.36 .

For this solution, with maximized robustness and optimized performance, we are also interested in other quantities like gain and phase margin. Because we took only variations of the resonance frequency $\tilde{\omega}$ into account in the uncertainty modelling, these quantities can give us additional information, independently of the uncertainty modelling, concerning the stability robustness for variations of other parameters like the gain $\tilde{K}$. For this reason the open-loop Bode plots and the Nyquist curve are depicted in Fig. 5.37 and 5.38 . We can see that the peak value of the process transfer function is completely eliminated using the nominal process parameters. The gain and phase margin are determined from the open-loop bode plot in Fig. 5.37. In this case, the gain and phase margin, gain-margin = 8.928 dB and phase-margin = 45.57° , are sufficient. In Fig. 5.38

besides the Nyquist curve also the M = 1.3 circle is depicted. This circle gives more information about the response-speed and the overshoot of the closed-loop system. When the Nyquist curve does not enter the area, enclosed by the M = 1.3 circle, the step-response and the overshoot (~23 %) of the closed-loop system are acceptable. By the Nyquist stability criterion the closed-loop system is stable if and only if the nyquist plot of the open-loop system does not encircle the point -1 , which is satisfied in our case.
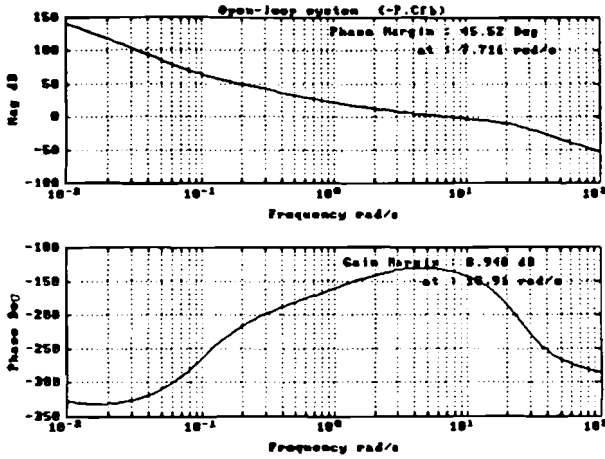
Fig. 5.37 : Open-loop Bode Plots
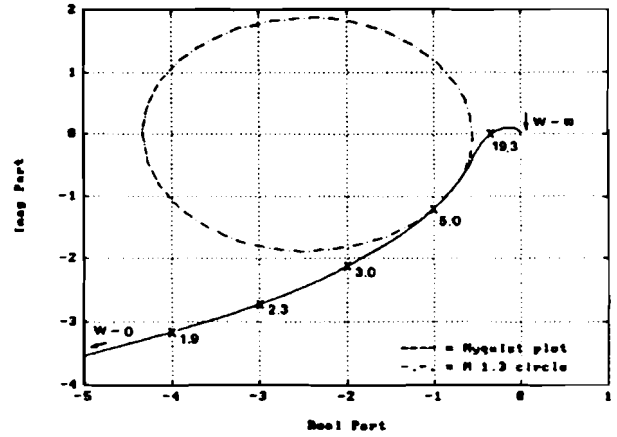
Fig. 5.38 : Nyquist Curve
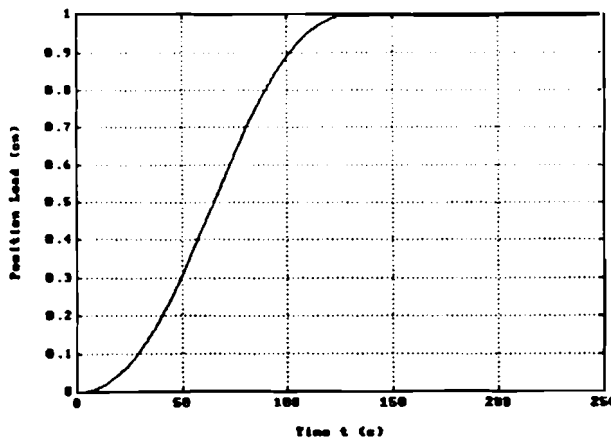
Fig. 5.39 : Simulation Output Signal

The simulations of the important time signals (output, error and control signal) are depicted in Fig. 5.39 , 5.40 and 5.41 . We can see that the new controller has become more active due to the optimization of the reference filter V_r , because the error signal tends to zero during constant acceleration. This has been achieved because frequencies below 0.1 rad/s are suppressed more using a first order reference filter V_r . The hatched

61

area in Fig. 5.34 depicts the gain compared to Fig. 5.23 . Only the steps in the acceleration signal cause peak values in the error signal. But we can see that the main peaks have an opposite direction compared to the acceleration signal. Examining the simulation of the error signal (Fig. 5.40) in more details at for example t = 129 s , we see that the error signal has a peak in positive direction first before the peak in negative direction occurs. The peak in positive direction is due to the positive step in the acceleration signal at t = 129 s. The peak in negative direction however, is due to the increased differentiating action in the feed-forward controller which tries to compensate the first peak. As mentioned earlier, the first peak can be eliminated using a smoother profile as reference signal. But the second peak can only be reduced by reducing the differentiating action in the controller. By optimizing V_r , we are weighting low frequencies stronger as before (Fig. 5.34 : -180 dB = 10^{-9}), which results in a smaller steady state error as can be seen in Fig 5.40 . The final position error is almost reduced to zero now. The settling time is still within the specified 63 seconds. Comparing Fig. 5.30 and 5.41 , we see that the control signal 'u_p' has hardly changed for low frequencies. The peak values however increased with a factor 2 which might cause saturation in a practical implementation.
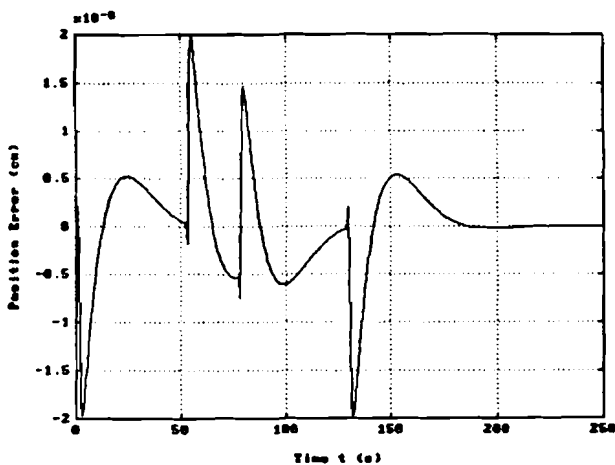
Fig. 5.40 : Simulation Error Signal   Fig. 5.41 : Simulation Control Signal
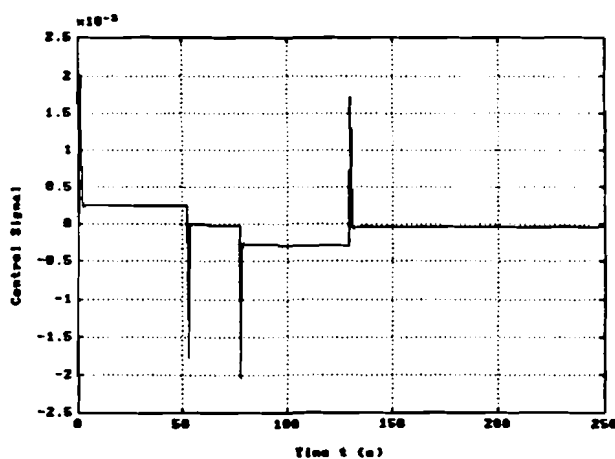
5.5 Robustness Analysis

The standard rules used so far (gain-margin , phase-margin and Nyquist stability criterion) tell us only something about stability robustness. The major problem we are dealing with, is however not the stability robustness but the performance robustness. To get more information about the performance robustness, we derived the maximum and minimum values of the parameters $\bar{K}$, $\bar{\omega}$ and $\bar{\beta}$ for which the closed-loop system is stable. Changing one parameter, the other parameters are set to their nominal values. Table 5.5 shows the results.

Table 5.5 : Parameter Variations

	Minimum Value	Maximum Value
$\bar{K}$	0.021	2.800
$\tilde{\omega}$	0.78	1.60
$\tilde{\beta}$	< 0.001	0.16

The values in Table 5.5 determine the stability ranges for all parameters. To illustrate the performance robustness for parameters variations, we derived the maximum position error (positive as well as negative) for the whole stability range of every parameter. Changing one parameter at the time , we find the results which are depicted in Fig. 5.42 , 5.43 and 5.44 .
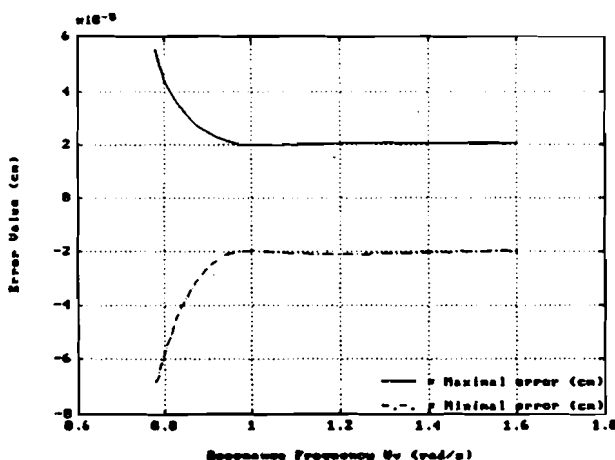
Fig. 5.42 :   Performance Robustness $\tilde{\omega}$
(Maximum Position Error)

The derived performance robustness is acceptable. The maximum position error remains almost constant for all parameter variations in the interesting stability ranges. For the resonance frequency $\tilde{\omega}$ we are only interested in the stability range starting with the nominal value $\omega_o = 1$ rad/s ($\tilde{\omega} > \omega_o$). Comparing Fig. 5.31 with 5.42 , we can see that the performance robustness for variations of $\tilde{\omega}$ has been improved. The maximum position error is decreased due to the optimization of the reference filter V_r . The maximum error value remains almost constant when the resonance frequency is increased.
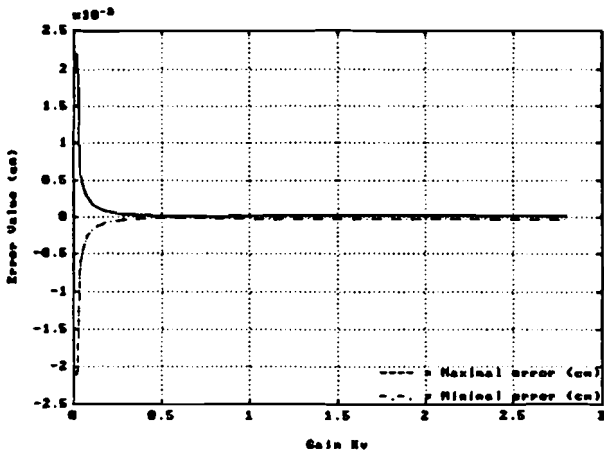
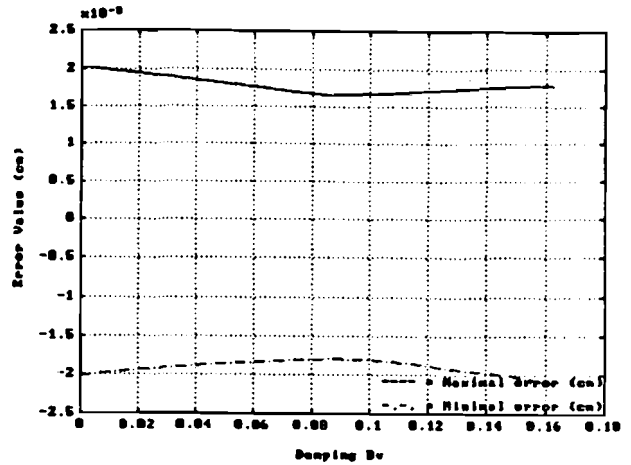Fig. 5.43 : Performance Robustness $\tilde{K}$
(Maximum Position Error)

Fig. 5.44 : Performance Robustness $\tilde{\beta}$
(Maximum Position Error)

The performance robustness of $\tilde{K}$ is almost constant for positive variations. For negative variations however, $\tilde{K}$ shouldn't become smaller than 0.2 to ensure an acceptable performance robustness. For values of $\tilde{K}$ smaller than 0.2 the position error increases significantly.

The derived performance robustness for variations of $\tilde{\beta}$ is good. We have designed the system for the worst case value (β_o = 0.01) and we are basicly interested in the performance behaviour for larger values. But we can see in Fig. 5.44 that for the whole stability range of $\tilde{\beta}$, also for values smaller than the worst case value, the maximum position error changes only slightly for variations of $\tilde{\beta}$.

The information we have showed so far, gives a basic idea about the performance robustness. The situations outlined until now, however, are idealistic in a way that we changed only one parameter at the time. Therefore we will derive the stability as well as the performance robustness for all possible parameter variations. The values in Table 5.5 will be used as the bounds of the parameters ranges and the stepsize is defined as 1/20 part of the interval. To show stability robustness we derived two 3D-graphs, because we have for every combination of $\tilde{K}$ and $\tilde{\omega}$ a minimum and maximum value of $\tilde{\beta}$ for which the closed-loop system is stable. Fig. 5.45 depicts now the upper bound of $\tilde{\beta}$ and Fig. 5.46 the lower bound. The graph is not plotted for those parameter combinations for which the system is unstable.
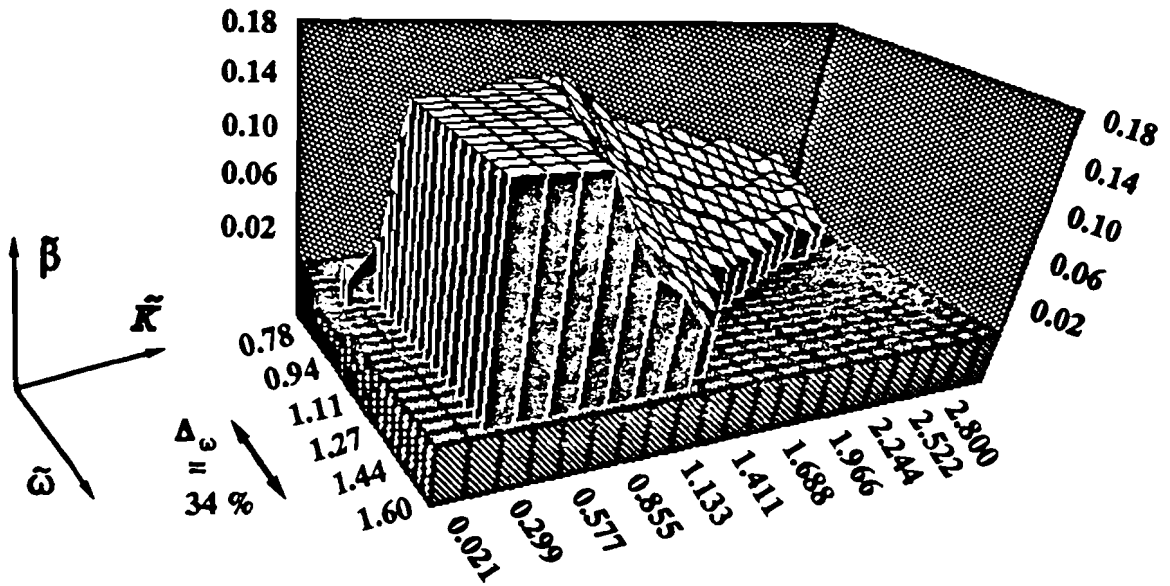
Fig. 5.45 : Stability Robustness ; Upper Bound $\overset{\smile}{\beta}$
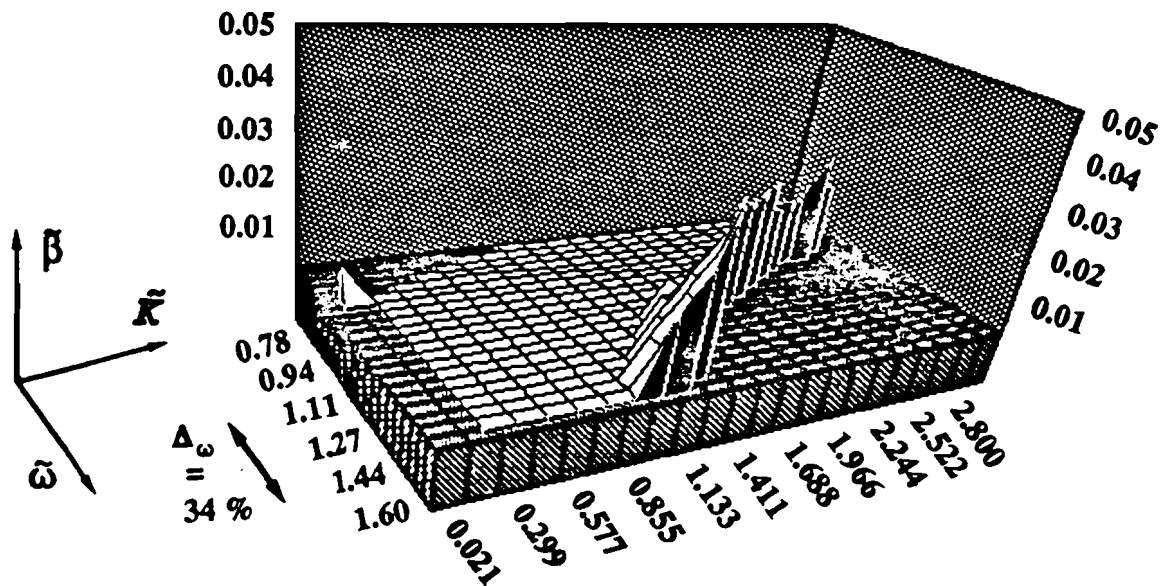
Fig. 5.46 : Stability Robustness : Lower Bound $\overset{\smile}{\beta}$

Examining Fig. 5.45 , we can see that for combinations of extreme high values or extreme low values of the resonance frequency $\tilde{\omega}$ and the gain $\tilde{K}$ the controller is not stabilizing anymore. For all parameter combinations of the process which are stabilized by the controller, the maximum and minimum position error are depicted in Fig. 5.47 . We can see that for some parameter combinations the position error increases significantly. Checking the parameter values, we found that this occurs whenever the gain $\tilde{K}$ becomes smaller than 0.2 . But we concluded already from Fig. 5.43 that $\tilde{K}$ shouldn't become smaller than 0.2 , to keep the position error small enough. All parameter combinations with $\tilde{K}$ greater than 0.2 are bounded by the box depicted in Fig. 5.47 . We

65

can see that an acceptable performance robustness is achieved.
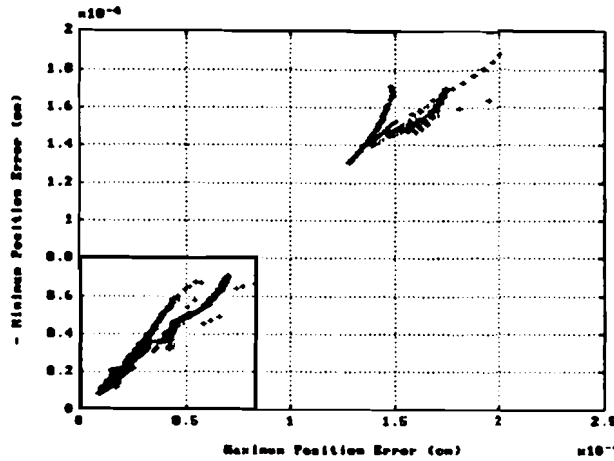
Fig. 5.47 : Performance Robustness (Maximum position error)

We used stable factor perturbations to design a controller which is robust with respect to stability as well as performance. According to the theory, the maximum possible variation of the resonance frequency $\bar{\omega}$ for which the controller is robust is 34% . The final controller however, is robust for a much larger range of variations of the resonance frequency $\bar{\omega}$ (60 %). We can conclude that the conditions derived using stable factor perturbations are sufficient but not necessary.

The derived solution ensures robustness with respect to stability as well as performance for variations of all parameters. Basicly, there is one degree of freedom left to improve the result, redesigning the disturbance filter V_v. As mentioned before, the disturbance filter V_v can be used to manipulate the phase margin derived from the open-loop system. The chosen filter , b = 0.1 , is optimal which can be explained as follows. In Fig. 5.37 , a breakpoint in the magnitude plot around 0.1 (= b) rad/s is clearly visible. The phase margin is build up after this breakpoint. The value of b is chosen in such a way that a phase margin slightly larger than 45° is achieved. Increasing b will result in a phase margin smaller than 45° which is not acceptable and decreasing b makes the phase margin unnecessary larger than 45° .

A last remark about the controllers. We have chosen a two-degree-of-freedom configuration, using a feed-back as well as a feed-forward controller, to improve the overall system behaviour with respect to robustness maximization and performance optimization. Due to the fact that the Model Robustness criterion is dominant in our design, it was only possible to improve the Signal Tracking, using a first order reference filter V_r , for low frequencies. This frequency range is, however not depicted in the Bode-plots of the controllers. Therefore it might seem that the feed-back and the feed-forward controller are almost the same (Fig. 5.36). This is in fact only true in the frequency range around the resonance frequency where the Model Robustness is dominant.

5.6 Summary Robustness Design

The robustness design is structured in the design sequence of the filters. The disturbance filter V_v is used on one hand to derive uncertainty models and on the other hand to achieve a phase margin just above 45°. Using the chosen disturbance filter V_v we find robustness constraints for the weighting filters. The envelop description of the uncertainty Δ_s with the process input weighting filter W_u should be optimized to reduce the conservatism in the design. The error weighting filter W_e has to be designed in such a way that it is an envelop description of the uncertainty Δ_i, but improves the signal tracking as well. The final step in the design is a further optimization of the signal tracking using the reference filter V_r.

With the proposed robustness approach it is possible to design controllers which are robust with respect to stability as well as performance for variations of all process parameters. To achieve robustness for variations of process parameters, stable factor perturbations have been used to derive uncertainty models. The derived robustness constraints, however, lead only to sufficient and not necessary conditions. According to the theory the resonance frequency $\bar\omega$ can vary only 34%. Simulations afterwards show however that variations of $\bar\omega$ up to 60% are acceptable for performance robustness.

The achieved stability robustness for variations of the process parameters is much larger than specified in the design criteria ($0.021 \leq \bar K \leq 2.8$ with $K_o - 1$, $0.078 \leq \bar\omega \leq 1.6$ with $\omega_o - 1$ *rad/s* and $0.001 \leq \bar\beta \leq 0.16$ with $\beta_o - 0.01$). The performance robustness has been simulated for all possible parameter combinations for which the closed-loop system is stable. For this purpose we used a second order position signal as reference signal (Motion time = 129 seconds). The maximum position error during the movement (Displacement of 1 cm) is smaller than 8.10^{-5} cm . The only condition is that the disturbed process gain has to be $\bar K > 0.2$. The steady state position error is reduced to 10^{-9} cm. The design criteria were 10^{-3} cm for the maximum position error respectively 10^{-6} cm for the steady state position error. Also the obtained settling time of 56 seconds is within the specifications (63 seconds).

By applying the H_∞ theory we obtain controllers which are of 11th order. Because of pole-zero cancellation we can reduce the feed-back controller to order 6 and the feed-forward controller to order 7.

6 Alternative Design Performance Approach

6.1 Introduction

Until now, the design has been focused entirely on the robustness constraints. We used stable factor perturbations to design a controller which is robust with respect to stability as well as performance. It turned out however that the conditions derived with stable factor perturbations are sufficient but not necessary. For this reason we will describe in this chapter an alternative design method. We will use no robustness information at all and focus our design entirely on the signal tracking performance. Finally we will compare the results obtained using the performance approach with the results of the robustness approach.

6.2 Design Strategy for Performance Approach

As we did for the robustness approach, we will introduce again a global design strategy but now suitable for the performance approach. The design sequence of the several filters is quite different. The design can be divided in two parts, the performance maximization and the robustness optimization. The first part has the following phases :

1) Design the disturbance filter V_v and the process input weighting filter W_u in such a way that the **Disturbance Reduction** criterion, defined by :

$$M_{11} = - W_e (I - P_o C_{fb})^{-1} V_v \; ,$$

the **Input Saturation** criterion, defined by :

$$M_{22} = W_u (I - P_o C_{fb})^{-1} C_{ff} V_r$$

and the **Model Robustness** criterion, defined by :

$$M_{21} = W_u C_{fb} (I - P_o C_{fb})^{-1} V_v$$

are not the limiting functions.

68

2)   The control system will be excited with a known reference signal. Characterize the reference filter V_r with the power spectral density of this reference signal.

3)   Maximize the **Signal Tracking** performance using the error weighting filter W_e. This can be achieved by weighting lower frequencies stronger and increase the bandwidth of the filter W_e as much as possible. Optimize W_e until a solution is found with $\gamma \leq 1$.

If the performance is maximized, the **Signal Tracking** criterion, defined by :

$$M_{12} - W_e \left[I - \left(I - P_o C_{fb} \right)^{-1} P_o C_{ff} \right] V_r$$

is the limiting function. The final transfer function from 'r' to 'e' will match the inverse weighting function $V_r W_e$ (scaled with γ) for a certain frequency range.

The second part of the design is the robustness optimization which can be divided in the following phases :

4)   Optimize the robustness using the disturbance filter V_v until the **Disturbance Reduction** criterion becomes the limiting function. This filter can be used mainly to optimize the shape of the open-loop Bode plot and achieve a phase margin just above 45°.

5)   Using the last degree of freedom, we can improve the **Model Robustness** by optimizing the process input weighting filter W_u. This can be done until either the **Input Saturation** criterion or/and the **Model Robustness** criterion will become the limiting function.

With the performance approach presented here, we didn't use any robustness information (Eq. 4.32) at all. Of course we have to check afterwards for which parameter variations of the process the controller is robust with respect to stability as well as performance.

6.3 Performance Maximization

In the previous section we introduced a general design strategy for the performance approach. Our goal in this section is to derive a controller for which the maximum position error during the movement is as small as possible.

To avoid that the **Input Saturation**, the **Disturbance Reduction** or the **Model Robustness** are the limiting functions (Design step 1), we will choose the disturbance filter V_v and the process input weighting filter W_u as follows :

69

$$V_v = \frac{0.01\left(s^2 + 0.1\sqrt{2}s + 0.01\right)}{s^2}$$ (6.1)

$$W_s = 0.001$$ (6.2)

The zeros of the disturbance filter V_v are the same as the one we have chosen in Chapter 5. Experiments showed that the decrease of the gain to $k_v = 0.01$ is necessary to avoid limitations in the **Disturbance Reduction**.

6.3.1 Design of Reference Filter V_r

In the previous chapter we used the robustness approach to derive a controller which is robust with respect to stability and performance. We didn't add any information to the system about the known reference signal, because a further performance optimization using the reference filter V_r was not possible. We could only improve the **Signal Tracking** using V_r for the lower frequencies but not in the important frequency range around the resonance frequency $\omega_e = 1$ rad/s . To reach an optimal signal tracking, we have to add this information to the system. The power spectral density of the used reference signal, described in Appendix D, is depicted in Fig. 6.1 .
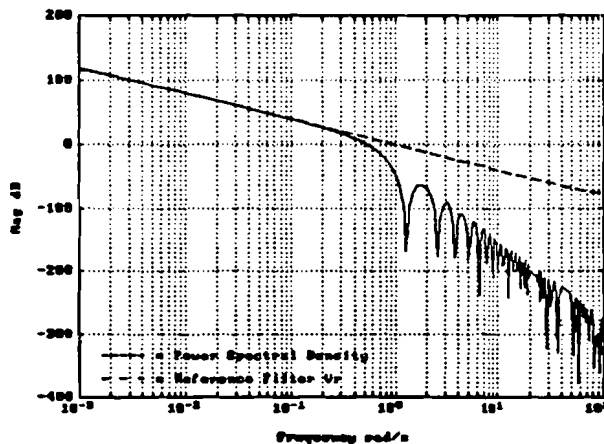
Fig. 6.1 : Power Spectral Density of Second Order Profile

We can see that the slope of the power spectral density for the lower frequencies is -2. Because of the limited sampling time in the frequency domain which is used to derive the power spectral density, the spectrum is not continuous anymore for high frequencies. In this high frequency range we have in fact a slope of -6 (Fig. 6.1). A proper characterization of this power spectral density for low frequencies is a second order filter (Design step 2). An optimal fit of the power spectral density can be achieved

using a 6th order reference filter V_r. Increasing the order of the reference filter V_r by 4 however, will also increase the controller order by 4 . To avoid this significant increase of the controller order we will use a second order reference filter V_r . Suppose we take :

$$V_r - \frac{10^{-4} \left(s^2 + 10^2 \sqrt{2}s + 10^4 \right)}{s^2 + 10^{-3}\sqrt{2}s + 10^{-6}} \qquad (6.3)$$

The poles of the reference filter V_r are chosen in such a way that frequencies below 10^{-3} rad/s are weighted with 120 dB to ensure that the steady state error will reduce to zero. The placing of the zeros has been determined by numerical limitations. Increasing the breakpoint at 10^2 rad/s due to the zeros of V_r is not possible because of numerical problems which occur solving the Riccati equations.

6.3.2 Optimization of Error Weighting Filter W_e

After designing the reference filter V_r , the next step (Design step 3) in our design is to maximize the **Signal Tracking** using the error weighting filter W_e . The bandwidth of the filter W_e is increased as far as possible (to decrease the maximal position error during the movement) and the low frequency behaviour is set to decrease the steady state position error even more. The optimal choice of the error weighting filter W_e for which a solution is found with $\gamma \leq 1$:

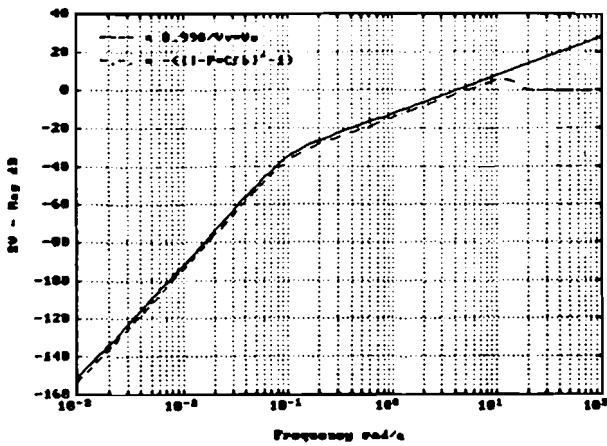$$W_e - \frac{0.01s + 400}{s + 4.10^{-4}} \qquad (6.4)$$
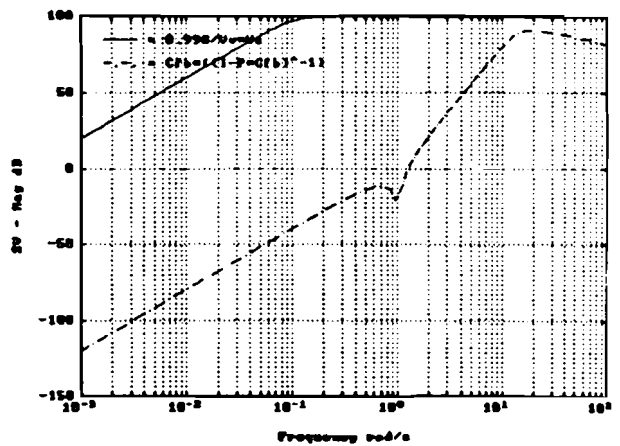

Fig. 6.2 : Disturbance Reduction

Fig. 6.3 : Model Robustness

Using the defined filters, a solution is found for $\gamma = 0.998$. All the transfer functions together with the corresponding inverse weighting functions are depicted in Fig. 6.2 , 6.3 , 6.4 and 6.5 .
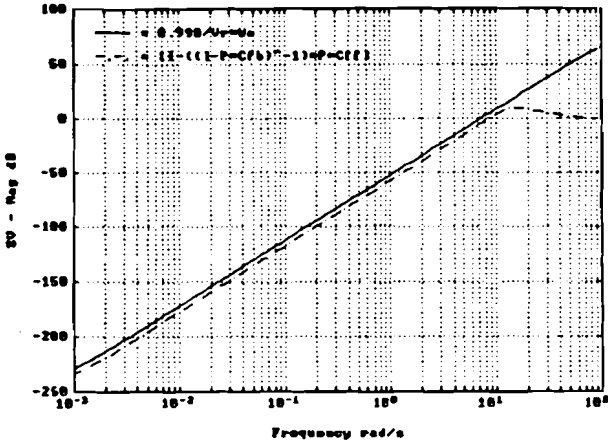
Fig. 6.4 : Signal Tracking   Fig. 6.5 : Input Saturation
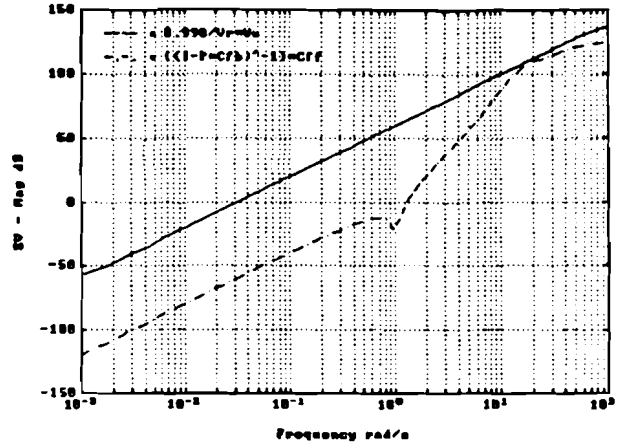
Our primary design function in this performance approach is the **Signal Tracking**. Comparing Fig. 5.34 and 6.4 , we can see that the bandwidth of the **Signal Tracking** function has increased and frequencies around and below the resonance frequency $\omega_o = 1$ rad/s are suppressed stronger. Increasing the bandwidth of the **Signal Tracking** function and suppressing the corresponding frequencies stronger will decrease the maximum position error during the movement as well as the settling time.

Nevertheless , the **Disturbance Reduction** and the **Input Saturation** functions have reached their bounds as well (Fig. 6.2 and 6.5). Experiments showed however, that these criteria are not the limiting functions in this design.

6.4 Robustness Optimization

After optimizing the **Signal Tracking** criterion we have to improve the robustness with respect to stability and performance.

6.4.1 Optimization of the Disturbance Filter V_v

Continuing our design (Design step 4) , we have to improve the **Disturbance Reduction** by optimizing the disturbance filter V_v . As mentioned earlier, the main purpose of the disturbance filter V_v is to characterize the model disturbances and to achieve a phase margin just above 45° . For this reason we will show first the open-loop Bode plot (Fig. 6.6) derived with the results of the previous section (Using the filters in Eq. 6.1 , 6.2 , 6.3 and 6.4).

72
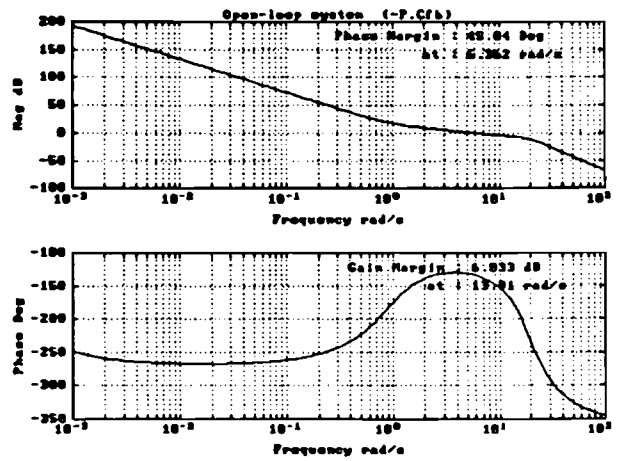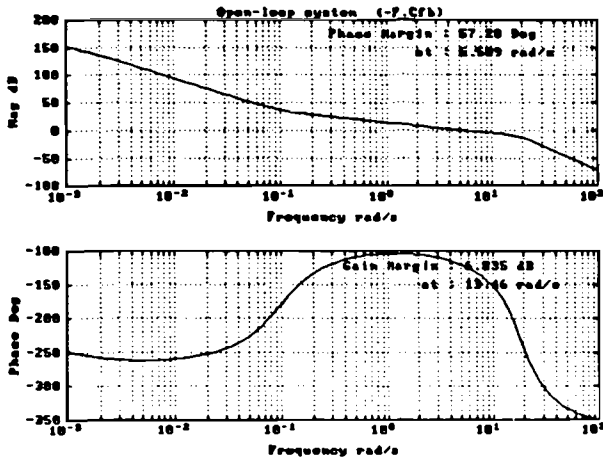
Fig. 6.6 : Open-loop Bode Plot (b = 0.1)   Fig. 6.7 : Open-loop Bode Plot (b = 1)

Table 6.1 : Margins in relation to zeros of disturbance filter V_v

b (in rad/s)	Phase Margin (in degrees)	Gain Margin (in dB)
0.1	57.28	6.853
0.2	55.58	6.724
0.3	53.99	6.620
0.4	52.50	6.521
0.5	51.10	6.427
0.6	49.79	6.339
0.7	48.57	6.256
0.8	47.39	6.179
0.9	46.18	6.105
1.0	45.04	6.033
1.1	43.98	5.964

We have achieved a phase margin of 57.28° . The breakpoint in the magnitude plot at 0.1 rad/s is clearly visible. Because the phase margin is build up after this breakpoint, the resulting phase margin is much larger than the necessary 45° . If we use the complex conjugated zeros as variable (b) the disturbance filter V_v in Eq. 6.1 is given by :

$$V_v = \frac{0.01 \left(s^2 + b\sqrt{2}s + b^2 \right)}{s^2} \tag{6.5}$$

To show the influence of the disturbance filter V_v on the phase margin, Table 6.1 contains the values of b, which is the cut-off frequency of V_v caused by the zeros, and the corresponding phase and gain margin.

From Table 6.1 , it is obvious that if we try to achieve a phase margin just above 45°, an appropriate choice for the placement of the zeros is at b = 1 rad/s . The open-loop Bode plot for this solution is depicted in Fig. 6.7 . The move of the breakpoint in the magnitude plot from 0.1 rad/s to 1 rad/s is clearly visible. Increasing the bandwidth of the filter V_v increased also the magnitude of the open-loop Bode plot for lower frequencies, which results in a stronger suppression of external disturbances for these frequencies. For this new situations, the four transfer functions with the corresponding inverse weighting functions are depicted in Fig. 6.8 , 6.9 , 6.10 and 6.11 .
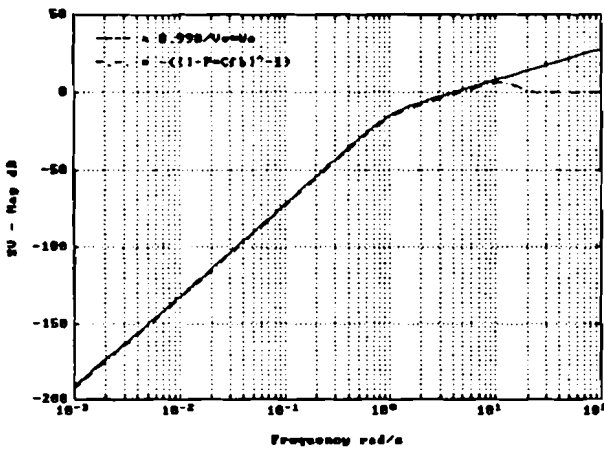
Fig. 6.8 : Disturbance Reduction
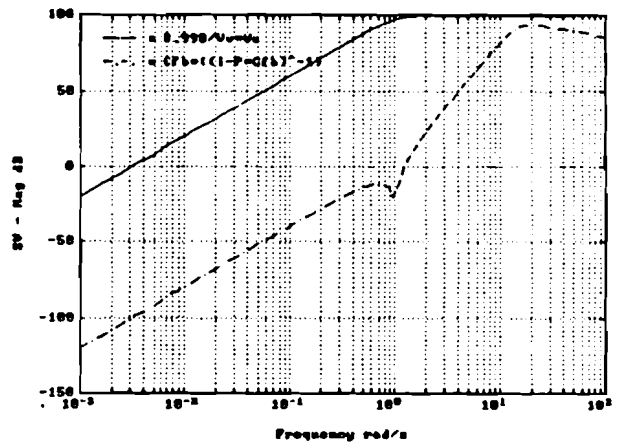
Fig. 6.9 : Model Robustness
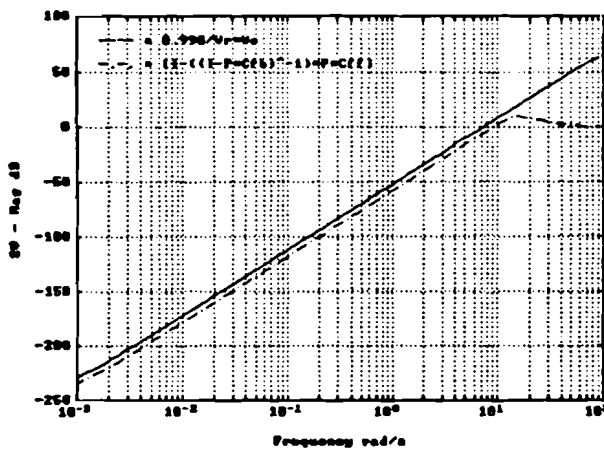
Fig. 6.10 : Signal Tracking
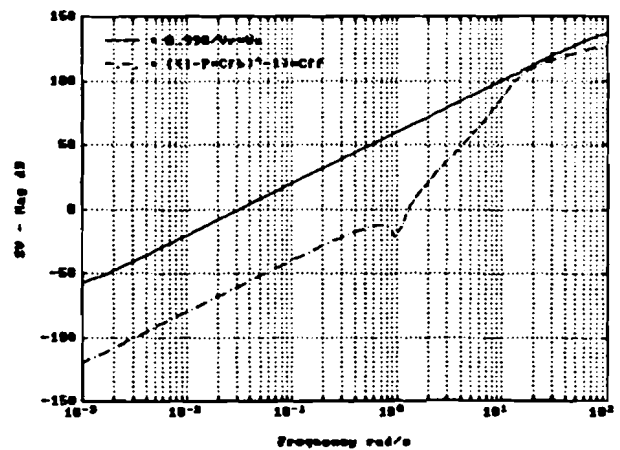
Fig. 6.11 : Input Saturation

74

Comparing the new transfer functions with those of Section 6.3.2 (Fig. 6.2 - 6.5) , we can see that only the **Disturbance Reduction** function is affected by changing the disturbance filter V_v . The transfer function from 'v' to 'e' still matches the inverse weighting function $\hat{V}_v W_e$ for frequencies up to 10 rad/s, but lower frequencies are suppressed stronger as before.

6.4.2 Optimization of Process Input Weighting Filter W_u

There is one degree of freedom left to improve the **Model Robustness** (Design step 5), using the process input weighting filter W_u . Considering Fig. 6.9 and 6.11 , there are still some possibilities left to improve the filter W_u , especially for lower frequencies. Only the **Input Saturation** function matches the inverse weighting function $V_r W_u$ almost at 16 rad/s. In Fig. 6.11 we see that in the frequency range from 1.5 rad/s to 16 rad/s the difference in slope of the **Input Saturation** function and the corresponding inverse weighting function is -2. Therefore we choose a second order weighting filter W_u to optimize the robustness. Experiments showed that an appropriate choice for W_u is :

$$W_u = \frac{0.001 \left(s^2 + 16\sqrt{2}s + 256 \right)}{s^2 + 0.02s + 1} \tag{6.6}$$
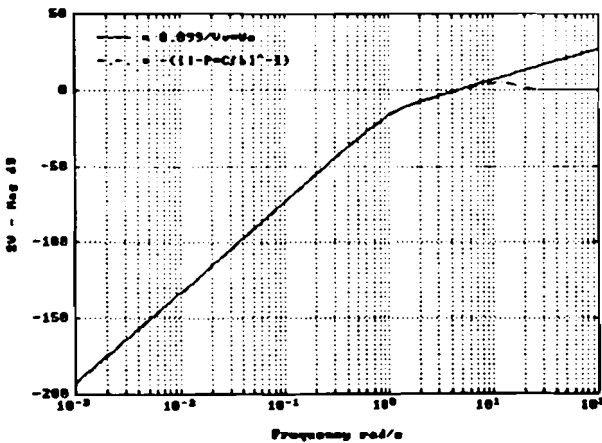
Fig. 6.12 : Disturbance Reduction   Fig. 6.13 : Model Robustness
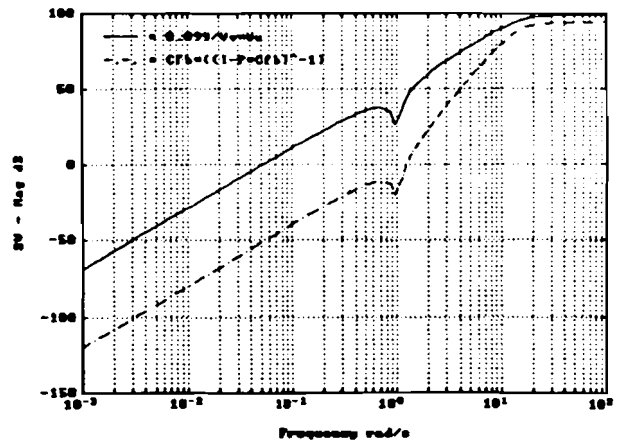
With this new process input weighting filter, a solution is found for $\gamma = 0.899$. Fig. 6.12 , 6.13 , 6.14 and 6.15 depict the new transfer functions with the corresponding inverse weighting functions.

In our design, the **Input Saturation** criterion has become the limiting function. Looking at Fig. 6.15 , it seems that further optimization might be possible. Considering

75

the whole frequency range however, a further optimization results in $\gamma > 1$. Because the **Input Saturation** criterion becomes the limiting function before the **Model Robustness** criterion, we cannot improve the robustness using the process input weighting filter W_u. All possible degrees of freedom have been used already and all transfer functions, except the **Model Robustness** function, match the corresponding inverse weighting function. This implies, using the proposed performance approach, a further optimization of the **Model Robustness** is not possible.
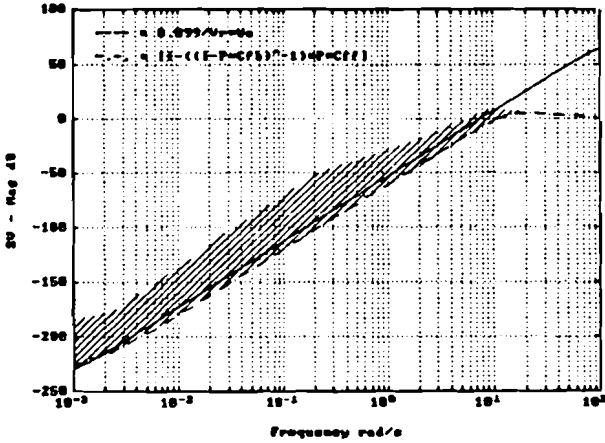
Fig. 6.14 : Signal Tracking
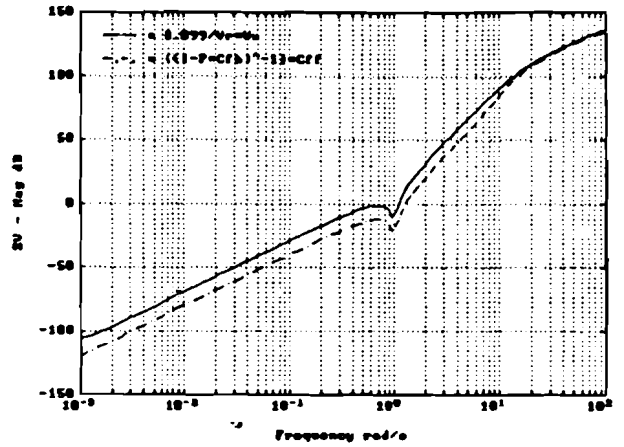
Fig. 6.15 : Input Saturation

Table 6.2 : Feed-forward Controller (gain C_{ff} : 7.25e + 10)
1) zero at ∞
2) Pole - zero cancellation

Poles C_{ff}		Zeros C_{ff}	
- 9.7268e + 03		4.1061e + 43	- 1.9935e + 39 j [1]
- 1.0965e + 01	1.7321e + 01 j	- 5.1376e + 00	5.1696e + 00 j
- 1.0965e + 01	- 1.7321e + 01 j	- 5.1376e + 00	- 5.1696e + 00 j
- 1.9113e + 01		- 7.0711e -01	7.0711e -01 j
- 1.0000e -02	9.9995e -01 j [2]	- 7.0711e -01	- 7.0711e -01 j
- 1.0000e -02	- 9.9995e -01 j [2]	- 1.0000e -02	- 9.9995e -01 j [2]
- 4.0000e -04		- 1.0000e -02	- 9.9995e -01 j
- 7.0711e + 01	7.0711e + 01 j	- 1.0000e -02	9.9995e -01 j [2]
- 7.0711e + 01	- 7.0711e + 01 j	- 1.0000e -02	9.9995e -01 j

The Tables 6.2 and 6.3 contain the poles and the zeros of the derived controllers for this solution. The order of the augmented plant is 9, so the basic controllers found with the H_∞ theory have also order 9. Inspection of the values in the tables show, that both

76

controllers have a zero which can be assumed to be at ∞ . The poles and zeros which can be reduced through pole-zero cancellation are marked as well.

Table 6.3 :   Feed-back Controller (gain C_{fb} : -4.889e+08)
1) zero at ∞
2) Pole - zero cancellation

Poles C_{fb}		Zeros C_{fb}	
- 9.7268e+03		- 4.9362e+24	- 7.4140e+22 j [1]
- 1.0965e+01	1.7321e+01 j	- 6.2753e -01	- 6.2755e -01 j
- 1.0965e+01	- 1.7321e+01 j	- 6.2753e -01	6.2755e -01 j
- 1.9113e+01		- 1.0000e -02	- 9.9995e -01 j [2]
- 1.0000e -02	9.9995e -01 j [2]	- 1.0000e -02	- 9.9995e -01 j
- 1.0000e -02	- 9.9995e -01 j [2]	- 1.0000e -02	9.9995e -01 j [2]
- 4.0000e -04		- 1.0000e -02	9.9995e -01 j
- 7.0711e+01	7.0711e+01 j [2]	- 7.0711e+01	- 7.0711e+01 j [2]
- 7.0711e+01	- 7.0711e+01 j [2]	- 7.0711e+01	7.0711e+01 j [2]

The Bode plots of the reduced controllers (satisfying the notes in the header of the tables) are depicted in Fig. 6.16 . In contradistinction to Chapter 5 is the difference between the feed-back and the feed-forward controller clearly visible.
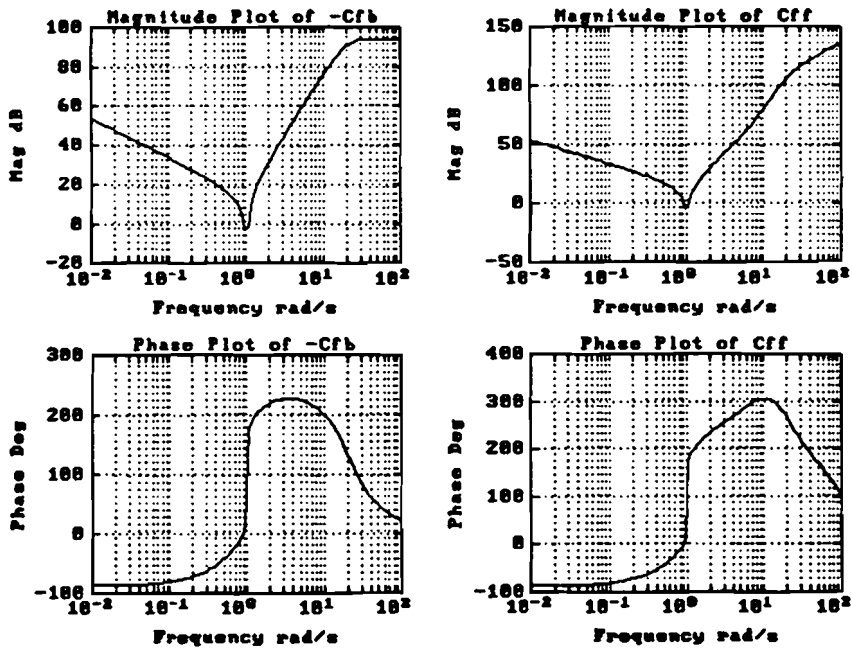
Fig. 6.16 : Bode Plots Controllers

If we look at Fig. 6.17 and 6.18 , which depict the open-loop Bode plot respectively the Nyquist curve for this solution, we can see that the phase margin has increased slightly, but the increase of the gain margin is significant. Due to this increased gain margin we can expect a larger stability range for the gain $\tilde{K}$.
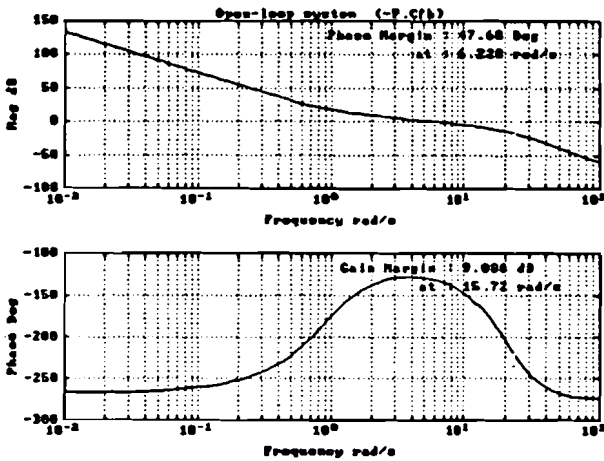
Fig. 6.17 : Open-loop Bode Plots
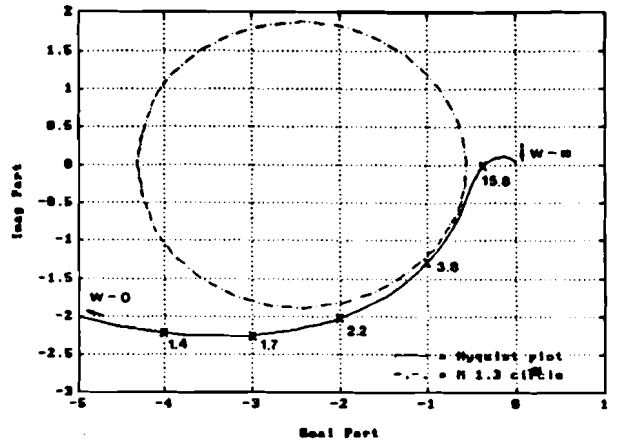
Fig. 6.18 : Nyquist curve

Using the optimized shaping and weighting filters derived with the performance approach, the simulations of the output, the error and the control signal are depicted in Fig. 6.19 , 6.20 and 6.21 .
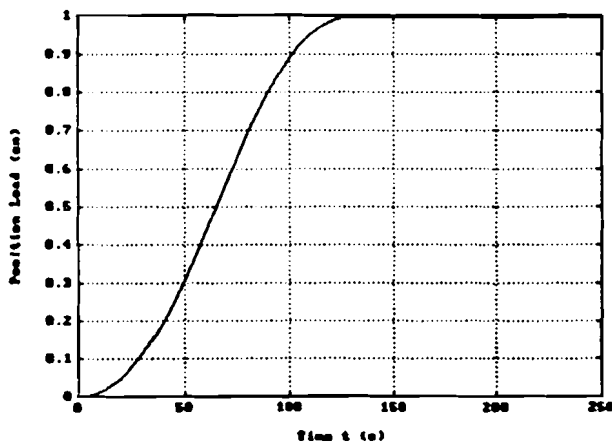
Fig. 6.19 : Simulation Output Signal

Because of the increased bandwidth of the **Signal Tracking** function the maximum position error as well as the settling time have been decreased significantly as we expected. The maximum position error reduces almost to zero when the acceleration signal is constant due to the fact that the bandwidth of the **Signal Tracking** function has been increased and frequencies below the bandwidth are suppressed stronger. This can

78

be explained by comparing the **Signal Tracking** functions in Fig. 5.34 and 6.14 together with the corresponding simulations of the error signal. The hatched area in Fig. 6.14 depicts the difference between the **Signal Tracking** functions in the robustness design and the performance design. In the performance approach the intersection with 0 dB of the **Signal Tracking** is at 10 rad/s (Fig. 6.14), in contradistinction with the robustness approach where the intersection was at 5 rad/s (Fig. 5.34). Another reason of the decrease of the maximum position error is the stronger suppression of the frequencies below the bandwidth, for example 60 dB in Fig. 6.14 and only 20 dB in Fig. 5.34 at 1 rad/s.
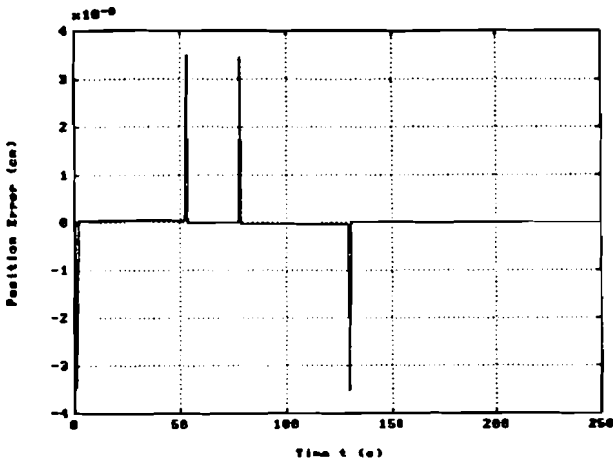
Fig. 6.20 : Simulation Error Signal   Fig. 6.21 : Simulation Control Signal
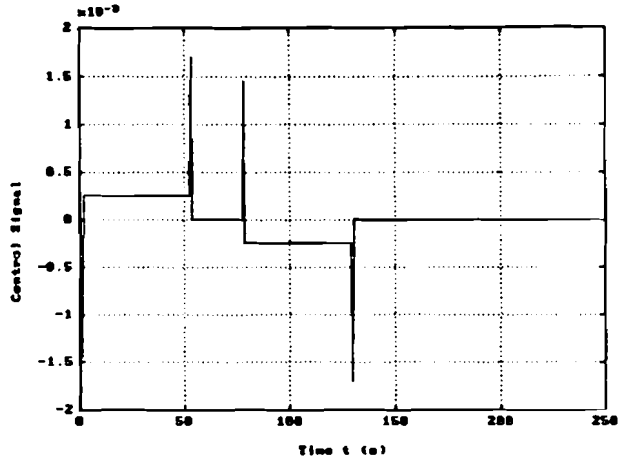
The peak values in the error signal are caused by the large differentiating action in the feed-forward controller (Fig. 6.16) because the direction of the peaks is opposite to the direction of the steps in the acceleration signal. The compensation by the controller of the step in the acceleration signal is too large which results in this negative affect. We noticed this problem already in Section 5.4 . In Fig. 5.40 we saw that the error signal tends first in the same direction as the step in the acceleration signal and then in the opposite direction due to the large differentiating action in the feed-forward controller . This affect has only been increased because of a further increase of the differentiating action in the feed-forward controller. The only way to avoid these problems is to reduce this differentiating action.

6.5 Robustness Analysis

We didn't include any robustness information at all and therefore we are of course interested in the robustness behaviour of the derived controllers with respect to stability as well as performance. To get more information about stability robustness we derived the maximal and minimal value of the parameters $\bar{K}$, $\bar{\omega}$ and β for which the closed-loop system is stable. The values in Table 6.4 determine the stability robustness range

for variations of the process parameters. The values of both design methods, the robustness as well as the performance approach have been included. The stability ranges for variations of the process parameters for both methods are almost the same. The only difference is the increase of the minimum value of $\tilde{K}$ and the decrease of the maximum value of $\tilde{\beta}$ in the performance design.

Table 6.4 : Parameter Variations

Process Parameter	Performance Design		Robustness Design	
	Minimum Value	Maximum Value	Minimum Value	Maximum Value
$\tilde{K}$	0.12	2.85	0.021	2.80
$\tilde{\omega}$	0.79	1.61	0.78	1.60
$\tilde{\beta}$	0.001	0.084	0.001	0.16

To illustrate the performance robustness for parameter variations, we derived the maximum position error (positive as well as negative) for the whole stability range of every parameter (Table 6.4), changing one parameter at the time and setting the other two parameters to their nominal values. The results are depicted in Fig. 6.22 , 6.23 and 6.24 .
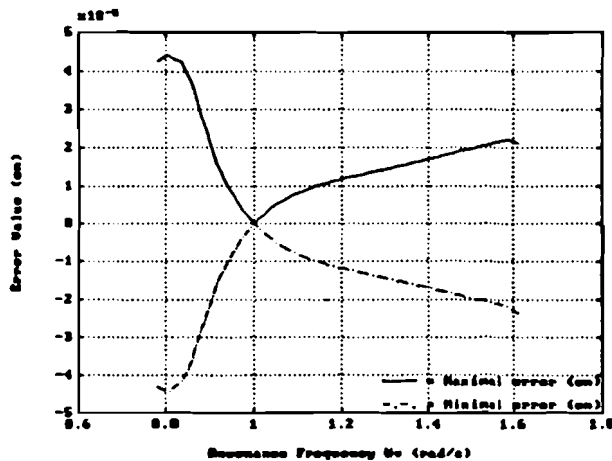
Fig. 6.22 :   Performance Robustness $\tilde{\omega}$
(Maximum Position Error)
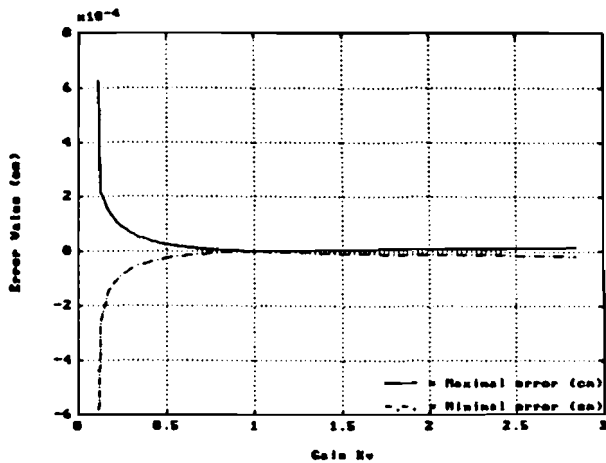
Fig. 6.23 : Performance Robustness $\tilde{K}$
(Maximum Position Error)
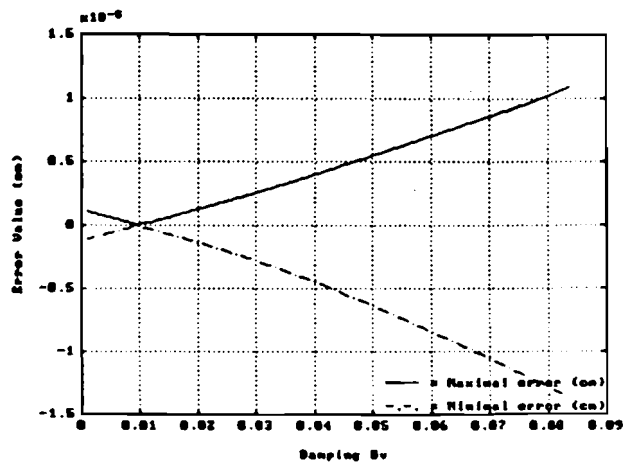
Fig. 6.24 : Performance Robustness $\tilde{\beta}$
(Maximum Position Error)

The stability range of the process parameters is almost the same for both design methods. But the controller is not robust at all with respect to performance. If the parameters vary from the nominal value, the maximum position error increases significantly (Fig. 6.22 , 6.23 and 6.24). Looking at Fig. 6.22 , performance robustness for variations of $\tilde{\omega}$, we see that the maximum position error which occurs if $\tilde{\omega}$ is increased as much as possible, is about the same size as the optimal error value we achieved in the previous chapter (Fig. 5.39). Comparing Fig. 6.23 and 5.40 we see that the robustness range for variations of the gain $\tilde{K}$ with respect to performance has become much smaller too. The same is true for the variations of the damping $\tilde{\beta}$.

Because we put all the effort in performance maximization for the nominal process parameters, it was not possible to achieve a controller which is robust with respect to performance for a wide range of parameter variations. The controller has been designed for a very small range of process parameters for high performance applications. But as soon as the disturbed process is outside the specified range the performance behaviour will decrease significantly.

Until now, we changed only one parameter at the time. Changing all parameters at once, which gives more realistic information, we can derive two 3D-graphs showing the values of the parameters for which the closed-loop system is stable. The values in Table 6.4 will be used as bounds of the parameter ranges. The stepsize is defined as 1/20 part of the interval. Fig. 6.25 shows now the upper bound of β and Fig. 6.26 the lower bound. Examining Fig. 6.25 and 6.26 , we see again that for combinations of extreme high values or extreme low values of the resonance frequency $\tilde{\omega}$ and the gain $\tilde{K}$, the controller is not stabilizing anymore.

81
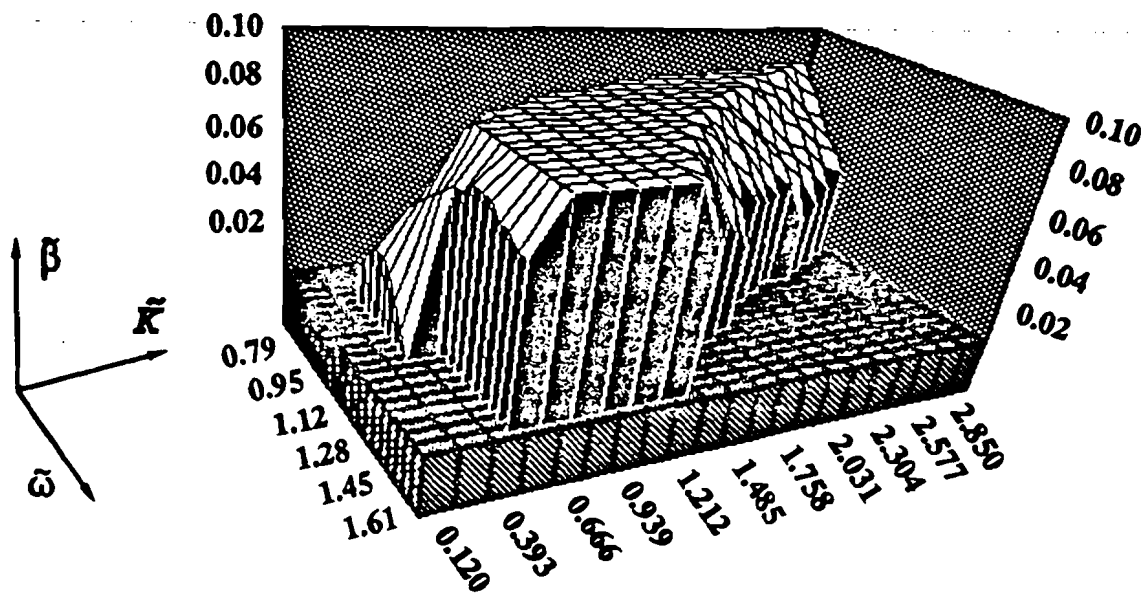
Fig. 6.25 : Stability Robustness ; Upper bound $\bar{\beta}$
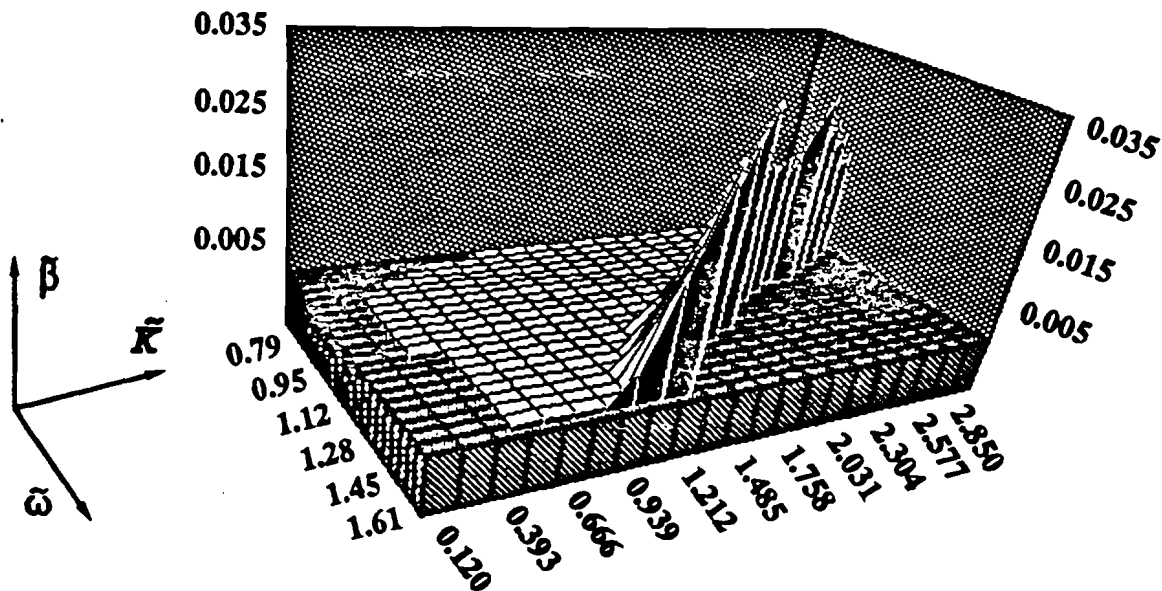
Fig. 6.26 : Stability Robustness ; Lower bound $\underline{\beta}$

To illustrate the performance robustness in a better way, Fig. 6.27 depicts the maximum and minimum position error of all parameter combinations of the process which are stabilized by the controllers. We see that the maximum position error is concentrated in the lower left corner of Fig. 5.27 . This corresponds to variations of the process parameters close to the nominal values. The achieved position error (Fig.

82

6.20) is only valid for the nominal values of the parameters. As soon as the variations of the perturbed process parameters increase, the maximum position error increases as well which is clearly visible in Fig. 6.27 .
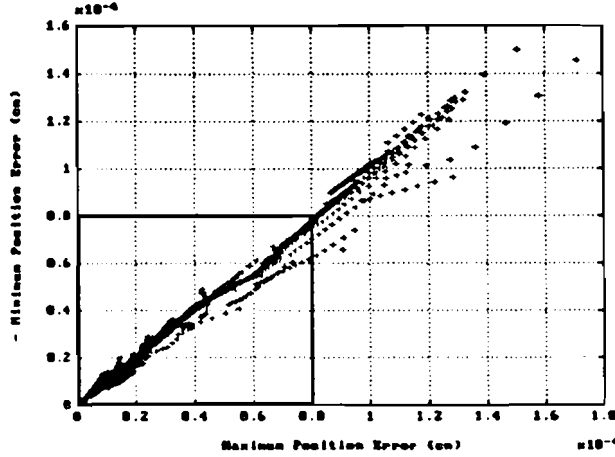
Fig. 6.27 : Performance Robustness ; Maximum position error

Suppose we accept the same maximum position error (< 8.10^{-5} cm) as we achieved in the previous chapter. The box depicted in the lower left corner of Fig. 6.27 is the bound of this range. The maximum parameter variations which correspond to this bound are given in Table 6.5 .

Table 6.5 : Parameter Variations
           (Maximum position error < 8.10^{-5} cm)
           + : All values
           - : No Values

$\tilde{K}$	$\tilde{\omega}$	$\tilde{\beta}$
$\tilde{K} \geq 0.6$	+	+
$0.45 \leq \tilde{K} < 0.6$	$\tilde{\omega} < 1.4$	+
$0.3 \leq \tilde{K} < 0.45$	$\tilde{\omega} < 1.2$	+
$\tilde{K} < 0.3$	−	−

It is obvious that the range of parameter variations for which the performance of the closed-loop system is acceptable has become smaller. The basic restriction we have is that the gain should be $\tilde{K} > 0.6$. If $\tilde{K}$ decreases we find first restrictions for the variations

of the resonance frequency and finally the performance becomes unacceptable for all parameter combinations.

6.6 Summary Performance Design

The design sequence of the filters in the performance design is structured but basicly different as in the robustness design. First we characterized the reference filter V_r with the power spectral density of the reference signal. The **Signal Tracking** can be improved by optimizing the error weighting filter W_e. Low frequencies should be weighed stronger to reduce the steady state position error and the bandwidth should be increased as much as possible to reduce the maximum position error during the movement. The disturbance filter V_v is used again to achieve a phase margin just above 45°. The final step in the design is a further optimization of the robustness using the process input weighting filter W_u.

With the proposed performance approach it is possible to design controllers for high performance applications. The maximum position error during the movement has been reduced to 4.10^{-8} cm and the settling time is less than 5 seconds (Motion time = 129 seconds) using a parabolic position signal as reference signal. The steady state position error is reduced to 10^{-11} cm. Large peak values however occur in the simulation of the error signal due to an increase of the differentiating action in the feed-forward controller. These peak values also occur in the process input signal and might cause saturation in a practical implementation.

Because of the proposed design sequence of the filters together with the optimization of the **Signal Tracking** it was not possible to include any robustness information. It turned out during the design that the **Input Saturation** became the limiting function before the **Model Robustness** could be improved. Because of the high performance design the mentioned values with respect to position error and settling time are only valid for the nominal process parameters ($K_o - 1$, $\omega_o - 1$ and $\beta_o - 0.01$). As soon as the perturbed process parameters vary from the nominal values the maximum position error increases significantly.

The robustness range for variations of the process parameters with respect to performance reduced significantly compared to the robustness design. The achieved stability robustness for variations of the process parameters remained however almost the same ($0.12 \le \bar{K} \le 2.85$, $0.79 \le \bar{\omega} \le 1.61$ and $0.001 \le \bar{\beta} \le 0.084$).

By applying the H_∞ theory we obtain controllers which are of 9th order. Because of pole-zero cancellation we can reduce the feed-back controller to order 5 and the feed-forward controller to order 7.

The robustness and performance approach have been presented here to show the worst and the best possible performance behaviour of the closed-loop system using these two extreme design techniques.

7 Conclusions & Recommendations

7.1 Conclusions

This report describes the analysis of the H_∞ theory and an application of H_∞ control. The general conclusions of this report will be discussed in this section. The more detailed conclusions related to the two design methods, the robustness and the performance approach, have been discussed at the end of Chapter 5 respectively Chapter 6.

The application of H_∞ to an electromechanical servo system has led to insight into the problems (restrictions and advantages) which might arise using H_∞ control design techniques. To solve the H_∞ optimization problem, the state-space approach is recommended above the polynomial approach because of the explicitness of the formulas involving only the solution to two Riccati equations together with a substantial reduction in computation.

The controllers in the Two-Degree-of-Freedom configuration have been derived from two different point of views. This Two-Degree-of-Freedom configuration has been introduced to optimize the trade off between robustness and performance. The objective of the first method is robustness maximization. This robustness procedure has been focused on the design of a controller which is robust for the maximum range of process parameter variations with respect to stability as well as performance. The objective of the second method is performance maximization. The controller design of this performance procedure has been focused on the optimization of the signal tracking. The design sequence of the shaping and weighting filters which is different for both design methods, is the proper way to achieve our design goals. The proposed design procedures however can also be used in general for the Two-Degree-of-Freedom configuration.

The main objective of this research was to design a controller for an electromechanical servo system which is robust with respect to stability as well as performance. To achieve stability robustness for variations of the process parameters, stable factor perturbations have been used to derive uncertainty models. The way in which uncertainty is modelled, affects the control design seriously. Taking all process uncertainties into account, can lead to very conservative uncertainty models because the H_∞ theory takes only amplitude information into account and no phase information. Because of the trade off between robustness and performance, a too conservative uncertainty model automatically leads to bad performance. The derivation of the uncertainty models has to be done very carefully to achieve an optimal performance. Although the uncertainty model has been reduced to the variation of only one process parameter, the resonance frequency, the derived robustness constraints using stable factor perturbations lead only to sufficient and not necessary conditions. The obtained controller is robust with respect to stability as well as performance for a much larger range of parameter variations as specified in the

85

uncertainty model. The achieved performance (maximum position error during movement, settling time) of the final controller is within the range of defined specifications.

Because the derived robustness constraints are sufficient but not necessary conditions, a controller without uncertainty model is designed emphasizing the performance optimization. A design without assuming uncertainty showed satisfying stability robustness but is not robust at all with respect to performance.

For practical applications it is necessary to reduce the order of the controllers as much as possible (4th order controllers are acceptable). To achieve low order controllers, it is necessary to design low order weighting functions as well. These low order weighting functions (satisfying the robustness constraints) result however in poor descriptions of the uncertainty models, which leads to conservatism and therefore loss of performance. To obtain an optimal performance, high order weighting functions are necessary which implies automatically high order controllers.

7.2 Recommendations

Until now a parabolic position signal (second order) is used as reference signal. But the mechanics are still excited too much due to the fact that the acceleration signal of the parabolic position signal has a steplike character. The peak values in the error signal become clearly visible. To optimize the performance, it is necessary to introduce a even smoother profile, like a cubic position signal (third order). Partly however, these peaks are caused by the designed controllers. Therefore it is necessary to reduce the differentiating action in the controllers as well to eliminate these peaks further. In a practical implementation these peaks which also occur in the process input signal, might cause saturation.

In this report stable factor perturbations have been used to derive uncertainty models. The obtained robustness constraints are however sufficient and not necessary conditions. Other techniques such should be studied to reduce the conservatism in the uncertainty models.

Two extreme design methods with the robustness optimization on one hand and the performance optimization on the other hand, have been presented. This resulted in controllers with optimal robustness and "poor performance" (the derived maximum position error and the settling time are still within the range of defined specifications) respectively poor robustness and optimal performance. A more quantitive approach for the range in between has to be made. Bounds should be derived for the ranges of parameter variations for which the closed-loop system is robust together with the corresponding optimal performance, to improve the use in practical applications.

Until now high order controllers are obtained. For practical applications it is necessary to reduce the order of the controllers. Several controller reduction techniques have been proposed in literature. The affect of the controller reduction with respect to performance behaviour (maximum position error, settling time), stability and performance robustness should be tested.

A last remark about the implementation using motion control cards. Until now we designed a continuous-time servo system, but in practical implementations we will use digital controllers. It should be tested if a controller obtained with continuous-time design techniques which is transformed to the discrete-time gives acceptable results.

Appendix A

References :

[1]   Anderson, B.D.O. and Liu, Y
           Controller Reduction : Concepts and Approaches
           IEEE Transactions on Automatic Control, Vol 34, No 8, 1989, pp 802-812

[2]   Boekhoudt, P.
           The H$_\infty$ Control Design Method ; A Polynomial Approach
           University of Twente Enschede, The Netherlands

[3]   Boom, A.J.J. van den
           H$_\infty$ Control ; An Exploratory Study
           University of Technology Eindhoven, The Netherlands
           Faculty of Electrical Engineering, EUT Report 88-E-211

[4]   Boom, A.J.J. van den , Klompstra, M. and Damen, A.
           A Comparison of PDD, LQG, H$_\infty$ and H$_2$ Controllers for a
           Laboratory Process
           Eindhoven University of Technology, The Netherlands
           Faculty of Electrical Engineering, Measurement and Control Group

[5]   Bouwens, H.J.J.
           Electromechanical Position Servos, Design Procedures
           Philips CFT Eindhoven, The Netherlands
           CFT Report 15/83

[6]   Doyle, J.C. , Glover, K. , Khargonekar, P.P. and Francis, B.A.
           State-space Solutions to Standard H$_2$ and H$_\infty$ Control Problems
           IEEE Transactions on Automatic Control, Vol 34, No 8, 1989, pp 831-847

[7]   Eisaka, T. , Zhong, Y. , Bai, S. and Tagawa, K.
           Evaluation of robust model matching for the control of a DC servo motor
           International Journal of Control, Vol 50, No 2, 1989, pp 479-493

[8]   Falkus, H.M.
           H$_\infty$ Control Design Toolbox for an Electromechanical Servo System
           in a Two-Degree-of-Freedom Configuration
           Philips CFT Eindhoven, The Netherlands
           Under preparation

[9]   Francis, B.A.
A Course in H_e Control Theory
Lecture Notes in Control and Information Sciences
Springer Verlag 88

[10]   Geerts - van Dalen, J.E.D. and Tosseram, B.G.M.G.
Introduction of H_e Theory on an Electromechanical Servo System
Philips CFT Eindhoven, The Netherlands
Technical Note 040/89 EN

[11]   Glover, K.
All optimal Hankel-norm approximations of linear multivariable systems and their L_e - error bounds
International Journal of Control, 1984, Vol 39, No 6, pp 1115-1193

[12]   Glover, K. and Doyle, J.C.
State-space formulae for all stabilizing controllers that satisfy an H_e - norm bound and relations to risk sensitivity
Systems & Control Letters, Vol 11, 1988, pp 167-172

[13]   Hostetter, G.H. , Savant, Jr C.J. and Stefani, R.T.
Design of Feedback Control Systems
Holt-Saunders International Editions 1982

[14]   Kruk, R.J. van der
Motion Control System, Concepts
Philips CFT Eindhoven, The Netherlands
CFT Report 032/87 EN

[15]   Kwakernaak, H.
Polynomial Approach to Robustness Optimization
First Philips Conference on Applications of Systems & Control Theory
Brussels, Belgium, January 27-29, 1988
University of Twente Enschede, The Netherlands

[16]   Kwakernaak, H.
Minimax Frequency Domain Performance and Robustness Optimization of Linear Feedback Systems
IEEE Transactions on Automatic Control
Vol Ac - 30 , No 10 , October 1985

[17]   Kwakernaak, H.
A Polynomial Approach to Minimax Frequency Domain Optimization of Multivariable Feedback Systems
International Journal of Control, Vol 44, 1986, pp 117 - 156

[18]   McFarlane, D.
        Robust Controller Design using Normalized Coprime Factor Descriptions
        Ph. D. Thesis, Queens' College, University of Cambridge,
        United Kingdom, 1988

[19]   Patel, R.V. and Munro, N.
        Multivariable System Theory and Design
        Pergamon Press, 1982
        Systems & Control, Volume 4

[20]   Swaanen, G.M.J. and Burg, R.A.J. van der
        Vierde Orde Electromechanische Servo Systemen
        Philips CFT Eindhoven, The Netherlands
        CFT Note 038/88 NE

[21]   Terlouw, J.C. and Smit, S.G.
        *Robust stability Analysis of a flexible mechanism assuming real and
        complex perturbations*
        Selected Topics in Modelling, Identification and Control
        Delft University of Technology, to appear 1990

[22]   Tosseram, B.G.M.G. and Burg, R.A.J. van der
        *State feedback based on a forth order model of an electromechanical
        servo system*
        First Philips Conference on Applications of Systems & Control Theory
        Brussels, Belgium, Januari 27-29, 1988
        Philips CFT Eindhoven, The Netherlands

[23]   Vidyasagar, M. and Kimura, H.
        Robust Controllers for uncertain Linear Multivariable Systems
        Automatica, Vol 22, No 1, 1986, pp 85-94

Appendix B

List of Symbols

A	: State matrix augmented plant G
$\hat{A}$	: State matrix controller K_a
A_e , B_e , C_e , D_e	: State space representation of W_e
A_p , B_p , C_p , D_p	: State space representation of P
A_r , B_r , C_r , D_r	: State space representation of V_r
A_u , B_u , C_u , D_u	: State space representation of W_u
A_v , B_v , C_v , D_v	: State space representation of V_v
α	: Standard problem
B	: Input matrix augmented plant G
B_1 , B_2	: Elements of B
$\hat{B}$	: Input matrix controller K_a
$\hat{B}_1$, $\hat{B}_2$	: Elements of $\hat{B}$
β_o	: Servo damping ratio
$\bar{\beta}$	: Disturbed servo damping
C	: Output matrix augmented plant G
C_1 , C_2	: Elements of C
$\hat{C}$	: Output matrix controller K_a
$\hat{C}_1$, $\hat{C}_2$	: Elements of $\hat{C}$
C_{fb}	: Feed-back controller
C_{ff} →	: Feed-forward controller
c	: Mechanical stiffnes [Nm^{-1}]
D	: Feedthrough matrix augmented plant G
D_{11} , D_{12} , D_{21} , D_{22}	: Elements of D
$D_{1.}$, $D_{.1}$	: Elements of D
$D_{11,11}$, $D_{11,12}$, $D_{11,21}$, $D_{11,22}$	: Elements of D_{11}
$\hat{D}$	: Feedthrough matrix controller K_a
$\hat{D}_{11}$, $\hat{D}_{12}$, $\hat{D}_{21}$	: Elements of $\hat{D}$
D_f , N_f	: Elements of polynomial matrix fraction
$D_{f,1}$, $D_{f,11}$, $D_{f,12}$, $D_{f,22}$	: Elements of polynomial matrix fraction
$\bar{D}_{f,11}$, $\bar{D}_{f,12}$, $\bar{D}_{f,22}$	: Elements of polynomial matrix fraction
$\bar{D}_f$	: Greatest common left factor
$\bar{D}_{f,22}$	: Element of polynomial matrix fraction
d_f	: Stable polynomial

91

Symbol	Description	Unit
d_i	Unstable part of d_0	
d_o	Nominal denominator of P_0	
d_s	Stable part of d_0	
d_1	Mechanical damping between rotor and load	
d_2	Friction between load and stator	
d_3	Friction between rotor and stator	
Δ_β	Error on β_0	
Δ_d	Error on d_0	
Δ_i	Model error on the inverse of P_i	
Δ_k	Error on K_0	
Δ_n	Error on n_0	
Δ_ω	Error on ω_0	
Δ_s	Model error on P_s	
e	Error signal	
$\tilde{e}$	Weighted error signal	
F	State feed-back matrix	
F_{11} , F_{12} , F_2	Elements of F	
F_m	Mechanical forces (in general)	[N]
F_{spring}	Force of spring	[N]
F_{damper_1}	Force of damper 1 (d_1)	[N]
F_{damper_2}	Force of damper 2 (d_2)	[N]
F_{damper_3}	Force of damper 3 (d_3)	[N]
Φ	Class of signals for v	
φ	Element of $\mathbf{RH}_\infty$	
G	Augmented plant	
G_{11}	Part of augmented plant ; transfer from w to z	
G_{12}	Part of augmented plant ; transfer from u to z	
G_{21}	Part of augmented plant ; transfer from w to y	
G_{22}	Part of augmented plant ; transfer from u to y	
γ	Scaling factor state-space approach	
H	Output injection matrix	
H_{11} , H_{12} , H_2	Elements of H	
H_∞	Hardy space of proper matrix functions in closed right half plane	
I	Motor current	[A]
i	Transmission ratio	[mrad^{-1}]
inf	infimum	
J	Inertia	[kgm^2]
j	Imaginary part ($j^2 = -1$)	
K	Controller (in general)	
K_a	State-space representation controller solution	
K_0	Gain constant	
K_r	Motor constant	[N]

K_a	: Stabilizing controller
$\tilde{K}$	: Disturbed gain
L_f	: Real rational matrix
L_2	: Inner product space
λ	: Scaling factor polynomial approach
$\lambda(.)$	: Eigenvalue
$MIMO$	: Multiple input multiple output
M_k	: Optimization function
$\lVert M_k \rVert$	: H_∞ optimization problem
M_t	: Total mass motor with load [kg]
M , N	: Left coprime factors of P
M_{11}	: Disturbance reduction criterion
M_{12}	: Signal tracking criterion
M_{21}	: Model robustness criterion
M_{22}	: Input saturation criterion
m	: Mass load [kg]
m_1	: Number of exogeneous inputs
m_2	: Number of control inputs
$N_{f,11} , N_{f,12} , N_{f,21} , N_{f,22}$	: Elements of polynomial matrix fraction
$\bar{N}_{f,11} , \bar{N}_{f,12} , \bar{N}_{f,21} , \bar{N}_{f,22}$	: Elements of polynomial matrix fraction
$\tilde{N}_{f,21} , \tilde{N}_{f,22}$	: Elements of polynomial matrix fraction
n	: Number of states
n_o	: Nominal numerator of P_o
n_r	: Input reference signal
n_v	: Disturbance signal
ω_o	: Nominal resonance frequency [rads^{-1}]
ω_b	: Scaling factor frequency axis
$\tilde{\omega}$	: Disturbed resonance frequency [rads^{-1}]
P	: Process (in general)
P_f , Q_f	: Polynomial fraction matrices
P_r , Q_r	: Elements algebraic Riccati equation
P_i	: Unstable part process P_o
P_o	: Nominal process
P_s	: Stable part process P_o
$\tilde{P}$	: Disturbed process
$\tilde{P}_i$	: Unstable part disturbed process $\tilde{P}$
$\tilde{P}_s$	: Stable part disturbed process $\tilde{P}$
p_1	: Number of outputs to be controlled
p_2	: Number of measured outputs
$R , \tilde{R}$	: Matrix definition state-space solution
$R_f , \bar{R}_f$	: Polynomial fraction matrices
r	: Shaped reference signal

Ric	: Riccati	
$\rho(\cdot)$	: Largest eigenvalue	
$\mathbb{R}$	: Real	
SISO	: Single input single output	
s	: Laplace operator	
$s_{\bullet}$	: Scaled laplace operator	
sup	: Supremum	
$T_{\bullet}$	: Motor Torque	[Nm]
θ	: Class of signals for r	
$u(t)$	: Control input	
u_p	: Process input	
$\bar{u}$	: Weighted control signal	
V_k	: Equalizing solutions	
V_r	: Shaping filter for reference signal	
V_v	: Shaping filter for disturbance signal	
v_p	: Shaped disturbance signal	
W_e	: Weighting filter for error signal	
W_u	: Weighting filter for control signal	
$w(t)$	: Exogeneous input	
X	: Solution Riccati equation (in general)	
X_{∞} , Y_{∞}	: Solution Riccati equations in H_{∞} control	
X_f , Y_f	: Polynomial fraction description controller	
x	: Displacement (in general)	[m]
$\dot{x}$	: Velocity (in general)	[ms^{-1}]
$\ddot{x}$	: Acceleration (in general)	[ms^{-2}]
$x(t)$	: State vector	
x_1	: Position of mass m	[m]
$\dot{x}_1$	: Velocity of mass m	[ms^{-1}]
x_2	: Angle position of inertia J	[rad]
$\dot{x}_2$	: Angle velocity of inertia J	[rads^{-1}]
x_p	: Position load	[m]
$\ddot{x}_p$	: Acceleration load	[ms^{-2}]
x_{P_o}	: States nominal process P_o	
x_{V_r}	: States reference filter V_r	
x_{W_e}	: States error weighting filter W_e	
x_{W_u}	: States process input weighting filter W_u	
$y(t)$	: Measured output	
$z(t)$	: Output to be controlled	
$\| \cdot \|_{\infty}$	: H_{∞} norm (in general)	

Appendix C

A Polynomial Approach

In this appendix the method to solve the "standard" H_∞ optimization problem via a polynomial approach is discussed shortly. The main reference we use in this section is the book "The H_∞ Control Design Method, A Polynomial Approach" of P. Boekhoudt [2].

The starting point is the definition of equalizing solutions. Define :

$$V_k := M_k^* M_k \qquad \text{(C.1)}$$

and

$$Z_{k,l} := V_k + L_f^* L_f \qquad \text{(C.2)}$$

where L is a real rational, not necessarily stable matrix of less than full rank. This is of no influence for the minimization problem. It ensures only that $Z_{k,l}$ is of full rank. We consider equalizing compensators, K, which have the property that :

$$Z_{k,l} - \lambda^2 I \qquad \lambda \in \mathbb{R} \qquad \text{(C.3)}$$

Let the general problem matrix G have a left coprime polynomial matrix fraction description :

$$G - D_f^{-1} N_f - \begin{pmatrix} D_{f,11} & D_{f,12} \\ 0 & D_{f,22} \end{pmatrix}^{-1} \begin{pmatrix} N_{f,11} & N_{f,12} \\ N_{f,21} & N_{f,22} \end{pmatrix} \qquad \text{(C.4)}$$

and the compensator transfer matrix a right fraction description :

$$K - Y_f X_f^{-1} \qquad \text{(C.5)}$$

then the closed-loop matrix is given by :

$$
\begin{aligned}
M_k &= G_{11} + G_{21} K \left(I - G_{22} K \right)^{-1} G_{21} \\
&= D_{f,11}^{-1} \left[N_{f,11} - \left(D_{f,12} X_f - N_{f,12} Y_f \right) \left(D_{f,22} X_f - N_{f,22} Y_f \right)^{-1} N_{f,21} \right]
\end{aligned}
\tag{C.6}
$$

Because polynomial matrices do (as constant matrices) not commute, we need polynomial matrix fraction conversion.

$$
\begin{pmatrix} D_{f,11} & 0 \\ 0 & I \end{pmatrix}^{-1}
\begin{pmatrix} D_{f,12} & -N_{f,12} \\ D_{f,22} & -N_{f,22} \end{pmatrix}
=
\begin{pmatrix} \bar{D}_{f,12} & -\bar{N}_{f,12} \\ \bar{D}_{f,22} & -\bar{N}_{f,22} \end{pmatrix}
\bar{D}_{f,11}^{-1}
\tag{C.7}
$$

then

$$
\begin{pmatrix} D_{f,11}^{-1} \left(D_{f,12} X_f - N_{f,12} Y_f \right) \\ D_{f,22} X_f - N_{f,22} Y_f \end{pmatrix}
=
\begin{pmatrix} \bar{D}_{f,12} & -\bar{N}_{f,12} \\ \bar{D}_{f,22} & -\bar{N}_{f,22} \end{pmatrix}
\bar{D}_{f,11}^{-1}
\begin{pmatrix} X_f \\ Y_f \end{pmatrix}
\tag{C.8}
$$

To make sure that $(D_{f,12} X_f - N_{f,12} Y_f)$ and $(D_{f,22} X_f - N_{f,22} Y_f)$ are polynomial and to satisfy Eq. C.2 , we require that :

$$
\bar{D}_{f,11}^{-1}
\begin{pmatrix} X_f \\ Y_f \end{pmatrix}
=
\begin{pmatrix} P_f \\ Q_f \end{pmatrix}
\tag{C.9}
$$

where P_f and Q_f are polynomial matrices to be determined. Combination of Eq. C.6 , C.8 and C.9 results in :

$$
\begin{aligned}
M_k &= D_{f,11}^{-1} N_{f,11} - D_{f,11}^{-1} \left(D_{f,12} X_f - N_{f,12} Y_f \right) \left(D_{f,22} X_f - N_{f,22} Y_f \right)^{-1} N_{f,21} \\
&= D_{f,11}^{-1} N_{f,11} - \left(\bar{D}_{f,12} P_f - \bar{N}_{f,12} Q_f \right) \left(\bar{D}_{f,22} P_f - \bar{N}_{f,22} Q_f \right)^{-1} N_{f,21}
\end{aligned}
\tag{C.10}
$$

We now define a greatest common left factor $\bar{D}_f$ of $\bar{D}_{f,22}$ and $\bar{N}_{f,22}$ such that :

$$
\bar{D}_{f,22} = \bar{D}_f \, \bar{\bar{D}}_{f,22} \quad , \quad \bar{N}_{f,22} = \bar{D}_f \, \bar{\bar{N}}_{f,22}
\tag{C.11}
$$

96

where $\bar{D}_{f22}$ and $\bar{N}_{f22}$ are left coprime. Then the polynomial matrix fraction conversion :

$$\begin{pmatrix} D_{f,11} & 0 \\ 0 & \tilde{D}_f \end{pmatrix}^{-1} \begin{pmatrix} N_{f,11} \\ N_{f21} \end{pmatrix} - \begin{pmatrix} \bar{N}_{f,11} \\ \bar{N}_{f21} \end{pmatrix} D_{f,1}^{-1} \qquad (C.12)$$

allows us to write M_k as :

$$\begin{aligned} M_k &- D_{f,11}^{-1} N_{f,11} - \left(\bar{D}_{f,12} P_f - \bar{N}_{f,12} Q_f \right) \left(\tilde{D}_{f22} P_f - \tilde{N}_{f22} Q_f \right)^{-1} N_{f21} \\ &- \bar{N}_{f,11} D_{f,1}^{-1} - \left(\bar{D}_{f,12} P_f - \bar{N}_{f21} Q_f \right)^{-1} \bar{N}_{f21} D_{f,1}^{-1} \\ &- \left(\bar{N}_{f,11} - \lambda S_f \bar{R}_f^{-1} \bar{N}_{f21} \right) D_{f,1}^{-1} \end{aligned} \qquad (C.13)$$

where :

$$S_f :- \bar{D}_{f,12} P_f - \bar{N}_{f,12} Q_f \qquad , \qquad \frac{1}{\lambda} \bar{R}_f :- \tilde{D}_{f22} P_f - \tilde{N}_{f22} Q_f \qquad (C.14)$$

The factor $1/\lambda$ has been inserted for later convienence. Finally, we perform the polynomial matrix conversion :

$$\bar{R}_f^{-1} \bar{N}_{f21} - \tilde{N}_{f21} R_f^{-1} \qquad \rightarrow \qquad \bar{N}_{f21} R_f - \bar{R}_f \tilde{N}_{f21} \qquad (C.15)$$

so that M_k becomes :

$$M_k - \left(\bar{N}_{f,11} R_f - \lambda S_f \tilde{N}_{f21} \right) R_f^{-1} D_{f,1}^{-1} \qquad (C.16)$$

Substitution of the new M_k in Z yields :

$$D_{f,1}^{-*} R_f^{-*} \left(\bar{N}_{f,11} R_f - \lambda S_f \tilde{N}_{f21} \right)^* \left(\bar{N}_{f,11} R_f - \lambda S_f \tilde{N}_{f21} \right) R_f^{-1} D_{f,1}^{-1} + L_f^* L_f - \lambda^2 I$$

$$\left(\bar{N}_{f,11} R_f - \lambda S_f \tilde{N}_{f21} \right)^* \left(\bar{N}_{f,11} R_f - \lambda S_f \tilde{N}_{f21} \right) + R_f^* D_{f,1}^* L_f^* L_f D_{f,1} R_f - \lambda^2 R_f^* D_{f,1}^* D_{f,1} R_f$$

$$(C.17)$$

Since the first term on the left and the term on the right-hand side of the expression are polynomial, also $R_f^* D_{f,1}^* L_f^* L D_{f,1} R_f$ is polynomial. Define :

$$\bar{L}_f^* \bar{L}_f := \frac{1}{\lambda^2} R_f^* D_{f,1}^* L^* L D_{f,1} R_f \qquad (C.18)$$

with $\bar{L}_f$ polynomial. We can rewrite the Eq. C.17 as :

$$\left(\frac{1}{\lambda} \bar{N}_{f,11} R_f - S_f \tilde{N}_{f,21} \right)^* \left(\frac{1}{\lambda} \bar{N}_{f,11} R_f - S_f \tilde{N}_{f,21} \right) + \bar{L}_f^* \bar{L}_f - R_f^* D_{f,1}^* D_{f,1} R_f \quad (C.19)$$

The equalizing solutions satisfy now the following polynomial matrix equations :

$$\left(\frac{1}{\lambda} \bar{N}_{f,11} R_f - S_f \tilde{N}_{f,21} \right)^* \left(\frac{1}{\lambda} \bar{N}_{f,11} R_f - S_f \tilde{N}_{f,21} \right) + \bar{L}_f^* \bar{L}_f - R_f^* D_{f,1}^* D_{f,1} R_f$$

$$S_f - \bar{D}_{f,12} P_f - \bar{N}_{f,12} Q_f$$

$$\frac{1}{\lambda} \bar{R}_f - \bar{D}_{f,22} P_f - \bar{N}_{f,22} Q_f \qquad (C.20)$$

$$\bar{N}_{f,21} R_f - \bar{R}_f \tilde{N}_{f,21}$$

The solution of the polynomial equations may be devided into 5 phases :

1) Solving the equations for $\lambda - \infty$. This solution is referred to as the starting solution.
2) Establishing the dimensions and the degrees of the unknown polynomial matrices.
3) Converting the set of polynomial equations, by equating coefficients of like powers, to a set of algebraic equations.
4) Solving the algebraic equations by using the solution at infinity as a starting solution and by decreasing $|\lambda|$ gradually.
5) Refining the solution for λ close to the optimal $\lambda - \lambda_{opt}$.

Appendix D

Parabolic Set Point Function

In practice step inputs are seldom used for motion trajectories. They cause saturation of the controller due to the limited acceleration and velocity of the motor and servo amplifier and therefore result in a poor position accuracy. High order set point functions are used to overcome these saturation problems. A well known function is the parabolic profile (second order) which is pointed out further in this appendix.

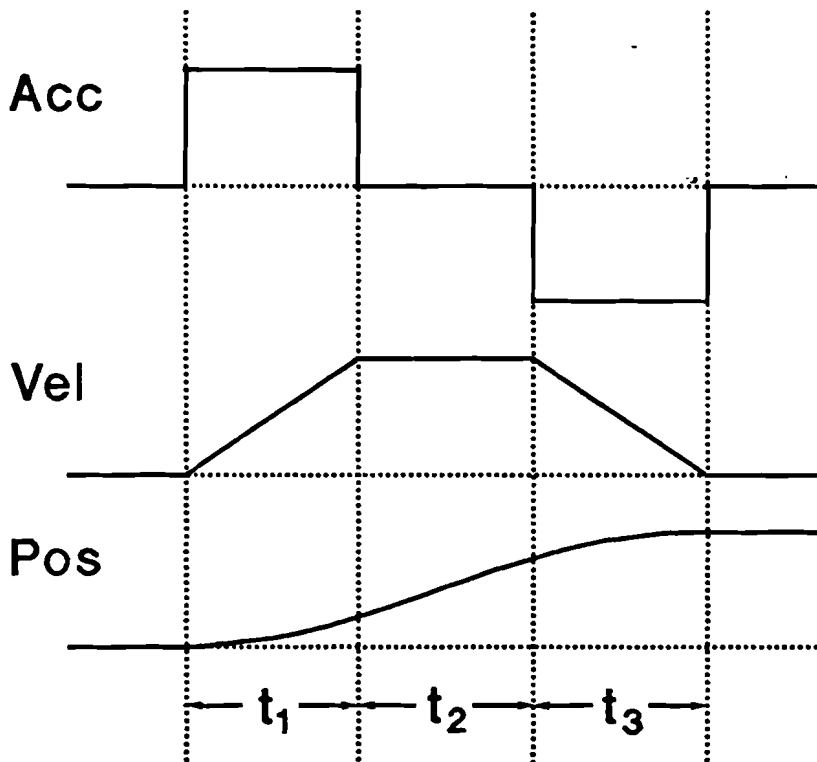The parabolic trajectory used for point-to-point control is depicted in Fig. D.1 .

Fig. D.1 : Parabolic Trajectory ($t_1 = t_3$)

Before we can derive the form of the parabolic trajectory (time intervals t_1 , t_2 and t_3) with the corresponding displacement, maximum acceleration and velocity, we will first consider these values in a theoretical case. Suppose we have an electromechanical servo system with a bandwidth of ω_s rad/s. In our simulation model the resonance frequency is scaled to 1 rad/s$_s$ ($_s$ stands for scaled). This implies we have to use the following scaling factor :

99

$$s - \omega_b \, s, \qquad\qquad\qquad\qquad \text{(D.1)}$$

The translation from s to s_s is the same as a division of ω_b on the frequency axis. In the time domain this is a multiplication of ω_b . Table D.1 shows the scaled design values which will be used in the simulations.

<div align="center">

Table D.1 : Scaled Design Values (omitting ._s)

Description	Value
Resonance Frequency	1 rad/s
Maximum Acceleration	$2.5\ 10^{-4}\ cm/s^2$
Maximum Velocity	$1.3\ 10^{-2}\ cm/s$
Motion Time	126 s
Settling Time	63 s

</div>

To achieve a displacement of 1 cm with the restrictions for maximum acceleration and velocity of Table D.1 , the time intervals of Fig. D.1 can be derived as follows. We will use the maximum acceleration and velocity to minimize the motion time as much as possible. We find :

$$t_{1,max}\ s\ *\ 2.5\,10^{-4}\ \frac{cm}{s^2}\ -\ 1.3\,10^{-2}\ \frac{cm}{s}$$
$$\rightarrow t_{1,max}\ -\ 52\ s \qquad\qquad \text{(D.2)}$$

The displacement due to the time intervals t_1 and t_3 ($t_1 = t_3$) is :

$$2\ *\ \left(\ \frac{1}{2}\ *\ t_{1,max}\ s\ *\ 1.3\,10^{-2}\ \frac{cm}{s}\ \right) - 0.676\ cm \qquad\qquad \text{(D.3)}$$

A total displacement of 1 cm can be achieved if the displacement during the time interval t_2 is (1 cm - 0.767 cm) = 0.324 cm . So, the time interval t_2 can be defined as :

$$t_2\ s\ *\ 1.3\,10^{-2}\ \frac{cm}{s^2}\ -\ 0.324\ cm$$
$$\rightarrow t_2\ -\ 25\ s \qquad\qquad \text{(D.4)}$$

The parabolic trajectory with a displacement of 1 cm using maximum acceleration and velocity is defined now. The total motion time is :

$$t_1 + t_2 + t_3 - 129 \ s \qquad\qquad (D.5)$$

The minimum motion time of 129 seconds is larger as specified in Table D.1 because of the limited acceleration and velocity. A smaller motion time can only be achieved if the maximum acceleration or (and) the velocity is increased.

Table D.2 shows the values of the position, velocity and acceleration for a displacement of 1 cm during 129 seconds.

Table D.2 : Parabolic point-to-point trajectory

Interval (s)	Position (cm)	Velocity (cm/s)	Acceleration (cm/s^2)
$t \le 0$	0	0	0
$0 < t \le 52$	$1.25 \ 10^{-4} \ t^2$	$2.5 \ 10^{-4} \ t$	$2.5 \ 10^{-4}$
$52 < t \le 77$	$1.3 \ 10^{-2} \ t + 0.338$	$1.3 \ 10^{-2}$	0
$77 < t \le 129$	$1 - 1.25 \ 10^{-4} \ (129 - t)^2$	$2.5 \ 10^{-4} \ (129 - t)$	$- 2.5 \ 10^{-4}$
$t > 129$	1	0	0